A model of the morphological behaviour and stability of channels and flats in tidal basins

M.Sc.Thesis, H 824.55

March 1992

TU Delft

Delft University of Technology

delft hydraulics

Summary

In this report, a model is derived which simulates the behavior of channels and flats in a tidal basin after a change in the exogenous parameters.

In chapter 1, a short introduction is given about the context in which this research has been done.

Chapter 2 discusses the general features of the tidal inlet system as well as its formation and classification. Also, an overview is given of the empirical relationships that have been derived.

In chapter 3, the shoaling process in a tidal basin is analyzed. Because of a slight deformation of the tidal wave, the tide-integrated residual transport flux causes the tidal basin to fill in. The continued influx of sediment will induce the growth of tidal flats, which are inundated during only part of the tidal cycle. These tidal flats in turn produce a mechanism which stops the import of sediment into the tidal basin. This means that an equilibrium relative tidal flats area exists.

In chapter 4, a model is derived based on the assumption that the behavior of the basic elements, the channels and the flats, is controlled by certain variables which try to attain their equilibrium value. These variables are the channel's cross-sectional area, the flats' surface area and the depth over the flats. With this model, four different scenarios, namely a partial closure of the tidal basin, a sea level rise, an increase in tidal range and a periodicity in the tidal range amplitude have been simulated. All these scenarios have been stacked to reproduce the morphological behavior in the Zoutkamperlaag, the Netherlands, which has undergone great changes since the closure of the Lauwerszee in 1969. Finally, a short assessment is made of the influence a changing tidal basin has on the other elements in the tidal inlet system.

A model of the morphological behaviour and stability of channels and flats in tidal basins

Ap van Dongeren

M.Sc. Thesis:

Group of Hydraulic Engineering
Department of Civil Engineering
Delft University of Technology

Thesis supervisors:

Prof.ir. K. d'Angremond
Dr.ir. H.J. de Vriend
Dr.ir. J. van de Graaff

Preface

This report on the morphological behavior and stability of channels and flats in tidal basins is submitted as my M.Sc thesis at Delft University of Technology.
It is based on an internship at Delft Hydraulics and has been funded by the research program ISOS*2 (Impact of Sea level On Society), which is sponsored by Rijkswaterstaat.

I wish to express my gratitude to my thesis supervisors prof. ir. K d'Angremond, dr. ir. H.J. de Vriend and dr. ir. J. van de Graaff for their advice, enthousiasm and valuable suggestions. Further, I would like to thank fellow Siberian ir. Ad Reniers for advice and support, all staff at Delft Hydraulics, and, last but not least, Gina Forno for support and correcting my English.

Ap van Dongeren
Delft, March 1992

CONTENTS

Preface
Summary
Contents
List of figures

Chapter 1 Introduction 1

Chapter 2 Tidal inlets 3

2.1 Elements of a tidal inlet 3
2.2 Formation 5
2.3 Classification 9
2.4 Empirical research on stability parameters . . 11

Chapter 3 Tidal basin shoaling 18

3.1 Basin lay-out 18
3.2 Boundary conditions 18
3.3 Governing equations 22
3.4 Shoaling simulation 24
3.5 Influence of geometry on tidal asymmetries and residual transports 26
3.6 Ebb dominance in existing tidal inlets 36
3.7 Conclusions 38

Chapter 4 Tidal basin model 40

4.1 Sediment distribution system 40
4.2 Tidal basin modeling 42
4.3 Tidal basin simulation model 47
4.4 Scenarios 48
4.5 Hindcast of the Zoutkamperlaag 53
4.6 Influence of changes in the tidal basin on other parts of the system 57

Conclusions and recommendations 58

REFERENCES 61

APPENDICES 66

List of figures

1.1 Schematization of a tidal inlet

2.1 Uninterrupted and interrupted coasts in the world (from Hayes, 1979)
2.2 Morphological elements of a tidal inlet (from Smith, 1984)
2.3 Bifurcating channels in a West Frisian tidal basin (from Massie, 1986)
2.4 Spit barrier formation (from Leatherman, 1982)
2.5 Barrier island development by cross-shore transport (from Leatherman, 1982)
2.6 Barrier island length vs. tidal range for the U.S. Mid-Atlantic coast (from Fitzgerald, 1988)
2.7 Ebb and flood flow fields (from Oertel, 1988)
2.8 Directional spreading of tidal currents in Texel inlet (from Sha, 1990)
2.9 Four different types of ebb tidal deltas (from Oertel, 1975)
2.10 Hydrodynamic classification based on offshore parameters (from Hayes, 1979)
2.11 No-inlet bathymetry (from Dean and Walton, 1976)
2.12 Tidal prism vs. ebb shoal volume for moderately exposed coasts (from Walton and Adams, 1976)
2.13 Tidal prism vs. ebb shoal volume for highly exposed coasts (from Walton and Adams, 1976)
2.14 V/P vs. W/D (from Marino and Mehta, 1987)

3.1 Channel schematization
3.2 A positive symmetric curve (from Boon and Byrne, 1981)
3.3 A positive anti-symmetric curve (from Boon and Byrne, 1981)
3.4 Time evolution of the channel profile
3.5 Time evolution of the channel with reflection
3.6 Lay-out of channel 1
3.7 Lay-out of channel 2
3.8 Lay-out of channel 3
3.9 Lay-out of channel 4
3.10 Lay-out of channel 5
3.11 Lay-out of channel 6
3.12 Evolution of the M_4/M_2 ratio in channels 1, 2 and 3
3.13 Growth of the relative phases in channels 1, 2 and 3
3.14 Net velocity flux in channel 1, 2 and 3
3.15 Evolution of the ratio in channels 4, 5 and 6
3.16 Growth of the relative phase in channels 4, 5 and 6
3.17 Net velocity flux in channels 4, 5 and 6
3.18 Lay-out of channel 7
3.19 Discharge per unit width curves and water level for sections I, II and total
3.20 Lay-out of channel 4a and 4b
3.21 Net velocity flux in channels 4a and 4b
3.22 Wachapreaque inlet, Virginia (from Boon and Byrne, 1981)
3.23 Stage-velocity curves in the Stiffkey marshes, Norfolk, England (from Pethick, 1980)
3.24 Velocity discharge and sediment discharge in Bolinas Lagoon, California (from Ritter, 1972)

4.1 Time evolution with constant τ
4.2 Summation of cross-sectional areas
4.3 Plan view of the tidal basin schematization
4.4 Schematized sediment flow
4.5 Influence of bank height on erosion
4.6 Situation before and after closure of the model basin
4.7 Zoutkamperlaag after 1969
4.8 Schematization of the Zoutkamperlaag before closure
4.9 Schematization of the Zoutkamperlaag after closure

Chapter 1 Introduction

Tidal inlets, short and narrow connections between bays or lagoons and the ocean, are important areas in many ways. Together with the basins, they provide natural harbors which propel economic activity, breeding grounds and natural habitats for fish and other marine animals, recreational space, fishing grounds and energy exploration sites.

The hydraulics and sediment transport processes in tidal inlets and adjacent inner and outer deltas prove to be very complex. Changes in conditions, caused either by human beings or by nature, force the inlet to adapt to a new unknown equilibrium which results in erosion or sedimentation of channels, deltas and barrier island shores. This in turn can cause unfavorable situations such as unnavigable entrance channels and loss of beaches and dunes on the barrier islands.

In the last fifty years, civil engineers have done much research to come to an understanding of the underlying physical processes in tidal inlets which in turn make it possible to predict changes in the morphology. In the Netherlands, with its extensive system of tidal inlets called the Wadden Sea, this research has been formatted into two programs called Kustgenese (Coastal Genesis) and ISOS*2 (Impact of Sea level On Society) sponsored by the Dutch Ministry of Public Works. This research is part of the latter program which has been developed to construct a dynamical model of long term changes in inlets based on empirical relationships.

This M.Sc. thesis (afstudeerrapport) is based on research that I carried out as a student researcher at Delft Hydraulics. During my internship, I focused on the morphological behavior of tidal basins in response to changes in the extrageneous conditions. The results of this research will be implemented into the model of a tidal inlet as proposed by De Vriend and Roelvink (1989), see Fig. 1.1.

Their model considers the various elements of a tidal inlet system, such as the tidal basin, outer delta and adjacent shores, to be sediment storage areas which can be described by their sand/sediment contents. The elements interact through transport relationships which are induced by deviations from the equilibrium state. The sediment balance of the elements serves as an equation of state. This model will give insight into the interconnectedness of the elements, the reaction to changing parameters and the effectiveness of remedies to counteract unfavorable situations.

This model is based upon the sand-sharing axiom as formulated by Dean (1988):

> If sand is removed or blocked from a portion of the sand-sharing system, the system will respond to restore equilibrium by transporting sand to the deficient area. The

adverse erosional effect on the remainder of the system by this removal or blockade is certain, only the timing and degree of its manifestation are uncertain beforehand.

De Vriend and Roelvink (1989) defined the system as follows:

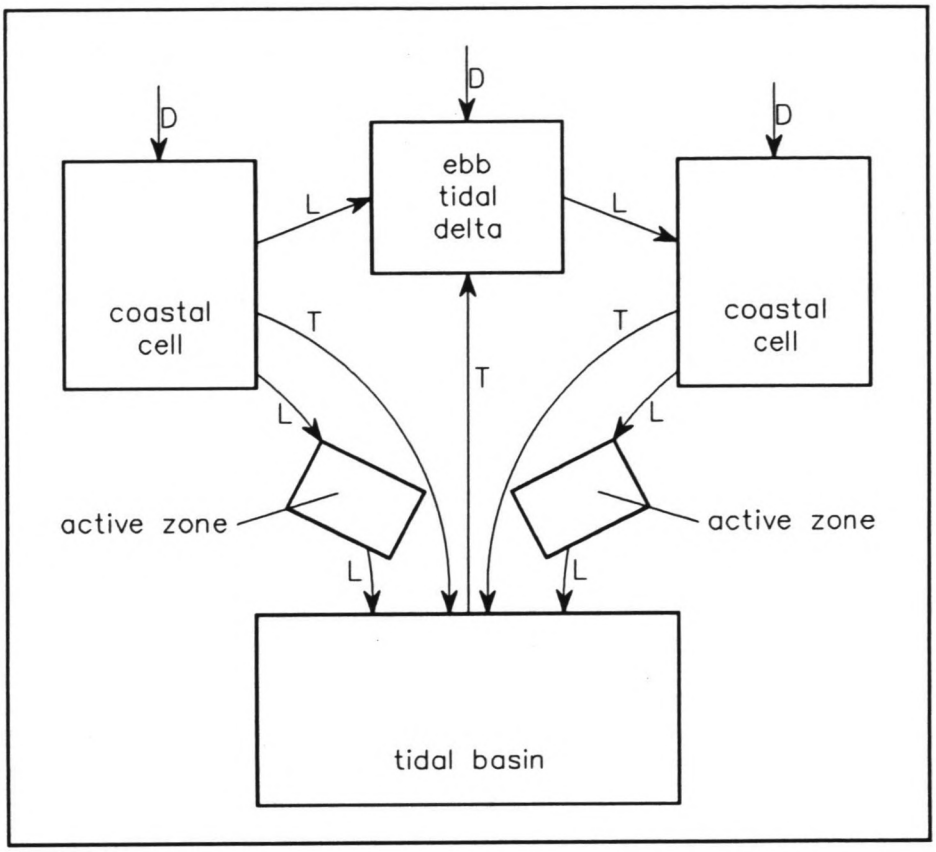

Fig. 1.1: Schematization of a tidal inlet

where D = cross-shore transport
L = longshore transport
T = channel transport

Chapter 2 Tidal inlets

In this chapter, some general features of tidal inlets as well as their formation and classification are discussed. Also, an overview of empirical relationships is given. In this chapter, use has been made of the literature survey written by Rob Steijn of Delft Hydraulics. We refer to his report and the literature that it is based upon for a comprehensive description of tidal inlets.

2.1 Elements of a tidal inlet

In classifying coasts, a distinction is made between uninterrupted and interrupted coasts. Uninterrupted coasts, like the Holland Coast, form the majority of the world's coastline. As can be seen in Fig. 2.1, interrupted coasts appear throughout the world. Major stretches of this type of coast include the U.S. East and Gulf coasts and the coast of Northwestern Europe.

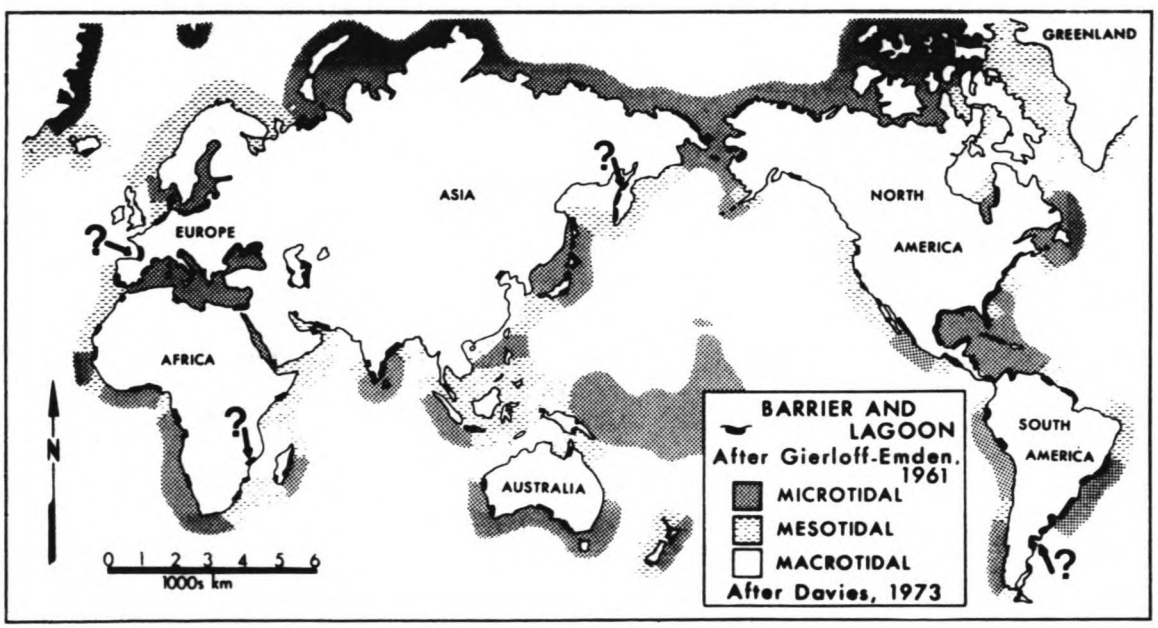

Fig. 2.1: Uninterrupted and interrupted coasts in the world (from Hayes, 1979)

The interrupted coasts can be classified according to the influence of tides and rivers on formation and maintenance of the interruptions (Steijn, 1991). One extreme is the delta coast of the Mississippi, which is strongly river-dominated. Estuaries such as the Western Scheldt in the Netherlands experience a mixed influence. This report concentrates on the other extreme: coastal interruptions which are maintained exclusively by marine action. These interruptions are called **tidal inlets**. One definition is given by Niemeyer (1990):

> A tidal inlet is a narrow passage that links two larger bodies of water (the sea and the tidal basin) through bi-

directional tidal flow.

A number of these inlets usually alternate with barrier islands to form barrier coasts which separate the sea from a basin like the Wadden Sea in the Netherlands, Germany and Denmark.
Strictly speaking, a tidal inlet consists only of the **gorge**, the short, narrow and deep waterway as defined by Niemeyer. Usually two other morphological elements, unique to the tidal inlet system, are also included in the definition: the ebb tidal delta and the flood tidal delta, see Fig. 2.2.

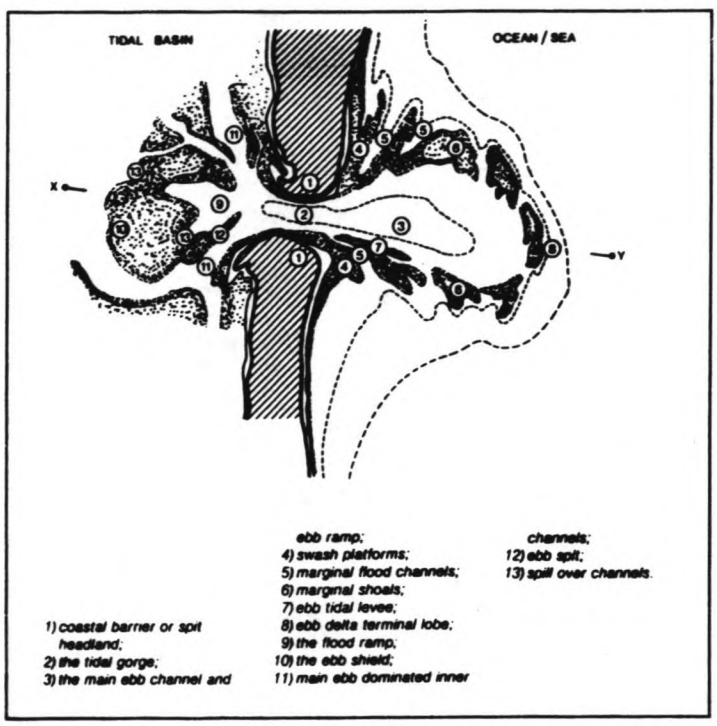

Fig. 2.2: Morphological elements of a tidal inlet (from Smith, 1984)

The **ebb tidal delta** is the accumulation of sediment seawards of the inlet. Its name is derived from the (not totally correct) notion that it is formed exclusively by the outflow (ebb flow) from a tidal inlet. Recent research has shown that the longshore current induced by waves is a major contributor to the build-up of the ebb tidal delta (Dean and Walton, 1975 and Marino and Mehta, 1988). For this reason, the word "outer delta", as proposed by Steijn (1991), would be a better term. In this report, both terms are used to describe the same morphological unit.
As can be seen in Fig. 2.2, the outer delta itself consists of a number of sub-elements. Note the central ebb channel which funnels the outflow, the flood channels through which the inflow is directed, the swash platforms that store sediment and the terminal lobe which forms the seaside perimeter of the delta. Sometimes these sub-elements are not easily recognized in nature. This "bulge" of sand is a vital part of the system and plays a central role in the sediment distribution to the

islands' coasts and the tidal basin. It probably stores sediment temporarily when the entire system is out of balance. Also, it protects the basin and the islands from wave attack.

The **flood tidal delta** is situated on the other side of the inlet. This delta has different appearances throughout the world. The sub-elements shown in Fig. 2.2 are defined on the basis of U.S. research and can not be recognized in tidal basins like the Wadden Sea. There, the flood tidal delta is better represented by a tree-like structure of bifurcating channels, see Fig. 2.3.

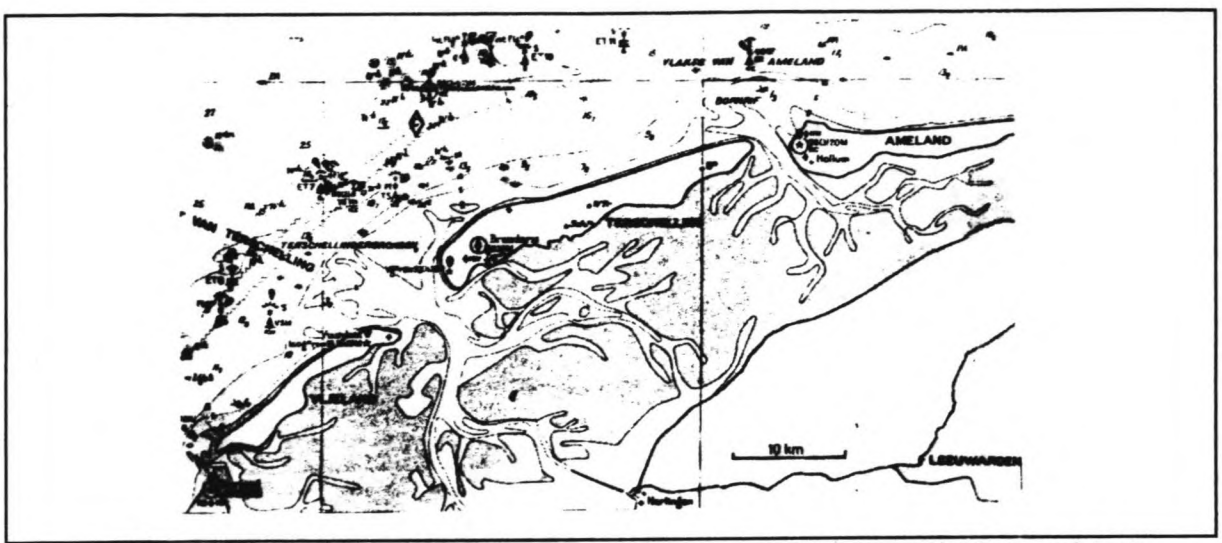

fig. 2.3: Bifurcating channels in a West Frisian tidal basin (from Massie, 1986)

Another part of the system are the **island headlands** on either side of the inlet gorge. These formations, sometimes called spits or recurved spits, probably play a role in temporarily storing sediment and constricting the inlet gorge to retain Escoffier's (1940) equilibrium inlet velocities after a change in the system. This mechanism could explain the formation of such a recurved spit in the Friesche Zeegat inlet. These headlands are denoted (1) and (4) in Fig. 2.2.

2.2 Formation

Tidal inlets are formed by different mechanisms: non-closure of an existing interruption, the break-through of a newly formed barrier coast and the flooding of river valleys (Steijn, 1991).

In the first case, ancient river mouths and natural basins serve as interruptions in an otherwise uniform coast. The longshore current moves sand along this coast and deposits its load at the coastal inlets when it loses momentum. Such deposits are called spits and can close the gap if the tidal flow is not strong enough.
Only tidal basins with a sufficiently large **prism** (the volume of water that has to pass through the inlet during flood to

fill up the basin) and consequently large velocities are able to maintain a cross-sectionally stable inlet (Niemeyer, 1990). These inlets may be in a fixed location, but it is also possible that the littoral drift causes the inlets to migrate along the coast.

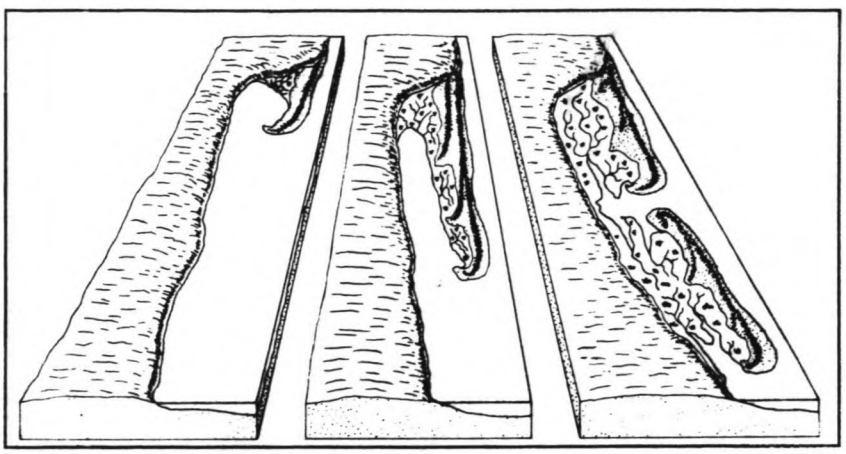

Fig. 2.4: Spit barrier formation (from Leatherman, 1982)

More important in the formation of many inlets is the breakthrough mechanism. In this scenario, waves and tides induce an onshore sediment transport through which sand is bulldozed into bars off the original coast (Hageman, 1969). When these bars fall dry at low water, wind forces have the opportunity to form dunes and whole islands. These islands are usually long and narrow.

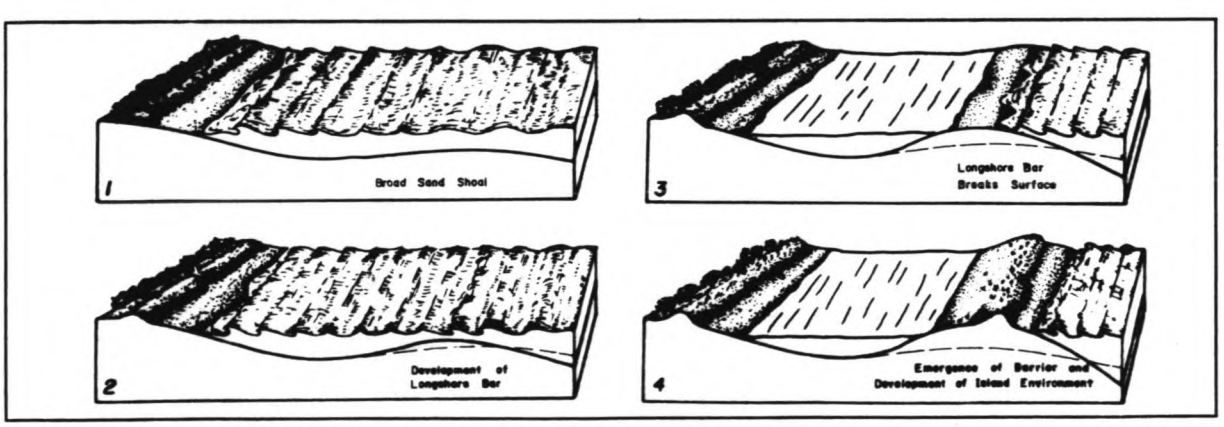

Fig. 2.5: Barrier island development by cross-shore transport (from Leatherman,1982)

Storm surges or river discharges can induce hydraulic gradients (Steijn, 1991) that cause break-throughs in the islands. Again, only under certain conditions will these inlets be stable.

The inlets in the Wadden Sea have formed in a slightly different way. Between 8000 and 7000 years ago the rising North Sea reached the area that is now known as the Wadden Sea and flooded the ancient river valleys. Through the bulldozer mechanism sand was deposited on the headlands separating the

valleys. As the sea level continued to rise, these sandy headlands formed the islands that we know today. The original location of the islands and the inlets is therefore primarily determined by geology. The islands and inlets probably migrated later (Steijn, 1991).

The spacing of these break-throughs is not entirely random. Apparently, there is a relationship between the **tidal range** (the difference between high and low water) and the island length. This is shown in Fig. 2.6 for the U.S. Mid-Atlantic coast (Fitzgerald, 1988). It also applies to the Georgia Bight (Hayes,1991) and the Wadden Coast (Wolff, 1986).

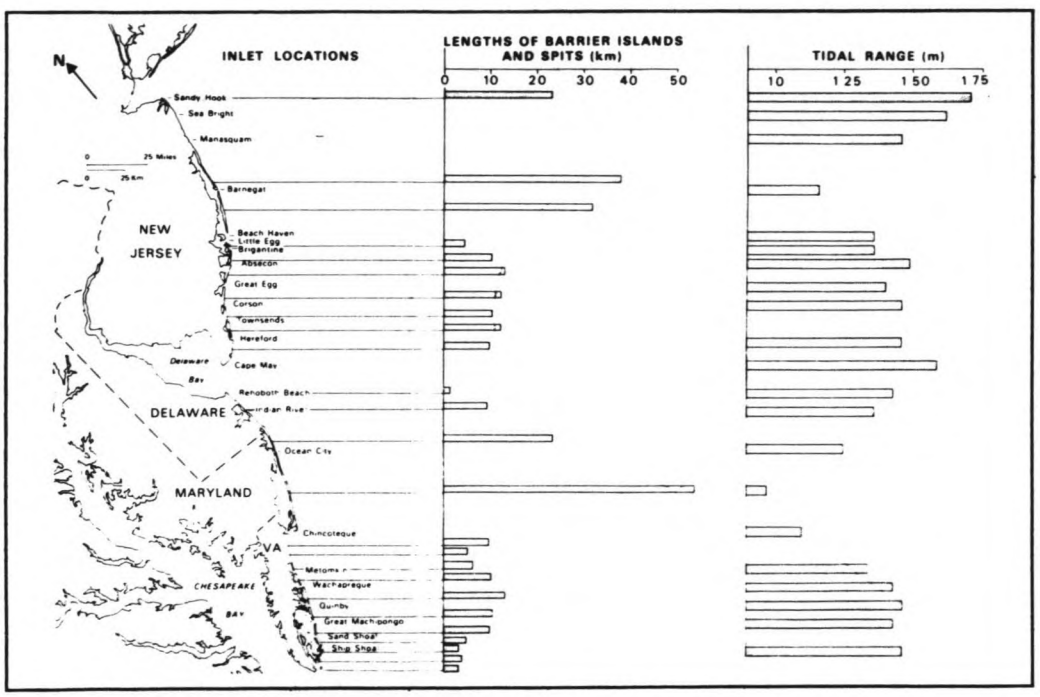

Fig. 2.6: Barrier island length vs. tidal range for the U.S. Mid-Atlantic coast (from Fitzgerald, 1988)

A larger tidal range increases the tidal prism. Since the inlet cross sectional area is a linear function of the prism, as O'Brien (1931, 1969) has shown, see section 2.4, this would imply a larger throat area. But apparently, it is more natural to create more inlets, thereby reducing the surface of the drainage areas served by the individual inlets, thus reducing the size of the prism.

After an inlet has developed, the asymmetry between the ebb flow, which acts like a free jet, and the flood flow, which acts like a convergent sheet flow (Oertel, 1988), establishes local areas of flood dominance and ebb dominance, see Fig. 2.7.

Interactions between the cross-shore tidal flow on the one hand and the longshore current - which is driven by the wave-induced radiation stress and the shore-parallel tidal forces (Van der Velden, 1989) - on the other, cause a local decelera-

tion (Niemeyer, 1990) and spreading (Sha, 1990) of velocities at the downdrift side of the inlet, which gives sediment the opportunity to settle and form the outer delta. Fig. 2.8 shows the directional spreading of the tidal currents in Texel inlet, the Netherlands.

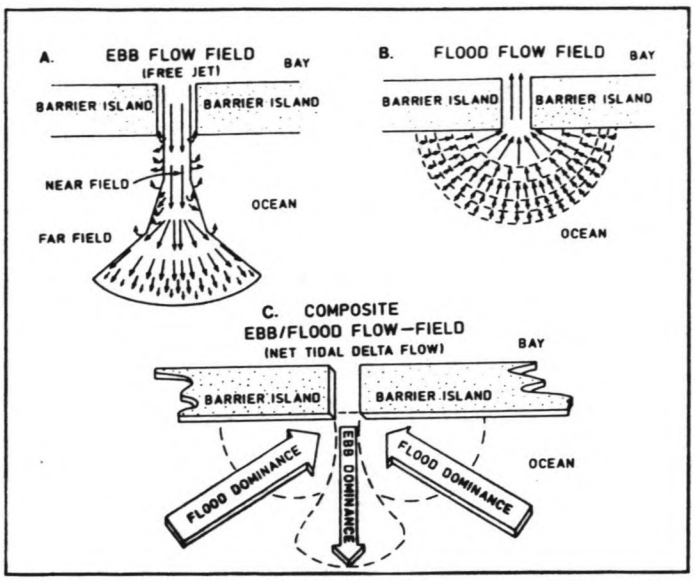

Fig. 2.7: Ebb and flood flow fields (from Oertel, 1988)

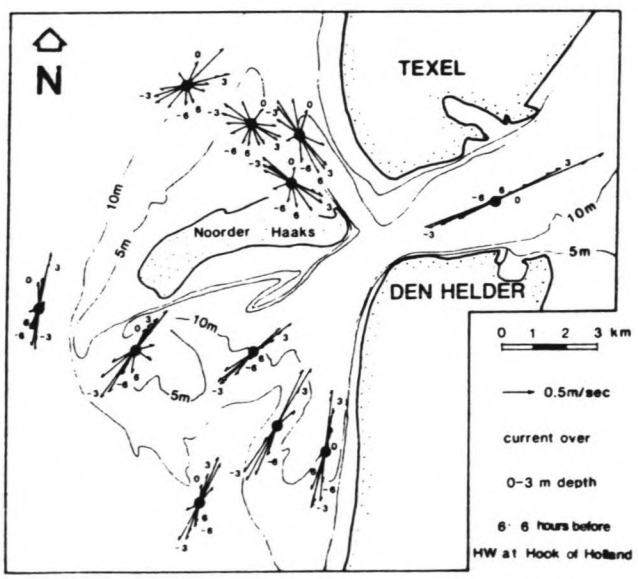

Fig. 2.8: Directional spreading of tidal currents in Texel inlet (from Sha, 1990)

The shape of the delta can thus be classified according to the ratio of the longshore and the cross-shore current as has been done by Oertel (1975). Two ends of the spectrum are the tide-dominated and wave-dominated inlets. In Fig. 2.9, type A is wave-dominated and type D is tide-dominated. Types B and C have asymmetric longshore currents, that could be caused by an asymmetrical distribution of wave energy around the inlet.

In natural inlets, the feedback between hydrodynamical and morphological processes will apparently result in a stable situation (Dean and Walton, 1975).

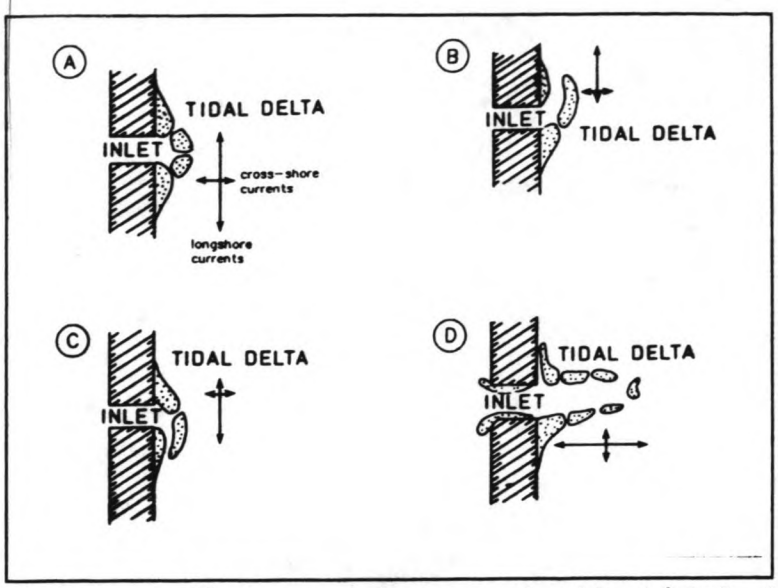

Fig. 2.9: Four different types of ebb tidal deltas (from Oertel, 1975)

One possible mechanism in the formation of the flood tidal delta (or better, the inner delta) is the distortion of the ocean tide inside the basin, which causes a difference in magnitude between flood velocities and ebb velocities. Because the sediment transport capacity is a function of the velocity, this asymmetry is responsible for so-called ebb or flood dominance. A flood dominant tidal basin experiences a net import of sediment and will shoal. This process is discussed further in chapter 3. Other possible mechanisms include transport by density currents and by settling and scouring lags of suspended sediment (Steijn, 1991).

2.3 Classification

Classification of tidal inlets is needed to be able to compare processes and to derive governing relationships. This can be done on the basis of geometric or hydrodynamic parameters.
One method classifies the inlets according to the shape of the tidal basin. This is not objective, as this shape could depend on a number of unknown parameters, such as the geological history.
A second type of classification is based on hydrodynamic parameters like tidal range and wave height. These two parameters do not depend on the inlet conFiguration itself, but rather on offshore conditions and large-scale coastal morphology (Niemeyer, 1990). This classification is therefore much more useful.
Hayes (1979) presented classifications for each parameter. He distinguished five classes of tidal range:

microtidal	< 1.0 m
low mesotidal	1.0 - 2.0 m
high mesotidal	2.0 - 3.5 m
low macrotidal	3.5 - 5.5 m
high macrotidal	> 5.5 m

He also defined three classes of wave energy, parameterized by the yearly-averaged mean wave height (H_s).

low wave energy	< 0.6 m
medium wave energy	0.6 - 1.5 m
high wave energy	> 1.5 m

These two sets of classifications were combined to determine five classes of coastal inlets, see Fig. 2.10. The figure also indicates the classification of the Friesche Zeegat, one of the West Frisian inlets.

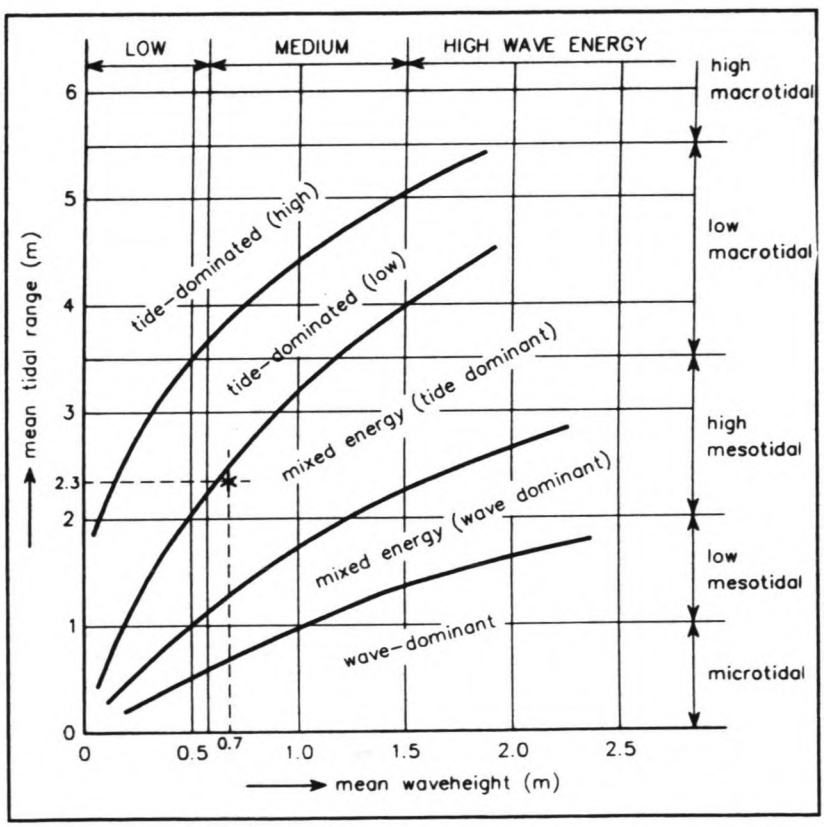

Fig. 2.10: Hydrodynamic classification based on offshore parameters (the x marks the Friesche Zeegat) (from Hayes, 1979)

Tidal inlets of different class have different appearances. Since most researched inlets fall in the medium wave energy classification (Hayes, 1979), the differences are usually attributed to the variation of tidal range. Microtidal inlets produce extensive flood tidal deltas and almost no ebb tidal deltas because of the small ebb flow. Macrotidal inlets are broad-mouthed and funnel-shaped because of the strong in and outflow. Mesotidal inlets (like those in the Wadden Sea) have

mixed features: pronounced ebb tidal deltas and - in volume - smaller flood tidal deltas.

This classification omits "onshore" parameters like the coastal physiography, the tidal prism (which is not only dependent on the tidal range, but also on the tidal basin surface area) and sediment availability (Steijn, 1991).

The class of dominance is of great importance to the shape of the outer delta, as described by Oertel (1975) and shown in Figure 2.9.

2.4 Empirical research on stability parameters

In the past, much research has been done to establish stability relationships between various properties of tidal inlets. It was found that the value of some properties can be expressed as a linear function of the tidal prism.

Inlet throat

O'Brien (1931,1969) found a linear relationship between the inlet cross-sectional area below MSL and the tidal prism:

$$A_c = c \cdot P \qquad (2.1)$$

where A_c = cross-sectional throat area below MSL (m^2)
c = empirical constant with value $6.56 \cdot 10^{-5}$ (m^{-1})
P = tidal prism (m^3), calculated as the product of the mean basin area and the spring tidal range

Jarrett (1976) expanded on this. He calculated the relationships for unjettied and single-jettied inlets at the three U.S. coasts.

$$A_c = 2.8 \cdot 10^{-4} \cdot P^{0.91} \qquad \textit{Pacific Coast}$$

$$A_c = 3.0 \cdot 10^{-5} \cdot P^{1.05} \qquad \textit{Atlantic Coast} \qquad (2.2)$$

$$A_c = 9.3 \cdot 10^{-4} \cdot P^{0.84} \qquad \textit{Gulf Coast}$$

The variation in the constants is caused by a difference in tidal regime (diurnal, semi-diurnal and mixed) and wave climate. Generally, a coast under higher wave attack has a larger throat area.
Similar relationships between the prism and the cross-sectional area have been found in many other parts of the world, including the Netherlands.
As Gerritsen and de Jong (1985) and Gerritsen (1990) have shown, these relationships can be applied to tidal channels as well. The authors found, however, that channel cross sections gave smaller values for the constant in the O'Brien relationship than the throat cross section did. They attributed this to the sheltering from wave energy. To correct for this, the stability shear stress τ_s, as introduced by Bruun and Gerritsen (1960), was used. With the proposed formula

$$A' = \frac{Q_{max}}{C\sqrt{\tau_s/\rho \cdot g}} \qquad (2.3)$$

where A'= the cross sectional area (m^2) at Q_{max}
ρ = the fluid density (kg/m^3)
C = the Chezy coefficient ($m^{\frac{1}{2}}/s$)

the channel cross sectional area can be calculated. Note that the prism is replaced by the maximum discharge, since maximum scouring of the bed takes place at the time of maximum discharge and sediment transport. The parameters depth and grain size are implicit in this formula, since they have an effect on both τ_s and C (Gerritsen, 1990).

Ebb tidal delta

Research has shown that the volume of the ebb tidal delta appears to be a function of the prism, too.
Walton and Adams (1976) measured the outer shoal volumes of 44 U.S. inlets using Walton and Adams' (1976) "no-inlet" bathymetry calculation procedure which calculates the volume of the outer bar as the difference between the volumes in the case of an inlet and in the case of no inlet. The procedure is explained in Fig. 2.11.

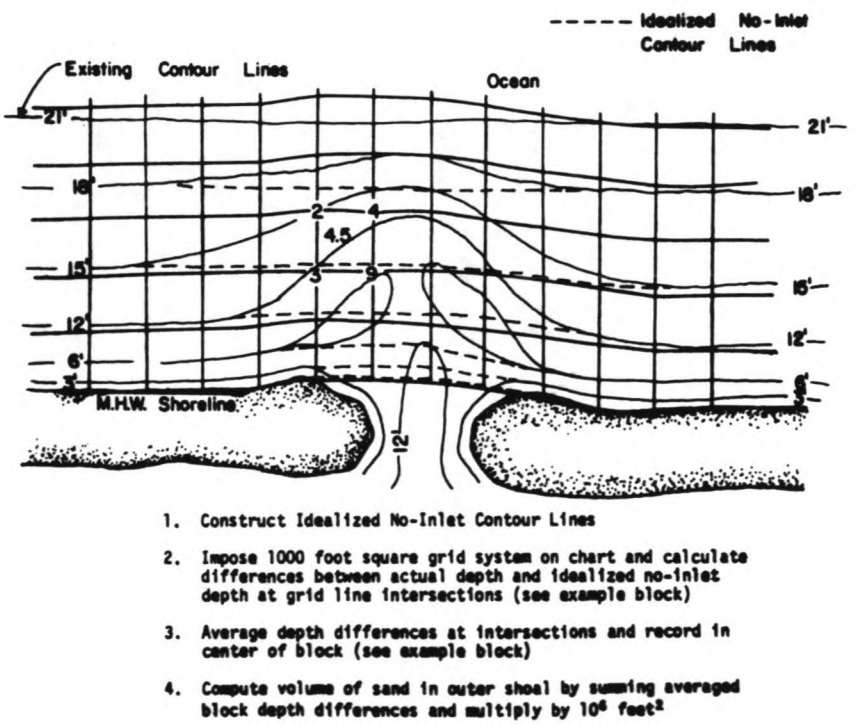

1. Construct Idealized No-Inlet Contour Lines
2. Impose 1000 foot square grid system on chart and calculate differences between actual depth and idealized no-inlet depth at grid line intersections (see example block)
3. Average depth differences at intersections and record in center of block (see example block)
4. Compute volume of sand in outer shoal by summing averaged block depth differences and multiply by 10^6 $feet^2$

Fig. 2.11: No-inlet bathymetry calculation procedure (from Dean and Walton, 1975)

Tidal prisms were calculated from current measurements in the throat and via the cubature method (Jarrett, 1976).

The inlets were classified according to the level of wave energy, parameterized by $H^2 \cdot T^2$, where H is the yearly-averaged significant wave height and T the wave period. This parameter is derived from the Airy Wave Theory (Marino and Metha, 1987). Converted to SI-units and rounded off to the nearest integer, the classes were defined in the following way:

exposure	$H^2 \cdot T^2$
mild	0-3
moderate	3-28
high	>28

For comparison: the measured significant wave height in the Friesche Zeegat, the Netherlands, is approximately 1.0 m. With $T_w = 5 \cdot \sqrt{H_s} = 5$ s, the parameter yields 25 m^2s^2 and falls just inside the moderately exposed range.

Even though many more parameters such as the longshore energy flux and the grain size distribution should influence this relationship, reasonable scattering was found. Fig. 2.12 shows the graph for moderately exposed coasts.

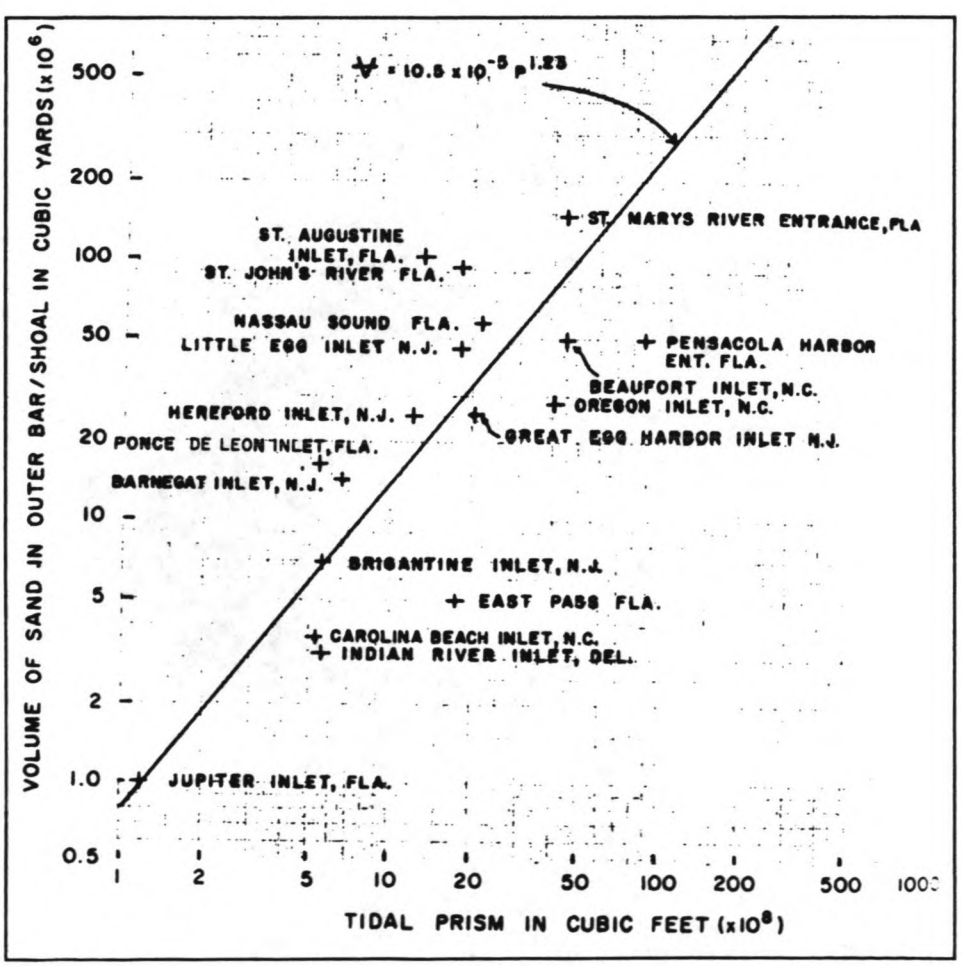

Fig. 2.12: Tidal prism vs. ebb shoal volume for moderately exposed coasts (from Walton and Adams, 1976)

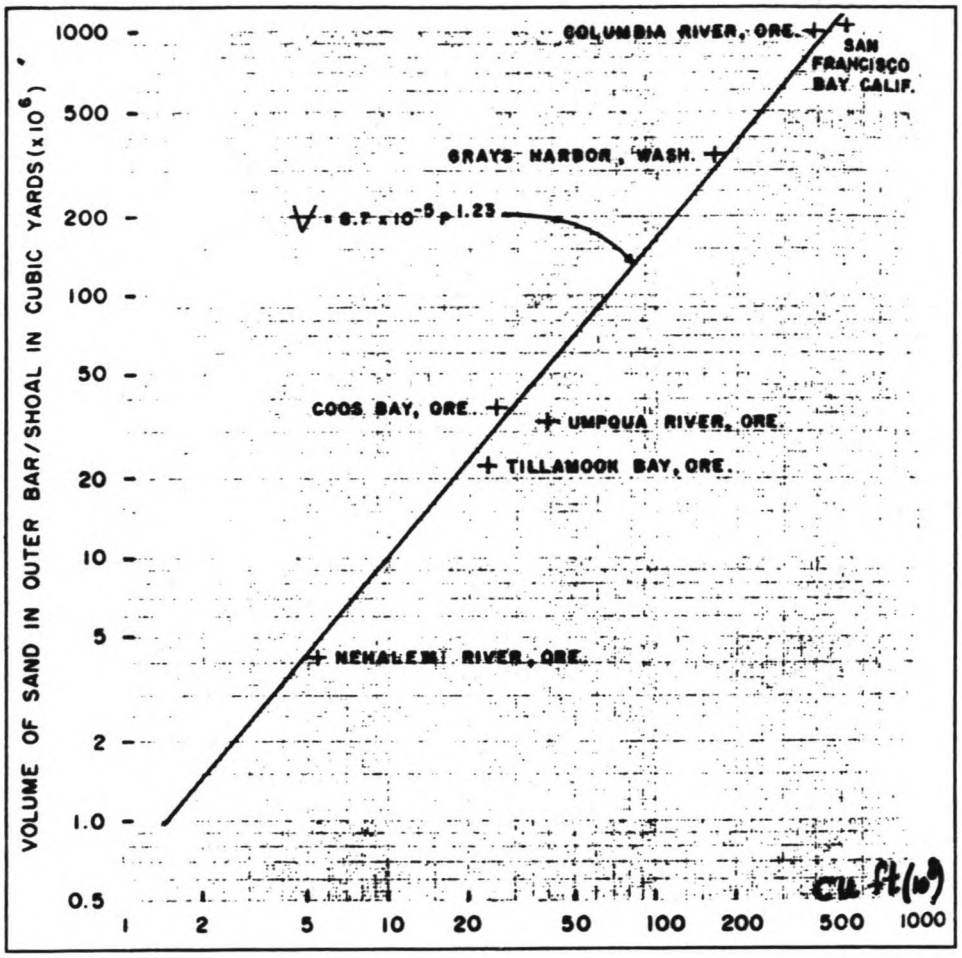

Fig. 2.13: Tidal prism vs. ebb shoal volume for highly exposed coasts (from Walton and Adams, 1976)

Through linear regression, Walton and Adams found the following equations (in SI-units):

$$V = 64.4 \cdot 10^{-4} \cdot P^{1.23} \quad \textit{moderately exposed}$$
$$V = 53.3 \cdot 10^{-4} \cdot P^{1.23} \quad \textit{highly exposed} \qquad (2.4)$$

where V = sand volume of outer delta (m^3)
P = tidal prism (m^3)

The constants in both formulas do not differ much. However, less scatter was found for the highly exposed coasts, because the authors assumed that the delta is a sediment sink with the coasts as the sole source of sediment. In other words, they only considered littoral sediment transport. This assumption holds better in the case of wave-dominated inlets where the wave-induced longshore transport is larger. Walton and Adams found that increasing wave action, parametrized by H^2T^2, decreases the volume of the ebb shoal, because waves drive the sand back to shore. Dean & Walton (1975) phrased this concept in a slightly different way: an equilibrium shoal volume is established when wave forces balance the tidal forces.

Marino and Mehta (1987) followed up on this research. They compared Walton and Adams' results with a number of Florida east coast inlets that all fall in the moderately exposed category. The authors found a slightly different relationship with about the same correlation coefficient (0.75). This led them to believe that other parameters have an influence on the outer shoal volume as well. They determined the significant variables and defined a functional relationship as follows:

$$f\left(\frac{V}{W^3}, \frac{P}{W^3}, \frac{W}{D}, \frac{A_c}{a_o^2}, \frac{E_w}{E_t}\right) = 0 \qquad (2.5)$$

where V = the ebb shoal volume (m^3)
W = the width of the inlet throat (m)
P = the tidal prism (m^3)
D = the depth of the throat (m)
A_c = the cross-sectional area of the throat (m^2)
a_o = the amplitude of the ocean spring tide (m)
E_w = the wave energy (Joule)
E_t = the tidal energy (Joule)

The last term is eliminated in their research, because in the moderately exposed range no identifiable relationship between the ebb shoal volume and this ratio could be established (Marino and Mehta, 1987, reference to Marino, 1986).

With this elimination the authors modified the function to

$$\frac{V}{W^3} = f\left(\frac{P}{W^3}, \frac{W}{D}, \frac{A_c}{a_o^2}\right) \qquad (2.6)$$

Since both V and P are a function of W^3, they were combined to form V/P. This ratio is plotted against W/D (see Fig. 2.14). The authors determined the function

$$\frac{V}{P} = -0.0033 \cdot \frac{W}{D} + 1 \qquad (2.7)$$

The function gives an estimation of the minimum boundary value of the ebb tidal delta volume when the ratio $A_c/a_o^2 > 1000$. Conversely, an estimation of the maximum value is given in the case that $A_c/a_o^2 < 1000$.

Marino and Metha (1987,1988) relate the variability in volume of the outer deltas with a constant prism to the W/D ratio. They argue that shallow inlets (with a large W/D ratio) could be related to shallow offshore depths. These inlets experience a higher wave-induced shear stress than deeper inlets with the same cross sectional area. This means that in these shallow inlets the critical shear stress, defined as "the effective average shear stress during maximum flow at spring tide conditions that determine the stability of a tidal channel" (Gerritsen, 1990), is reached sooner. Under these conditions, sediment is removed from the bar and is deposited on the

shore.

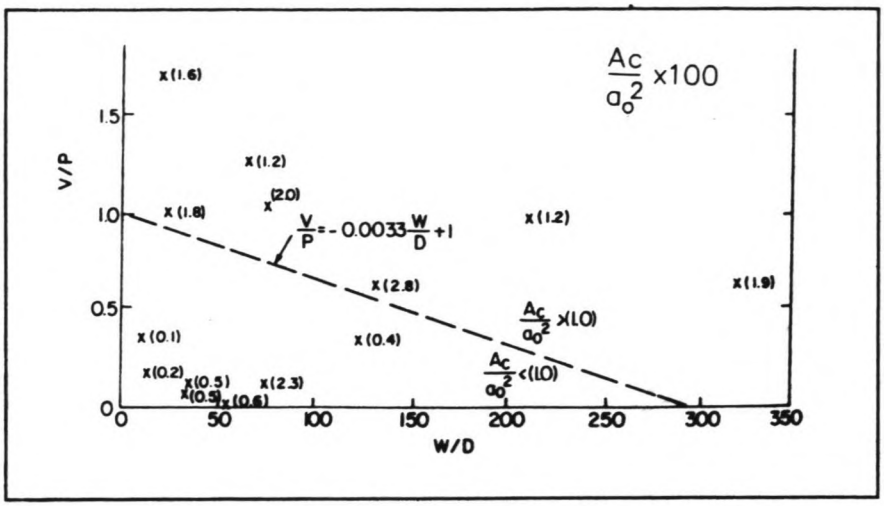

Fig. 2.14: V/P vs. W/D (from Marino and Metha, 1987)

The volume of the ebb tidal delta is thus dependent on the tidal prism and the depth to width ratio.

Tidal channel volume and tidal flat area

Research on the relationship between the volume of the tidal channels below a certain datum and the tidal prism has been performed by Renger (1976) and Eysink (1990), as reported by Eysink (1991). Both found similar relationships.
Renger found for German Bight inlets:

$$V_{MLW} = 8.839 \cdot 10^{-6} \cdot P^{1.566} \qquad (2.8)$$

where V_{MLW} = volume of tidal channels below MLW (m^3)

Eysink found for the Wadden Sea:

$$V_{MSL} = 65 \cdot 10^{-6} \cdot P^{1.5} \qquad (2.9)$$

where V_{MSL} = volume of tidal channels below MSL (m^3)

The constant in both formulas differ by a factor 10. This is due to the fact that the channel volumes have been calculated below different datums.
As Eysink (1991) describes, both relationships follow from the O'Brien's Ac-P relationship where the contents of the channel is calculated as the integral of the cross-sectional area over the length of the channel.

Renger and Partenscky (1974) and Eysink (1990) come to similar relationships describing the ratio of the tidal flat area and the gross basin area:

$$\frac{A_f}{A_b} = 1 - 0.025 \sqrt{A_b} \qquad (2.10)$$

where A_b = total basin area (10^6 m^3)
A_f = tidal flats area (10^6 m^3)

Although the coefficient is not dimensionless, this relationship might prove helpful in calculating a critical tidal flat area in chapter 4.

In the next chapters, these empirical relationships will form the basis of a model which will describe the morphological changes in a tidal basin in response to changes in the system parameters.

Chapter 3 Tidal basin shoaling

In this chapter, an attempt is made to simulate and analyze the shoaling process in a tidal basin based on the assumption that the evolution of such a tidal basin is dependent on the long-term direction and magnitude of the residual sediment flux. Short-term changes such as high deposits in the channels during storms are not considered.
First, a highly schematized basin topography is defined. Then the boundary conditions are determined, the governing equations are derived and a computer simulation is made. The results are checked against data from existing inlets and will be implemented into the model presented in chapter 4.

3.1 Basin lay-out

In the following schematization, the tidal basin is considered to be a rectangular channel with length L and initial bottom level at a constant depth, h(x,0) = H below MSL, see figure 3.1. Although in reality a tidal basin consists of a network of bifurcating channels with a decreasing depth in the landward direction, this schematization will suffice to investigate basic governing processes. In chapter 4, an actual tidal basin will be represented by a system of these one-dimensional channels.
Only tidal action is considered. The outer shoals of a tidal inlet absorb most of the ocean wave energy (Niemeyer, 1986) and the fetch inside a basin is usually too short to generate significant wind waves (Oertel, 1975). There is no fresh water inflow, the water column is well mixed and the flow unstratified.

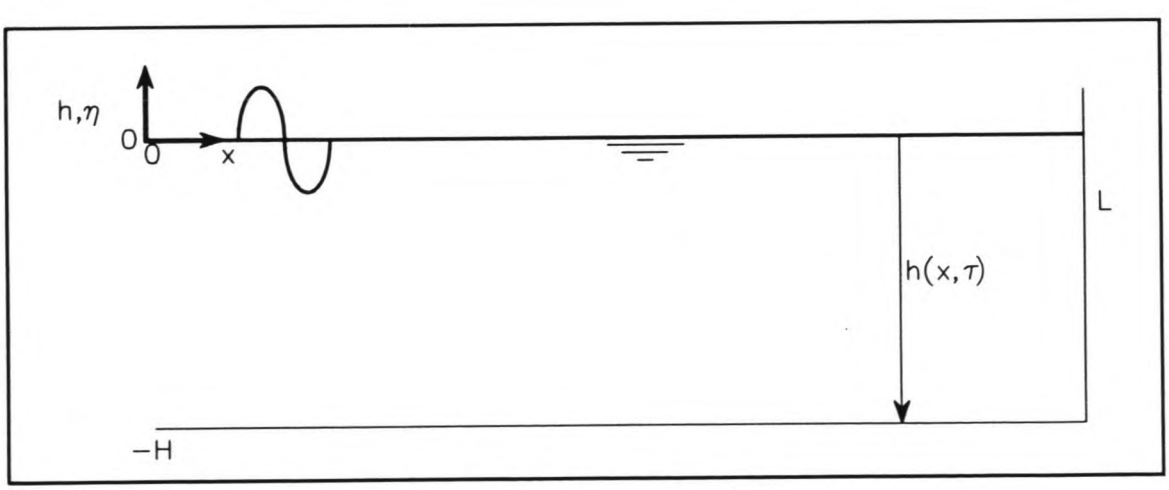

Fig. 3.1: Channel schematization

3.2 Boundary conditions

At the solid boundary the condition of no flux is valid, so Q(L,t) = 0 and therefore u(L,t) = 0.

At the entrance of the tidal basin the boundary condition is

given by a schematized vertical tide.
At deep sea, the astronomical ocean tide contains a number of periodic constituents - each with its own amplitude, period and phase shift - whose interactions cause a complex problem in itself (Aubrey and Speer, 1985). As the tide propagates into shallower waters such as the coastal shelf and the ebb tidal delta, energy from these constituents is dissipated and transferred to higher harmonic components, called "overtides" (DiLorenzo, 1988) with higher frequencies. This transfer is caused by the non-linearity of the wave, which will be explained in detail later. A simple explanation is that the crest of the wave propagates at a higher celerity than the through. This distortion can be represented by a summation of the fundamental wave and waves with higher frequencies.
The phenomenon of non-linear effects being enhanced during spring tide and reduced during neap tide is not yet taken into account in this model.

Of all constituents, the semi-diurnal (twice-daily) M_2 is far greater in amplitude than other components along U.S. and Dutch coasts (Aubrey and Speer, 1985 and Dronkers, 1986 respectively). Also, Seelig and Sorensen (1978) found that for a constant amount of tidal energy a semi-diurnal tide produces the largest net sediment transports, which is of importance in the following simulation. It is therefore warranted to focus on this constituent and its overtides. The vertical tide can thus be represented as follows (Boon and Byrne, 1981):

$$\eta(0,t) = \eta_o + \sum_{n=1}^{\infty} [M_{2n} \cdot \cos(\omega n t - \theta_n)] \qquad (3.1)$$

where $\eta(x,t)$ = sea surface elevation at x and t
η_o = 0 (as defined in Fig. 3.1)
M_{2n} = amplitude of the M_n constituent
ω = $2\pi/T$
T = period of the tidal wave = 12.42h = 44712s
θ^n = phase of the M_n constituent

Of the overtides ($n \geq 2$), the M_4-constituent with a quarter-diurnal frequency is the most important one in describing tidal asymmetries. For example, field recordings at Nauset Inlet, MA, show that the next overtide, M_6 was six times smaller (Aubrey and Speer, 1985). This finding is supported by theoretical work (as reported by Speer and Aubrey: Kreiss, 1957; Dronkers, 1964; Pingree and Griffiths, 1979). Thus, with n=2, eq. (3.1) becomes:

$$\eta(0,t) = M_2 \cdot \cos(\omega t - \theta_1) + M_4 \cdot \cos(2\omega t - \theta_2) \qquad (3.2)$$

The asymmetry or the non-linearity of the tidal wave is characterized by the ratio of M_4/M_2. The relative phase of the M_4-constituent is given by $2\theta_1 - \theta_2$. A positive value indicates a lead of M_4 over M_2, a negative value indicates a lag.
For $M_4 \neq 0$ this equation produces an asymmetrical tide. Depending on the relative phase, the distortion varies between

symmetric (equal rise and fall duration, unequal maxima and minima, see figure 3.2) and anti-symmetric (unequal rise and fall duration, equal maxima and minima, see figure 3.3). Positive symmetric curves have larger maxima than minima, whereas positive anti-symmetric curves give longer rise durations (Boon and Byrne, 1981).

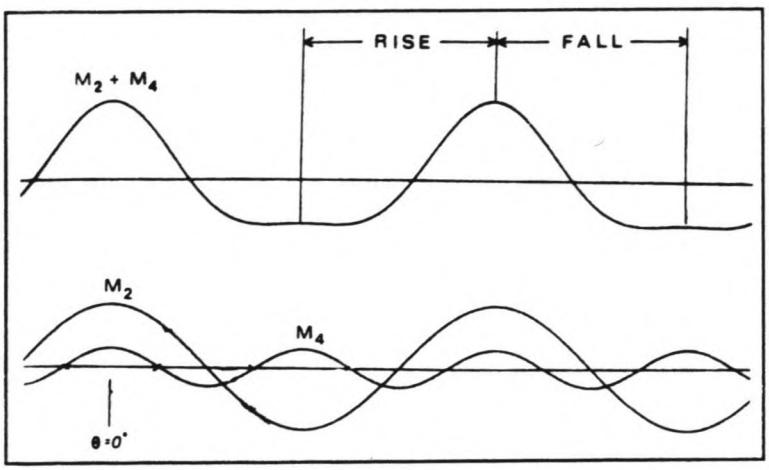

Fig. 3.2: A positive symmetric curve (lead = 0°) (from Boon and Byrne, 1981)

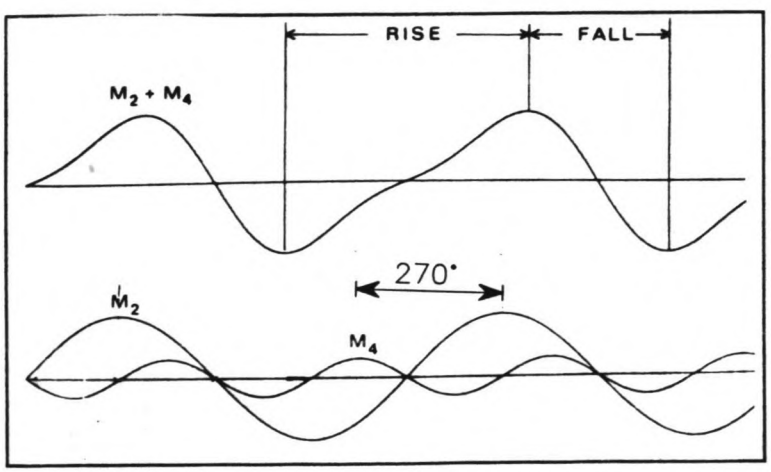

Fig. 3.3: A positive anti-symmetric curve (lag = 90° or lead = 270°) (from Boon and Byrne, 1981)

The impact of the relative phase on the type of distortion is illustrated in table 3.1, adapted from DiLorenzo (1988).

The type of asymmetry has a large impact on the morphological evolution of a shallow channel. A tidal wave with a larger ebb than flood duration produces - to meet the continuity requirement - shorter, but more intense flood currents than ebb currents. This is called flood dominance.

Because the bed-load transport of coarse sediment is roughly proportional to the velocity raised to some power n (for instance $n \approx 3$), flood dominance results in a net inward sediment transport over one tidal cycle, causing the channel to

shoal on a larger time-scale (Aubrey and Speer, 1985).

Suspended sediment transport is more difficult to quantify, since it is greatly dependent on low frequency tidal motions like spring and neap tides (Aubrey and Speer, 1985), and cohesive properties and time lags (Dronkers, 1986). According to Dronkers, a steeper rise than fall of water levels means that the duration of slack water before flood (the length of time the velocities are below the threshold value of sediment transport) is longer than the duration of slack water before ebb. This favors the import of fine sediment, just as it does coarse sediment.

Lead of basin M_4 relative to M_2 in degrees, where 360° = 6.21 h.	Distortion type
lead = 0°	positive symmetric (no dominance)
0° < lead < 90°	flood dominance
lead = 90°	negative antisymmetric (max. flood dominance)
90° < lead < 180°	flood dominance
lead = 180°	negative symmetric (no dominance)
180° < lead < 270°	ebb dominance
lead = 270°	positive antisymmetric (max. ebb dominance)
270° < lead < 360°	ebb dominance

table 3.1: Distortions in the horizontal tide for various M_2-M_4 phase leads in the vertical tide.

This simple picture becomes more complicated, however, when over one tidal cycle the variation of the wet basin surface is large. The standing wave which occurs in the case of no tidal flats is distorted into a partially progressive wave when tidal flats are present. This means that slack waters in the horizontal tide do not coincide with high or low water in the vertical tide and that maximum discharges no longer occur at midtide. Rather, the maximum flood discharge is shifted towards HW which reduces the value of the maximum velocity and makes ebb dominancy possible. The importance of this will be explained on page 34.

In the following channel model, a lead of 90° is used, making the forcing boundary condition negative anti-symmetric and the channel - without surface variation - flood dominant.

3.3 Governing equations

If the length of the basin, L, is small with respect to the length of the tidal wave, the channel can be considered as a storage basin and only the continuity equation per unit of width has to be taken into account:

$$\frac{\partial \eta}{\partial t} + \frac{\partial q}{\partial x} = 0 \qquad (3.3)$$

Substituting $q = (\eta - h) \cdot u$ (as defined in Fig. 3.1) in eq. (3.3) yields:

$$\frac{\partial \eta}{\partial t} + \frac{\partial (\eta - h) \cdot u}{\partial x} = 0 \qquad (3.4)$$

Rewriting and integrating over the basin length L:

$$(\eta - h) \cdot u = \int^{x} -\frac{d\eta}{dt}\, dx + constant \qquad (3.5)$$

Substituting the boundary condition u(L,t) = 0 and assuming that the sea surface elevation η is small compared to the depth of the channel h, the velocity can be approximated by

$$u(x,t) = \frac{L-x}{-h(x,\tau)} \cdot \frac{d\eta}{dt} \qquad (3.6)$$

where τ = the morphological time which is assumed to be constant during one tidal cycle.

The last assumption has to be made in order to be able to derive an analytical solution for the long-term sediment transport formula of eq. (3.11).

From this follows:

$$q(x,t) = (L-x) \cdot \frac{d\eta}{dt} \qquad (3.7)$$

Scaling the variables into a dimensionless form using:

$\eta = M2 \cdot \eta^*$
$x = L \cdot x^*$
$h = H \cdot h^*$
$t = t^* / \omega$
$\tau = \tau^* \cdot \tau_o$ with τ_o a scaling parameter ($\tau_o >> T$)

yields:

$$\eta^*(t^*) = \cos(t^* - \theta_1) + \frac{M_4}{M_2} \cdot \cos(2t^* - \theta_2) \qquad (3.2a)$$

and

$$u(x,t) = \frac{L - x}{-h(x,\tau)} \cdot \frac{d\eta}{dt}$$

$$= \frac{L - x}{-h(x,\tau)} \cdot [\, -M_2 \cdot \omega \cdot \sin(\omega t - \theta_1) - 2 \cdot M_4 \cdot \omega \cdot \sin(2\omega t - \theta_2)]$$

$$= \frac{L}{H} \cdot \frac{1-x^*}{h^*(x,\tau)} \cdot M_2 \cdot \omega \cdot [-\sin(t^* - \theta_1) - 2 \cdot \frac{M_4}{M_2} \cdot \sin(2t^* - \theta_2)] \quad (3.6a)$$

$$= \frac{L \cdot M_2 \cdot \omega}{H} \cdot \frac{1 - x^*}{h^*(x,\tau)} \cdot \frac{d\eta^*}{dt^*}$$

$$= \frac{L \cdot M_2 \cdot \omega}{H} \cdot u^*(x^*, t^*)$$

Likewise:

$$q(x,t) = u(x,t) \cdot -h(x,\tau)$$
$$= L \cdot M_2 \cdot \omega \cdot q^*(x^*, t^*) \quad (3.7a)$$

Using a simple - but according to Mota Oliveira (1970) useful - bed-load sediment transport formula

$$S^*(x^*, t^*) = m^* \cdot (u^*)^n$$
$$with \quad m^* \cdot \frac{m^{3-n}}{s^{1-n}} = m \quad (3.8)$$

with n = 3, the sediment transport rate at any point x can be calculated. Incorporating eq. (3.6a) into this equation yields

$$S^*(x^*, t^*) = m^* \cdot \left(\frac{q^*}{h^*}\right)^3 = m^* \cdot \left(\frac{1 - x^*}{h^*(x^*, \tau^*)} \cdot \frac{d\eta^*}{dt^*}\right)^3 \quad (3.9)$$

This formula is still based on the small hydrodynamic time scale t. To step up to the morphological time scale τ, S is integrated over one tidal cycle. The resulting residual transport is called S_T.

$$S^*(x^*, \tau^*) = m^* \cdot \left(\frac{1-x^*}{h^*(x^*, \tau^*)}\right)^3 \cdot \int_0^1 \left(\frac{d\eta^*}{dt^*}\right)^3 dt^* \quad (3.10)$$

and

$$S^*(x^*, \tau^*) = m^* \cdot \left(\frac{1-x^*}{h^*(x^*, \tau^*)}\right)^3 \cdot S_T \quad (3.11)$$

3.4 Shoaling simulation

The integral in eq. (3.10) is calculated for input parameters $\theta_1 = 0^\circ$, $\theta^\circ = -90^\circ$ and an arbitrary $M_4/M_2 = 0.14$. As stated above, the first two parameters cause the tidal distortion to be negative anti-symmetric and the channel flood dominant. The high value for the ratio produces a very pronounced asymmetry. As will be shown in section 5, this value is not reached in simulation runs with a tidal model, but is useful in this simulation to speed up the shoaling process. This value is not unnatural, however, because ratios up to 0.28 have been measured at some small-scale tidal inlets, for example Bourne's Pond, MA (Moody, 1988).

With the residual transport capacity, the level of bottom cell between two cross-sections follows from

$$\frac{\partial h^*}{\partial \tau^*} = -\frac{\partial S^*}{\partial x^*} = S(x^* + \Delta x^*) - S(x^*) \qquad (3.12)$$

where $S^*(x)$ = the transport rate in cross-section x^*

Substitution of eq. (3.11) into this equation shows that the parameter m influences only the rate of shoaling, thus only the time scale of the shoaling process, but not the character. The time evolution of the channel depth is shown in figure 3.4, where the letters A-M indicate different stages of shoaling. This shows that shoaling starts at the open boundary and

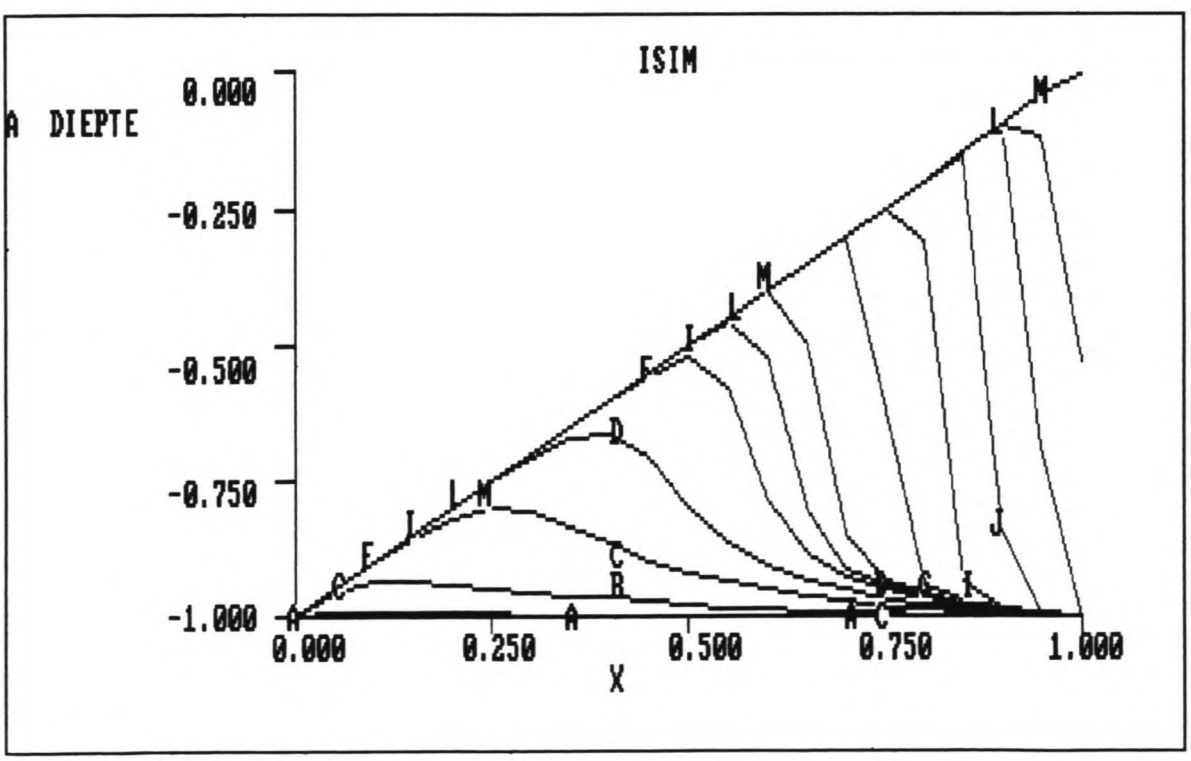

Fig. 3.4: Time evolution of the channel profile

that the sediment wave builds farther and farther into the channel, behaving like a non-linear wave (De Vriend, 1987), increasing in height (and consequently decreasing the water depth). This result is consistent with work done by Stauble et al (1988), who simulated the shoaling in Sebastian Inlet, Florida.

In this simulation, the bottom profile tends to an inclining plane, which can be considered a quasi-equilibrium state. According to O'Brien (1969), the equilibrium cross-sectional area of the throat of an inlet is given by:

$$A_c \sim P \tag{3.13}$$

where A_c = the cross-sectional area
P = the tidal prism

If O'Brien's relationship also applies to cross sections other than the throat as is suggested by Gerritsen and De Jong (1985), this inclining plane would be the equilibrium profile. Also, it can be derived from eq. (3.12) that on an equilibrium slope neither erosion nor accretion takes place, so that

$$\left(\frac{dS^*}{dx^*}\right)_{\tau_e^*} = 0 \Rightarrow S^*(x^*,\tau_e^*) = constant \quad \forall\, 0 < x^* < 1 \tag{3.14}$$

with τ_e^* = the time at which equilibrium is reached.

This can only be true if, in eq. (3.11),

$$\left(\frac{1-x^*}{h^*}\right)^3 = constant$$

and therefore

$$h_e^* = a\cdot(1-x^*)$$

This is a profile with a constant inclining slope, irrespective of the exponent n in eq. 3.8.

One problem remains: since the given right boundary condition yields $S(1,t) = S(1,\tau) = S(1,\tau_e) = 0$, the following conditions also have to be met.

1) $\left(\frac{dS}{dx}\right)_{\tau_e} = 0$

2) $S(0,\tau_e) = 0.$

Condition 1 is fulfilled if eq. (3.14) equals zero. Condition 2 cannot be met, because the asymmetrical tide which serves as the left boundary condition produces a non-zero transport rate. The profile indicate by the letter M in Fig. 3.4 is therefore not the final stage. Rather, thhe basin will conti-

nue to experience a net influx of sediment which will be passed on and reflected against the closed end (see Fig. 3.5), causing the channel to fill in completely, as is expected by Aubrey and Speer (1985).

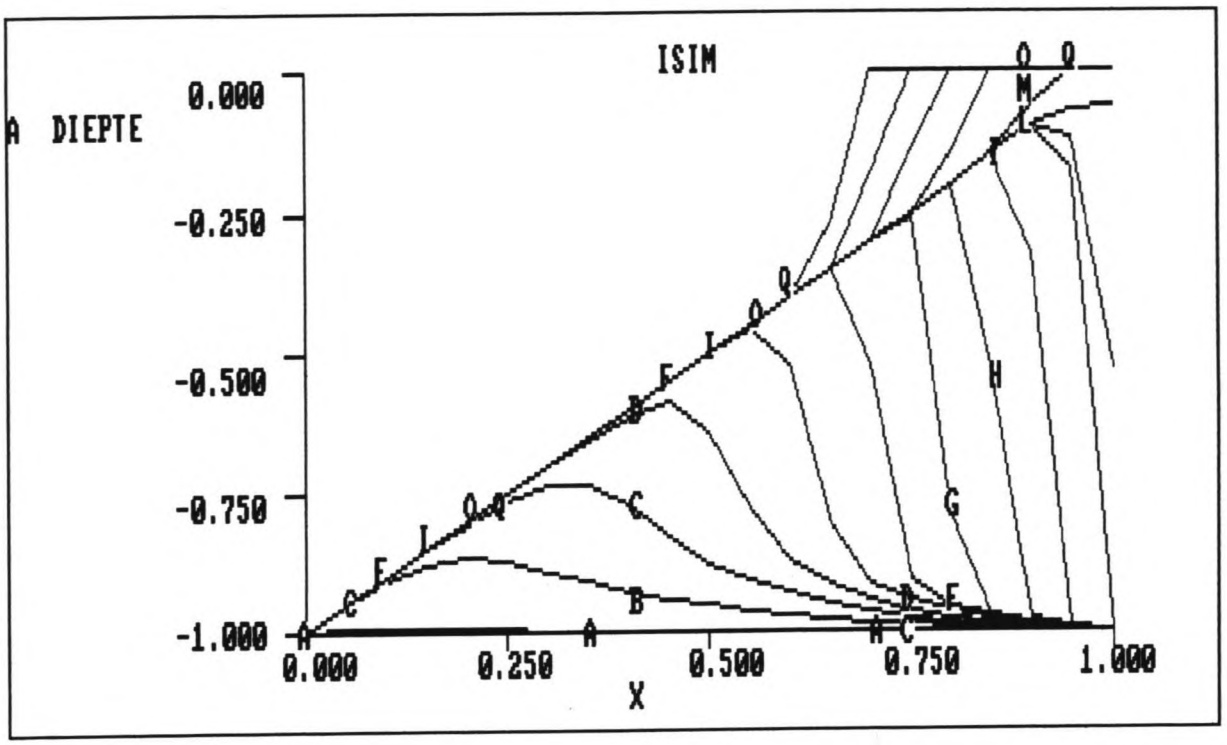

fig 3.5: Time evolution of the channel with reflection

The only way a stable basin would be able to exist is if the shoaling channel conditioned the vertical tide and the currents in such a way that the net transport would become zero (or more likely: fluctuate around zero, a dynamically stable situation).

In the next section, an investigation is made into this reaction of the tidal asymmetry and the residual transports on the changing geometry. As Aubrey and Speer state, the geometry does influence the harmonic growth and it is our hypothesis that this interaction is profound enough to reach a dynamically stable situation.

3.5 Influence of geometry on tidal asymmetries and residual transports

WENDY, the one-dimensional flow software package written by DELFT HYDRAULICS, was used to determine the relationship between the seaside boundary condition and the geometry in the channel. The program solves the continuity and momentum equations and provides output of water level, discharge and related variables at any place or time. WENDY was designed to solve practical problems and unfortunately does not accept non-dimensional variables.
The horizontal lay-out and input parameters were chosen follo-

wing work by Speer and Aubrey (1985), who modeled Nauset Inlet, MA and Wachapreague Inlet, VA. Relative to the previous shoaling model, the seaside boundary was moved farther out, so that a symmetrical tide, representing the astronomical ocean tide, can develop into an asymmetrical one naturally. The first 7000 m serve only as a 'running start stretch'. In an actual situation, the coastal shelf and the ebb tidal delta serve as such. Since the channel lengths are much smaller than the wave length ($l = \sqrt{(gh)} \cdot T = 343$ km), the longitudinal scale is not an important parameter (Speer and Aubrey, 1985).

Lay-out

The following channels were investigated:

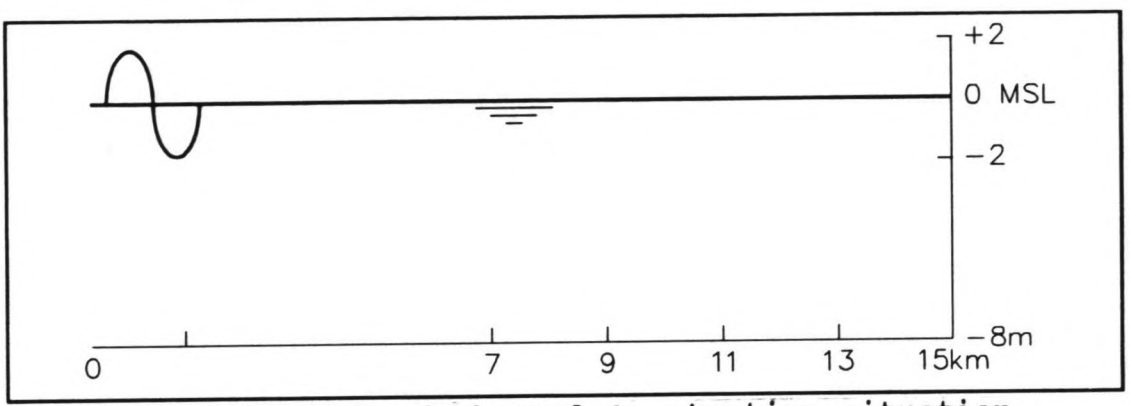

Fig. 3.6: Lay-out of channel 1: starting situation.

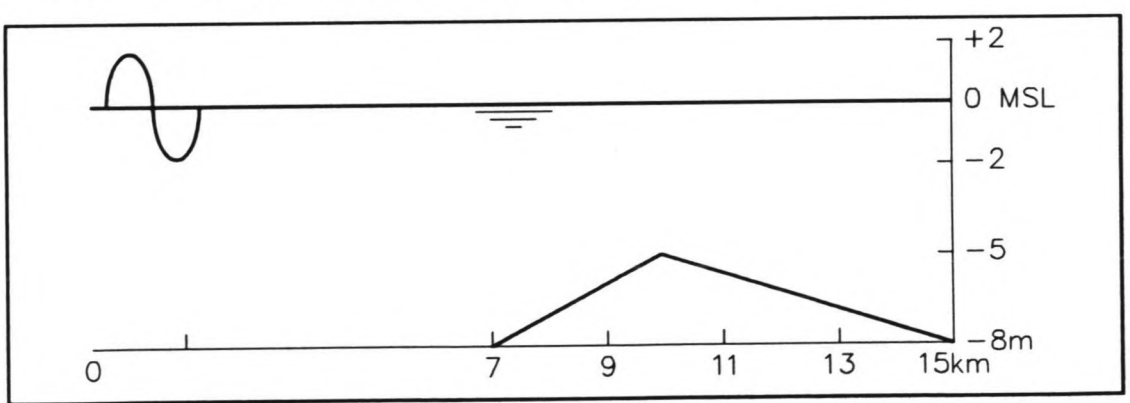

Fig. 3.7: Lay-out of channel 2: stage in the shoaling process indicated by letter D.

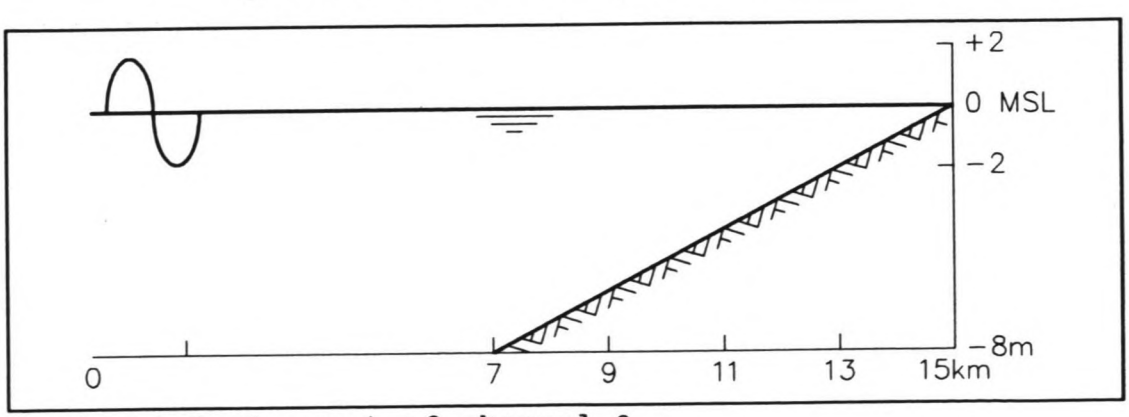

Fig. 3.8: Lay-out of channel 3

Channels 4, 5 and 6 represent the situation after the sediment is reflected and tidal flats have developed in the back of the basin. This lay-out is unlike that of Speer and Aubrey (1985) who defined the flats as storage regions along the channel axis which are not included in the momentum equation. In the model presented here, both equations are solved in the channel as well as on the flats. Because of the small length scale compared to the tidal wave length, the actual location of the flats, either along or at the terminal of the channel, is not important.

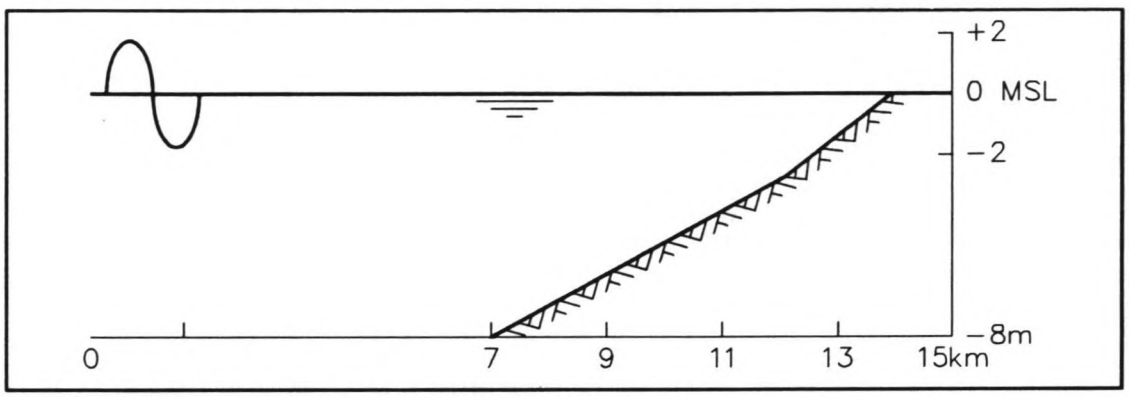

Fig. 3.9: Lay-out of channel 4

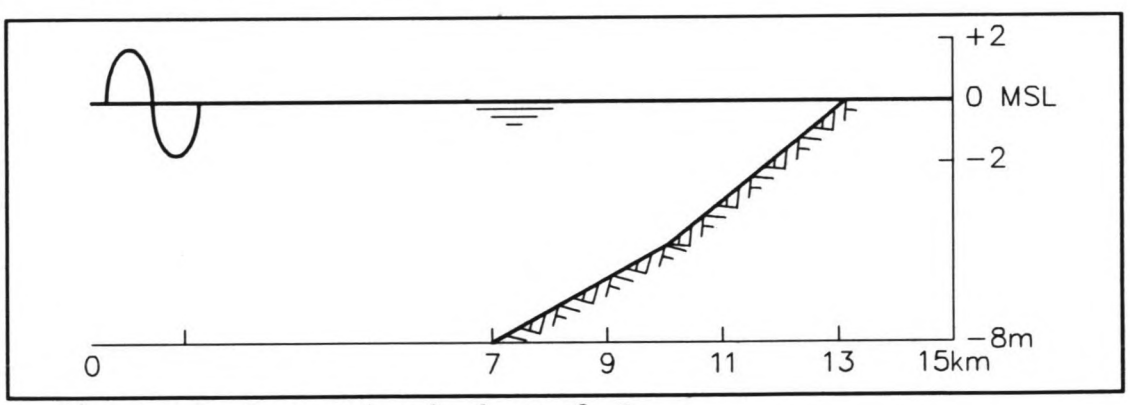

fig 3.10: Lay-out of channel 5

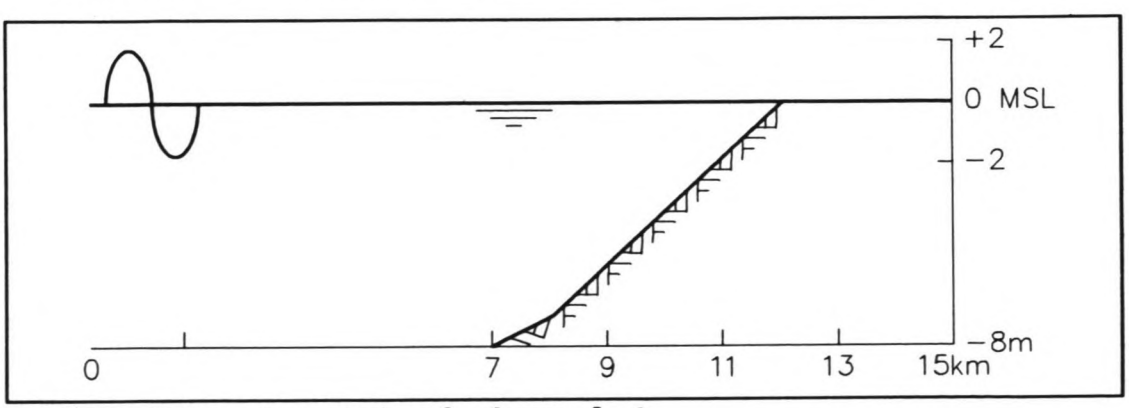

Fig. 3.11: Lay-out of channel 6

In WENDY, the flats were inclined slightly to ensure a better run-off from the flats during ebb. However, it could not be prevented that a small amount of water remained on the flats

at all times. This unnatural situation is taken into account in later calculations and does not affect the results.

Boundary conditions

On the left, the boundary condition is given by a symmetrical tide with T = 12.48h and an amplitude of 2 m. This means a large amplitude to depth ratio of 0.25, which makes the assumption in section 3 of neglible variation of the cross sectional area during a tidal cycle invalid.
On the right, the boundary condition of no flux is still valid.

Starting values

$$u(x,0) = 0$$
$$\eta(x,0) = 0$$

Friction coefficient

A friction factor of f=0.02, corresponding to a Chezy-coefficient of C=22 $m^{\frac{1}{2}}/s$, is used. This low value implies a very rough bottom, but this is valid in shallow estuaries with a strong tidal flow, large bed forms and high sediment transport rates (Speer and Aubrey, 1985). High friction rapidly distorts the tidal wave, so the length of the running start stretch can be kept short.

Results

For all channels the model reached stationary values for η and u after one tidal cycle. $\eta(x,t)$ tables were output for x = 1, 3, 5, 6, 7, 8, 9, 10, 11, 13 and 15 kms. For each of these points the unknowns of eq (3.2), namely η_o, M_2, M_4, θ_1 and θ_2, were solved using a least-squares program written by Zhu Weimin (1990). The results are listed in appendix 3A.

The space evolution of the ratio and relative phase of channels 1, 2 and 3 is shown in figs. 3.12 and 13, respectively. The results correspond to those of Speer and Aubrey (1985).

In general, the harmonic growth of the ratio and of the phase lead are attributable to two mechanisms: energy dissipation of the M_2-constituent by friction and transfer from the fundamental tide M_2 to the overtide M_4 by non-linear advection, non-linear continuity and friction (Speer and Aubrey, 1985).
However, in rectangular channels with relatively short lengths, friction is not effective in reducing the tidal amplitude (Dronkers, 1964). In other words, harmonic growth is in this case entirely due to energy transfer, not dissipation.

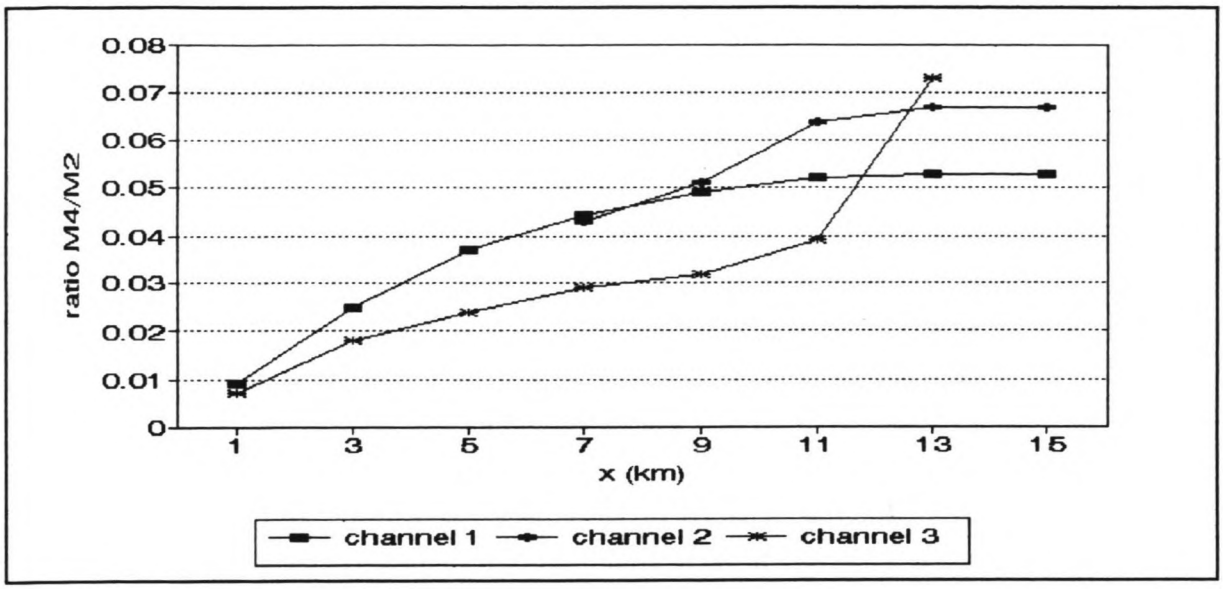

Fig. 3.12: Evolution of the M_4/M_2 ratio in chs 1, 2 & 3

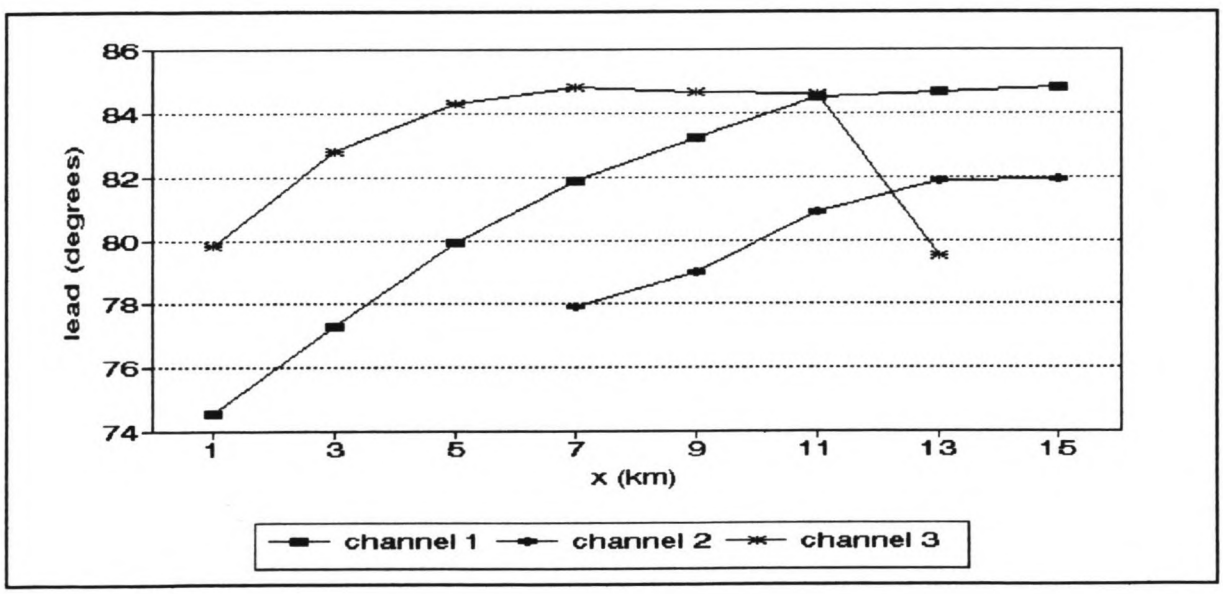

Fig. 3.13: Growth of the relative phase as defined in eq. (3.2) in channels 1, 2 and 3.

The non-linear advection term, $u \cdot \frac{\partial u}{\partial x}$, and the non-linear term in the continuity equation, $\frac{\partial \eta u}{\partial x}$, cause the crest to propagate at a higher celerity than the trough which yields a shorter flood period (Dronkers, 1986). Speer and Aubrey (1985) found that the friction term which has a higher value at LW than at HW has the greatest influence on the harmonic growth. The resulting distorted vertical tide can be represented by a summation of tidal constituents as in eq. (3.2). The stronger

the distortion, the larger the M_4-term, the greater the energy transfer.

Friction and advection, both functions of u, are strongest near the forcing boundary and decline rapidly down channel. The non-linear continuity term declines only slightly, since it is dependent on $\frac{\partial u}{\partial x}$, which is almost constant (Speer and Aubrey, 1985). Thus, the growth of the ratio and the relative phase is large near the forcing boundary and becomes smaller down channel. Both the M_4/M_2-ratio and the phase lead approach equilibrium values.

The different geometries appear to have some impact on the ratio. In channel 3, an intertidal area has formed. This results in a smaller tidal volume and velocities, which decreases the magnitude of the non-linear terms, especially the friction term which is the square of the velocity. The relative phase is almost the same in all three channels and close to 90°: the vertical tide is negative anti-symmetric. Note that the ratio and the lead for x = 13 km. in channel 3 do not fit in the curve properly. This is due to the fact that this point falls dry at LW, which deforms the tidal wave.

The (u,t)-curves produced by WENDY were used as input into a Pascal program that cubed the velocities and calculated the residual transport over one tidal cycle. Since the factor m as defined in eq. (3.8) has not been included, it is better to speak of residual velocity fluxes than of actual sediment transports.

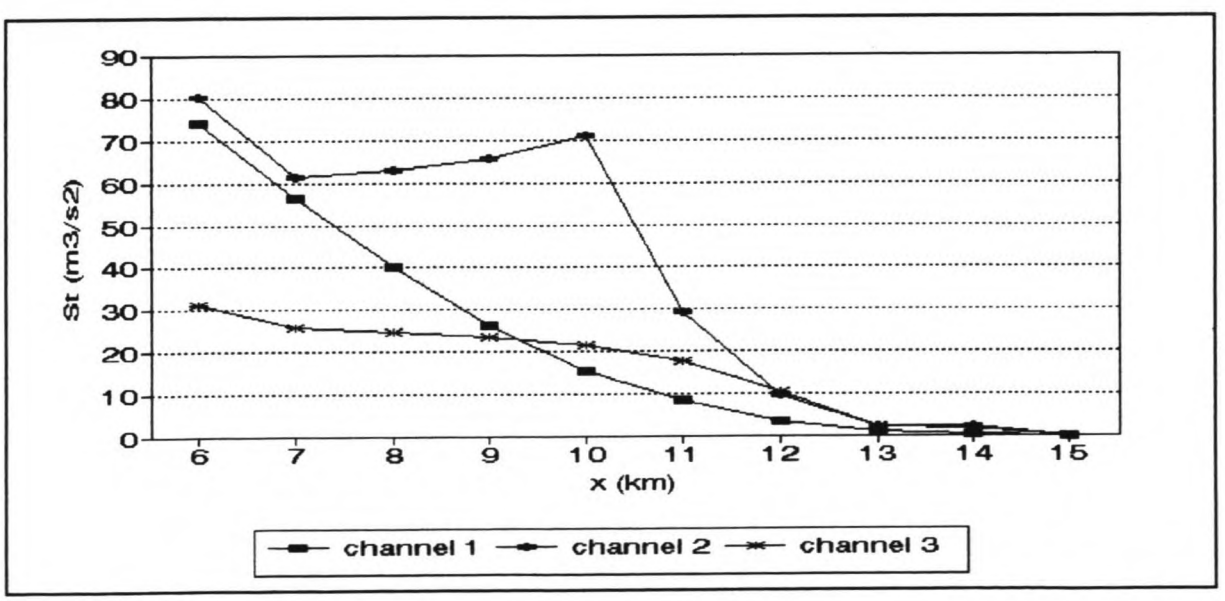

Fig. 3.14: Net velocity flux in channels 1, 2 and 3

Results are listed in appendix 3B and depicted in Fig. 3.14 which shows that all residual fluxes are inward: the channel is flood dominant. In channel 3 the residual transports are

smaller than in channel 1, which leads to the conclusion that the shoaling channel limits the influx of sediment. Channel 2 shows that the transport on top of the sediment wave is extreme: the tide flattens the upward slope.

The space evolution of the ratio and the relative phase of channels 4, 5 and 6 is shown in figs. 3.15 and 3.16 and listed in appendix 3C.

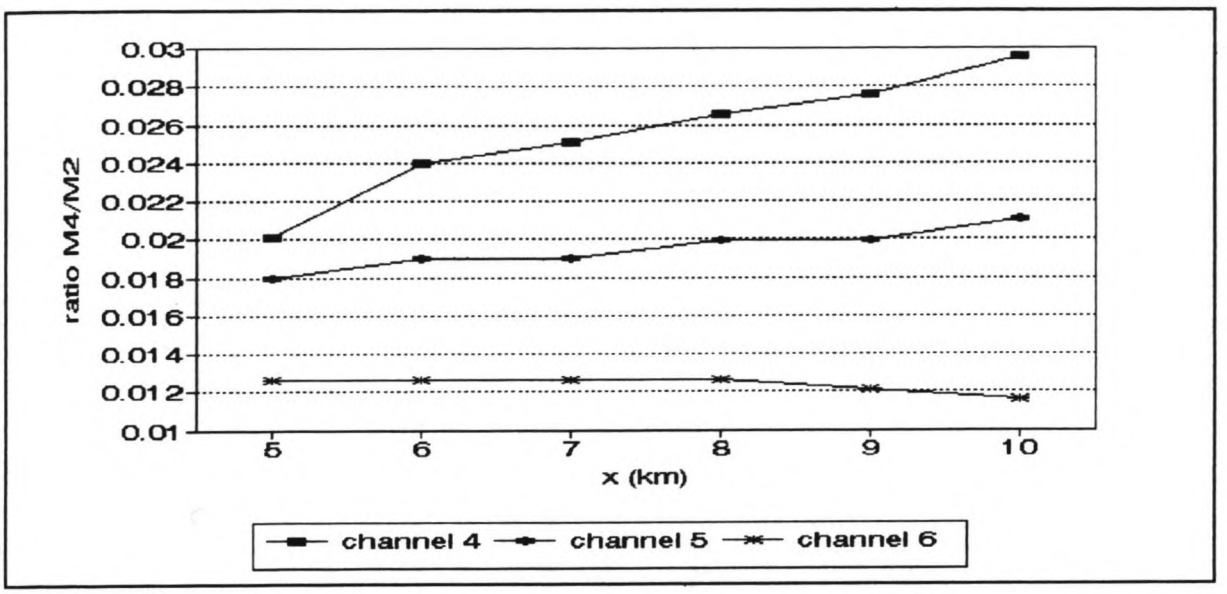

Fig. 3.15: Evolution of the ratio in channels 4, 5 and 6

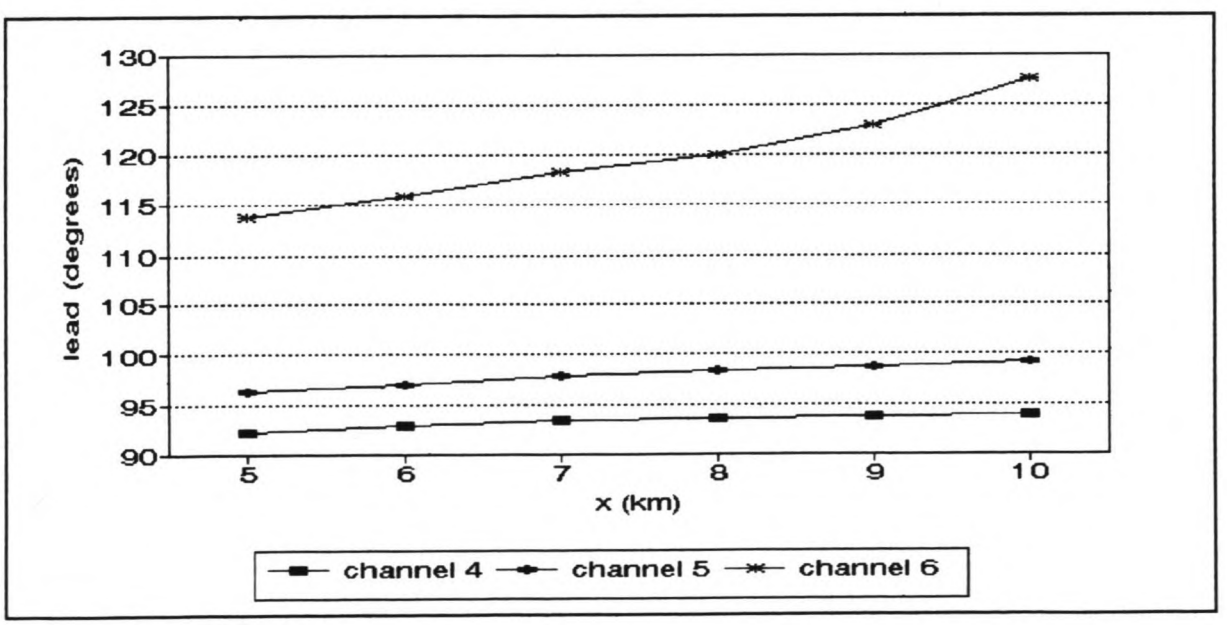

Fig. 3.16: Growth of the relative phase in chs. 4, 5, 6.

Fig 3.15 shows that the magnitudes of the ratios of M_4/M_2 are much smaller than in fig 3.12. This is caused by the reduction of tidal volume and velocities, which decreases the non-linear terms, especially friction.

Fig 3.16 shows that the relative phases increase considerably when the area of tidal flats is increased. The relative phase approaches 180°, which means that the difference between the maximum flood and ebb velocities becomes smaller. The mechanism which produces this is explained below. These graphs are consistent with findings by Speer and Aubrey. Note that all values are still less than 180° which, according to table 3.1 would indicate a flood dominant channel.

However, the residual velocity fluxes, calculated as explained above, show something else, see fig 3.17 and appendix 3D. As the relative area of tidal flats increases, the velocity flux becomes smaller and even negative. This indicates an ebb dominancy in terms of sediment transport.

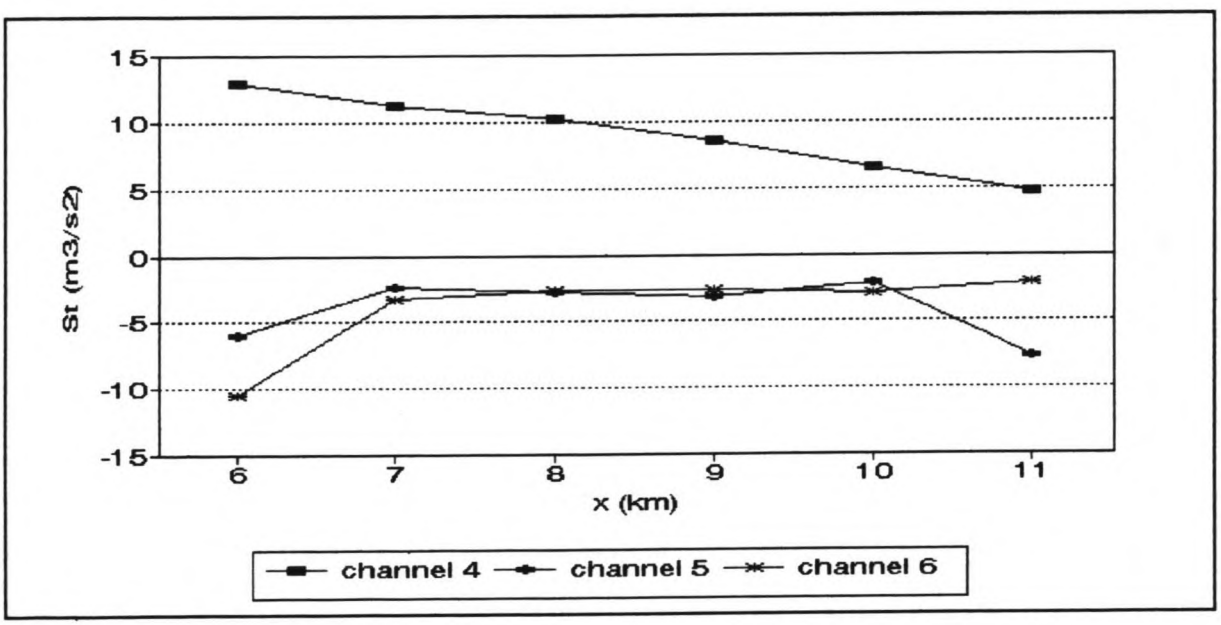

Fig. 3.17: Net velocity flux in channels 4, 5 and 6

The influence of tidal flats on the residual velocity flux can be explained as follows:
During flood, the water level in the channel rises and the flats are inundated. However, since the small depth on the flats limits the wave celerity through the dispersion relationship ($c = \sqrt{gh}$) and through friction, the water level on the flats does not rise uniformly, but experiences a landward slope. As the water level in the channel reaches high water, the flats are still being flooded which will continue even during ebb in the channel. In the channel, slack water before ebb does not occur at HW anymore, but is shifted towards LW, thus prolonging the duration of the flood period. Unlike the inundation, the drainage of the tidal flats is not a wave phenomenon, but is caused by gravity. The drainage is much more efficient than the inundation. At LW in the channels, the flow from the flats is negligible and here LW nearly coincides with slackwater.
Fig. 3.18 shows the lay-out of channel 7 with a large area of tidal flats, chosen to be able to demonstrate their influence.

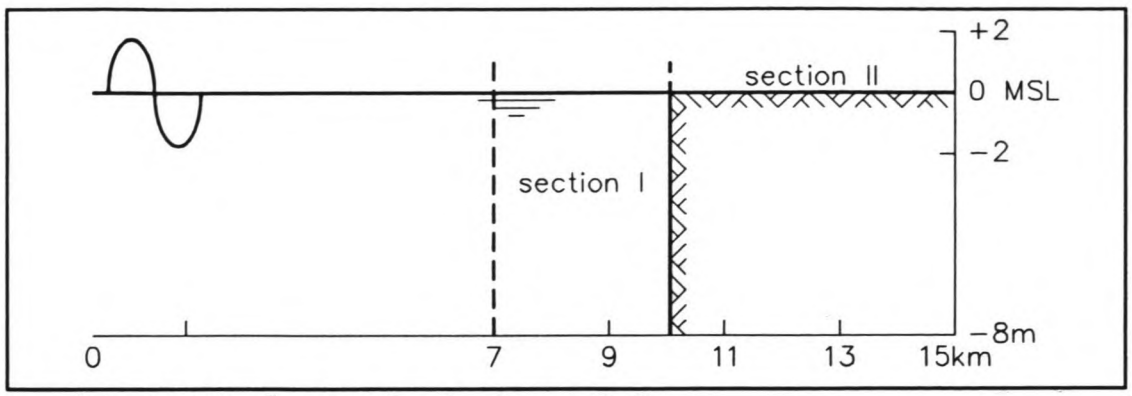

Fig. 3.18: Lay-out of channel 7

The time-discharge curves of this channel for section I only, section II only and their summation are given in Fig. 3.19. Considering section I only (from the cross-section at x=7 km to x=10 km), the discharge through the cross-section at x=7 km is the derivative of the water level fluctuation at that point.
Considering section II only, the discharge through the cross-section at x=10 km shows that inundation (positive values) is limited to a short time span and that drainage takes place over a much longer period of time.
By adding both discharge curves, the total discharge for sections I and II through the cross-section at x=7 km is obtained. The figure shows that the flats shift the slack water before ebb more than the slack water before flood.
Thus, the ebb period is shortened, in this example from 6.63 h (greater than ½T) to 6.11 h (less than ½T). This causes on average larger ebb velocities than flood velocities.

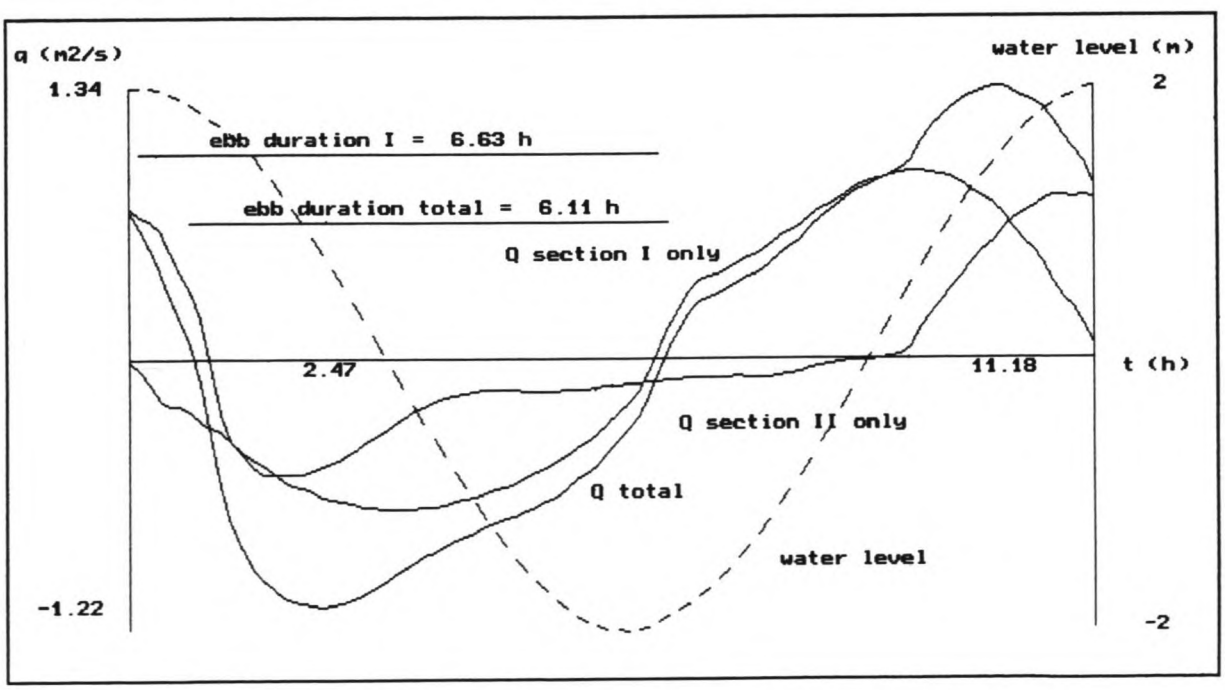

Fig. 3.19: Discharge per unit width curves and water level for sections I, II and total.

More importantly, the time of maximum flood discharge is shifted more towards HW than the time of max ebb discharge is, which causes a notable reduction in the maximum flood velocity since the cross-section is larger. In Fig. 3.19, $q_{max,flood}$ occurs at t = 11.18 h at which time the depth is 9.59 m. The maximum flood velocity is then 0.139 m/s. $q_{max,ebb}$ occurs at t= 2.47 h at a depth of 8.64 m. The maximum ebb velocity is thus 0.142 m/s.
In this lay-out, the average ebb velocity exceeds the average flood velocity and the ebb peak velocity is larger than the flood peak velocity. This leads to a negative velocity flux and an ebb-dominant channel.

The tidal wave is now partially progressive. Therefore, table 3.1 does not apply here. The difference in inundation and drainage explains the possibility of a situation of a "flood dominant" vertical tide and an "ebb dominant" horizontal tide. The influence of the area of tidal flats on ebb or flood dominance has also been shown by Seelig and Sorensen (1978) who investigated a tidal basin with a constant surface area below and a linearly increasing tidal flat area above the mean water level. A theoretical analysis has been made by Keulegan (1951) who also showed that the ebb current in the throat of an inlet is more efficient than the flood current in case of tidal flats.

Equilibrium seems to be the approximate configuration between channels 4 and 5. To determine a critical equilibrium flats area, two more lay-outs were investigated, see Fig. 3.20.

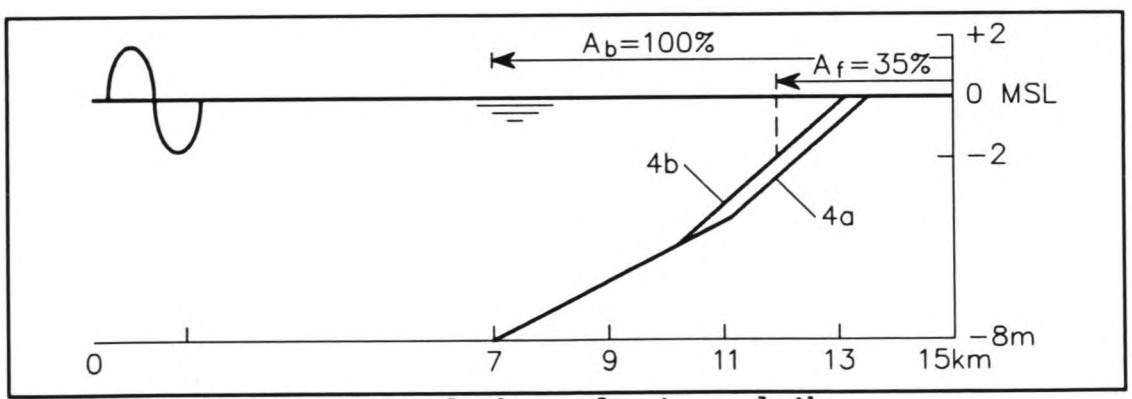

Fig. 3.20: Lay-out of channels 4a and 4b.

The net velocity fluxes are listed in appendix 3D and are depicted in Fig. 3.21. Channel 4a is flood dominant and channel 4b is ebb dominant in terms of sediment transport. Due to the grid size of 250 m no intermediate lay-outs could be investigated. The results indicate that the relative equilibrium flats area, where the net velocity flux equals zero, is about 35% in this schematization. However, this critical area of tidal flats is a function of the ratio of the amplitude of the tidal wave and the mean depth, of the variation of the cross-sectional area over one tidal cycle and of friction. These parameters were all assumed to be constant in this simulation. Also, in an actual tidal basin the flats are not

situated in the back of the basin as is assumed in this one-dimensional model. Rather, the two-dimensional effect of flats located along a channel will influence the equilibrium flats area since the inundation and drainage pattern is different.

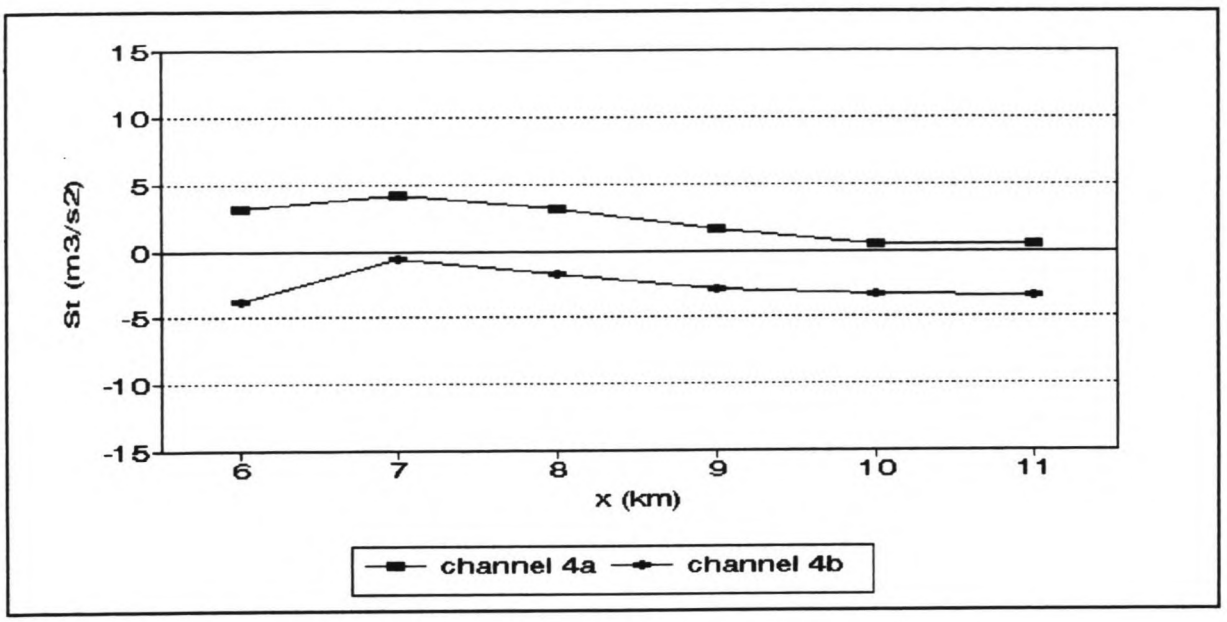

Fig. 3.21: Net velocity flux in channels 4a and 4b

It might be possible to deduce a critical relative flat area in an empirical way based on a study of many inlets, both flood and ebb dominant, throughout the world. In the simulation model in chapter 4, an empirical relationship between the tidal flat area and the gross basin area as given by Eysink (1991) could be used, see also section 2.4:

$$\frac{A_f}{A_b} = 1 - 0.025 \cdot \sqrt{A_b} \qquad (2.10)$$

where A_b = the gross basin area (mln m²)
A_f = the tidal flat area (mln m²)

This formula is based on data from German Bight inlets which are all flood dominant. The values for the equilibrium relative flat area found with this formula will therefore be too low. However, most of the inlets investigated have been approaching equilibrium for a long time, so calculated values might not be too far off.

3.6 Ebb dominance in existing tidal inlets

Only a minority of tidal inlets in the world exhibit ebb dominancy. All these inlets have a remarkably large relative area of tidal flats which feeds the hypothesis that this is one of the controling parameters.

Fig. 3.22: Wachapreague inlet, VA (from Boon and Byrne, 1981)

Byrne et al (1974) studied the Wachapreague, VA inlet and came to the hypothesis that infilling basins may change from flood to ebb dominancy. Boon and Byrne (1981) later sustained this idea with a numerical model of the inlet which has a high relative flat area, see Fig. 3.22. Fitzgerald and Nummedal (1983) note that most marsh-filled inlets in the Eastern U.S. show the same tendency.

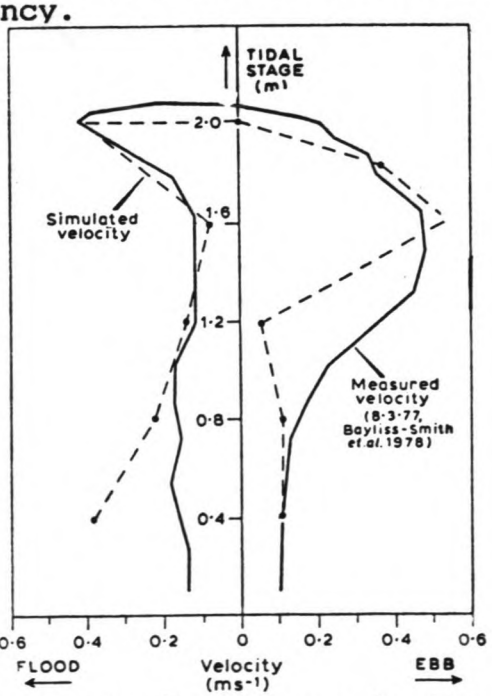

Fig. 3.23: Stage-velocity curves in the Stiffkey marshes, Norfolk, England (from Pethick, 1980)

Pethick (1980) measured velocity-stage curves in a lagoon near the Wash, England, see fig 3.23. This basin also has a large area of tidal flats. His measurements prove what has been shown in the previous section, namely that the maximum flood velocity occurs late in the flood cycle when water rises above the bank (in this figure at 1.6 m) and spills onto the flats. Maximum ebb discharge occurs at a lower stage and smaller cross section which results in relatively higher velocities.

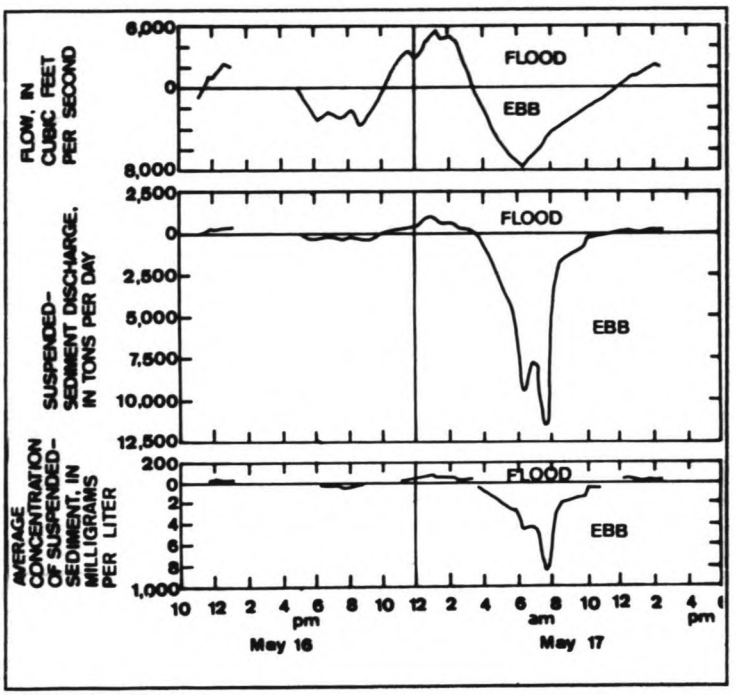

Fig. 3.24: Velocity, discharge and sediment discharge in Bolinas Lagoon, CA (from Ritter, 1972)

Ritter (1972) describes the velocity vs. time curves in Bolinas Lagoon, CA which is not a marsh system but exhibits an ebb dominancy, possible caused by its small size. It clearly shows the great influence the magnitude of the velocity has on sediment transports, see fig 3.24.

3.7 Conclusions

We come to the conclusion that shoaling takes place in an open basin. The rate of shoaling which is determined by the residual currents decreases as the basin fills in. The residual currents are controlled by the relative area of tidal flats which influence the inundation and drainage flow.
Therefore, the rate of shoaling does not become zero at a profile with a constant slope as was expected beforehand on page 25, but only after an equilibrium relative flat area is created. This situation is dynamically stable which means that the system will - after a change in the exogenous conditions - always try to reach a new equilibrium.

Inlets in the Dutch Wadden Sea are all believed to be flood

dominant. At the present time, all experience an import of sediment. If the conclusions from this report are true, the rate of infilling and the demand from the coastal shelf would decrease in time and become zero, if the exogenous conditions such as the mean sea level remained constant in time. Since these conditions are not constant, equilibrium will change too and might never be reached. The implications of this will be shown in chapter 4, where a model is presented based on the notion of and equilibrium flat area.

Chapter 4 Tidal basin model

In this chapter, a model is presented which describes the morphological behavior of a channel-flats system in a tidal basin. First, the mathematical basis is explained. Then, the model is defined in terms of variables, parameters and equations. With this model runs are made for four different scenarios. In the last section, various scenarios are stacked to simulate the behavior in the Zoutkamperlaag after the closure of the Lauwerszee in 1969.

4.1 Sediment distribution system

The basis of the model is the assumption that the main variables in the system, the channel cross-sectional area and the flats' surface area, tend to their equilibrium values according to a first order differential equation, also known as the decay function. For the channel cross-sectional area eq. (4.1) applies:

$$\frac{\partial A_c}{\partial t} = \frac{\overline{A_c} - A_c}{\tau_c} \qquad (4.1)$$

where A_c = area (m^2)

$\overline{A_c}$ = equilibrium area (m^2)

τ_c = inherent time scale (year)

For the flats' surface area eq. (4.8) applies. The equations state that the change in the area in one unit of time is proportional to the difference between its value at that time and its equilibrium value. The further a variable is out of balance, the faster it will adapt. Also, the closer a variable is to its equilibrium, the slower the process becomes.
In the tidal basin model, the adaption according to eq (4.1) can only occur if enough sediment is supplied. If this is not the case, the cross-sectional area will adapt in the following way:

$$\frac{\partial A_c}{\partial t} = - \frac{S}{\Delta x} \qquad (4.2)$$

where S = sediment inflow (m^3/year)

Δx = length of channel section (m)

Eq. (4.2) shows that all available sediment will be used to adjust the channel cross-sectional area. The sediment inflow S is determined by eq. (4.4) which will be explained later.

To show the time-evolution of a shoaling channel without flats a simulation model was made with the same lay-out as defined in Fig. 3.1, but based on the equations stated above, where in

this one-dimensional model A, the cross-sectional area, becomes h, the depth, and O'Brien's linear relationship $\overline{A} \sim P$ (see eq. (2.1) becomes $\overline{h} \sim (L-x)$ where L is the length of the basin. See Fig. 3.1 for definition of variables.

The results in Fig. 4.1 show that sediment which is input at the left boundary in one time-step is used to adapt the first section of the channel according to its inherent time-scale. Excess sediment is passed on to the next section to the right, which also adapts itself and transports the superfluous sediment until in one section demand exceeds supply and no sediment is passed on. Consequently, the sections on the right are not provided with any sediment and their depth will remain stable for some time. Only after several time-steps will demand in the first sections decrease according to eq. 4.1 to allow sediment to be passed on to the "back". Because of the nature of eq. (4.1), which states that the adjustment to equilibrium decreases as this equilibrium is reached, the top of the sand wave in fig 4.1 appears flatter in comparison to Fig. 3.4. Apart from this, the two figures show a strong resemblance.

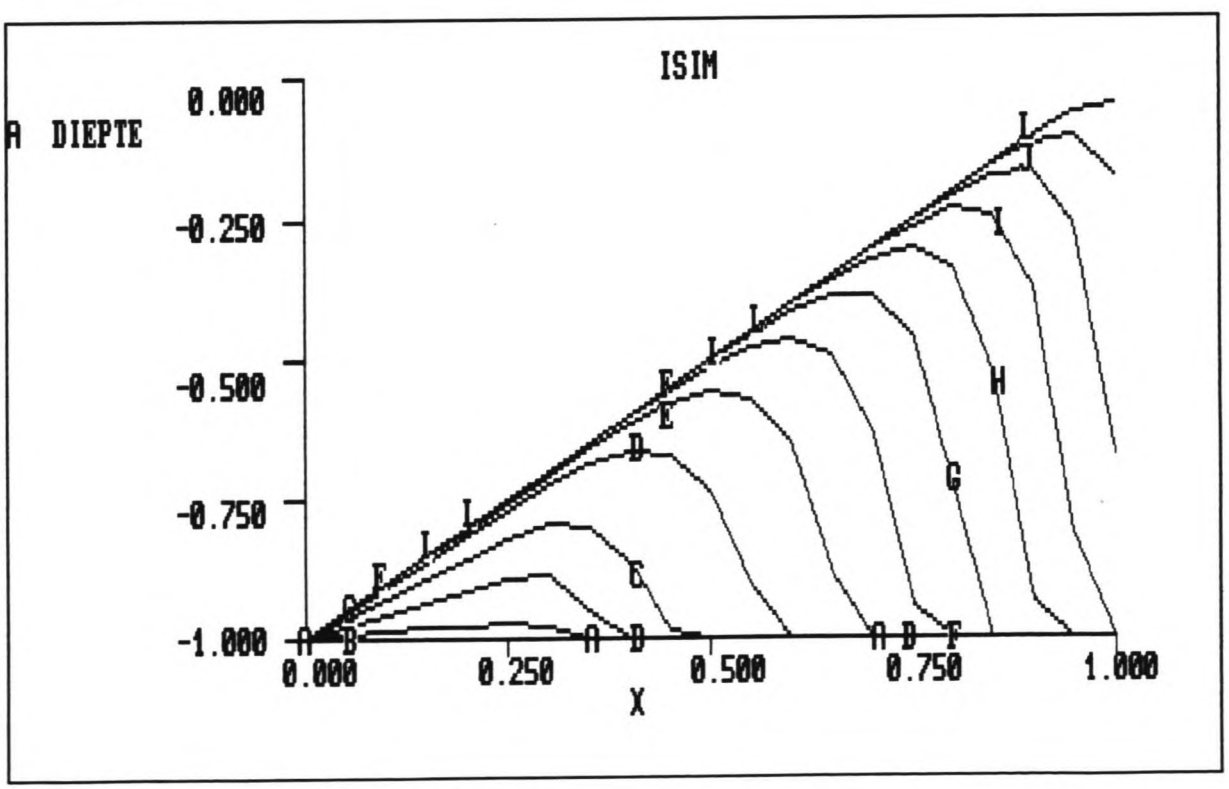

Fig. 4.1: Time-evolution with constant τ. The letters indicate different stages in the shoaling process.

For this reason, and because measurements in tidal basins show an exponential response after changes (e.g. Renger and Par-

tenscky, 1980), a model based on a decay function can be used to simulate morphological processes in a tidal basin. A decay function also served as the basis of a model for the Haringvliet (Allersma, 1988).

4.2 Tidal basin modeling

Schematization

A tidal basin is defined as the area enclosed by the barrier islands, the mainland and drainage divides. This area is inundated during at least part of the tidal cycle. In the model, the basin consists of two elements: channels and flats.
Channels are inundated throughout the tidal cycle. Since the channel cross-sectional area is a linear function of the prism, the areas of cross-sections of different branches at a certain distance from the gorge can be summated into one total cross-sectional area at that distance, see Fig. 4.2. This is done similar to Di Silvio (1989).

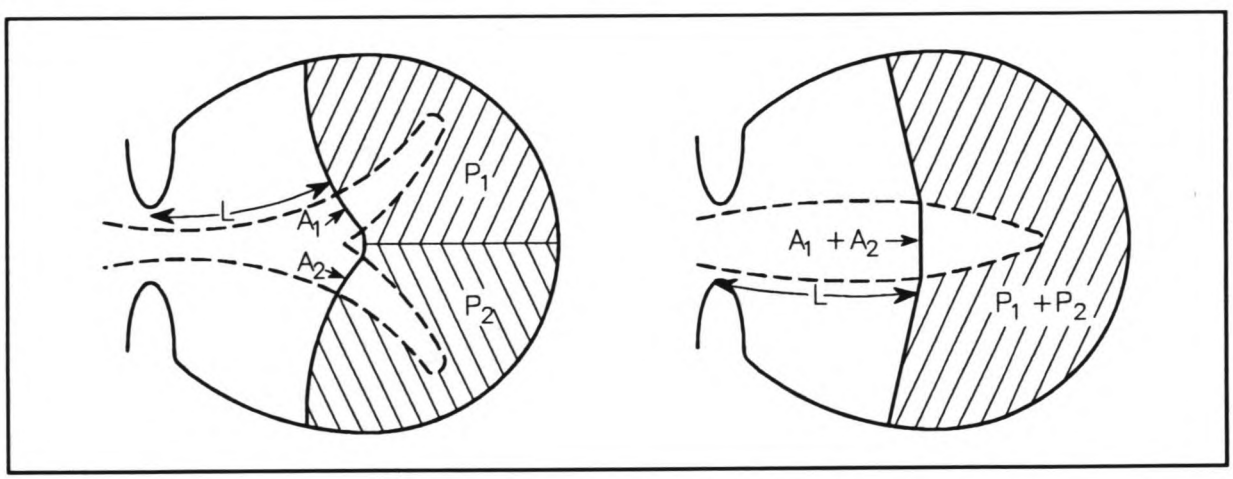

Fig. 4.2: Summation of cross-sectional areas.

Flats are inundated during only part of the tidal cycle. Although in nature the level of tidal flats does vary between HW and LW, it is set at MSL in this model. In many basins, the area of tidal flats is relatively larger in the back of the basin than at the gorge. In the model, the flats are assumed to have a triangular shape. The schematization based on these assumptions is depicted in Fig. 4.3.
The basin now consists of two discrete elements, the channels and the flats. Each of these elements is divided into sections with a specific length (for instance, Δx = 1000 m in the model).
Sediment exchange occurs between consecutive channel sections, much like the shoaling model of section 4.1 and between a channel section and a flats section with the same section index. This excludes sediment exchange between flats sections amongst themselves. External sediment exchange occurs through the gorge of the basin i.e. between the ebb tidal delta and

the first channel section. A possible sink is caused by sediment or gas mining which results in an areal-averaged land subsidence of the flats' section.

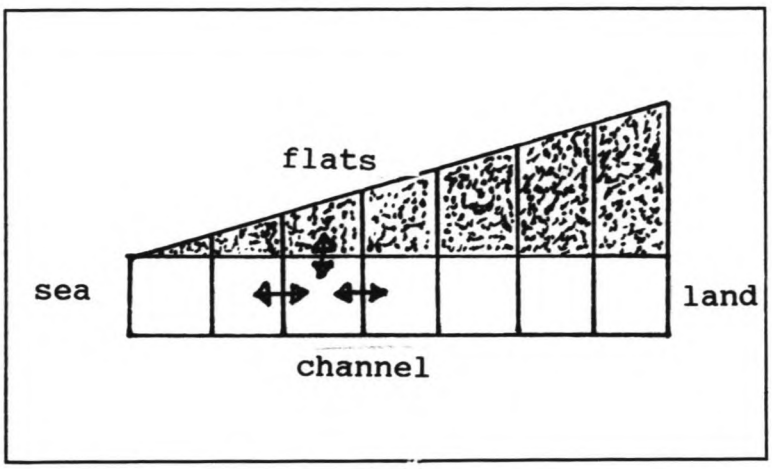

Fig. 4.3: Plan view of the tidal basin schematization

Equilibrium

The controlling variables are the cross-sectional area in the channels and the surface area and level of the flats. In each time-step and in each section, these variables are compared with their equilibrium values.

The equilibrium cross-sectional area in a channel is calculated with O'Brien's formula:

$$A_c = c \cdot P \qquad (4.3)$$

where $c = 6.56 \cdot 10^{-5}$ (m^{-1})

The prism through a cross-section is calculated as the sum of the storage volume in the channel (the tidal range multiplied by the horizontal storage area between the channel cross-section and the back of the channel) and the storage volume on the flats (the difference between HW and the flats' level multiplied by the area of flats between the cross-section and the back of the basin).

The equilibrium flats' area is based on eq. (2.10). As stated in section 3.5, this equation has some shortfalls. First of all, it is not non-dimensional and, more importantly, it is derived from data of flood dominant basins in the German Bight, which means that calculated values will actually be too low.
However, most of these basins have been approaching equilibrium for a long time, so relative flats' areas calculated with eq. (2.10) might not be too far off equilibrium. Also, to date no research has been done to determine the critical flats' area. This equation is therefore state-of-the-art. More importantly, the consequence of eq. (2.10), i.e. that smaller

basins need a relatively larger flats' area to influence the dominancy seems plausible, because the turn-around from flood to ebb dominant is due to the different character of inundation and drainage flows which becomes notable at a certain amount of tidal flats. In smaller basins this flats' area will be relatively larger. An equilibrium equation will then have the same appearance with different parameters.
Naturally, to use this equation for a clearly unintended purpose will affect results but not the trend in results. Since qualitative results are more important in this report, use of this equation will be made in this report.

The equilibrium seeking mechanism in the flats' level is explained in the following section under 'F'.

Equations

Sediment flow to and from one channel section can be schematized as follows:

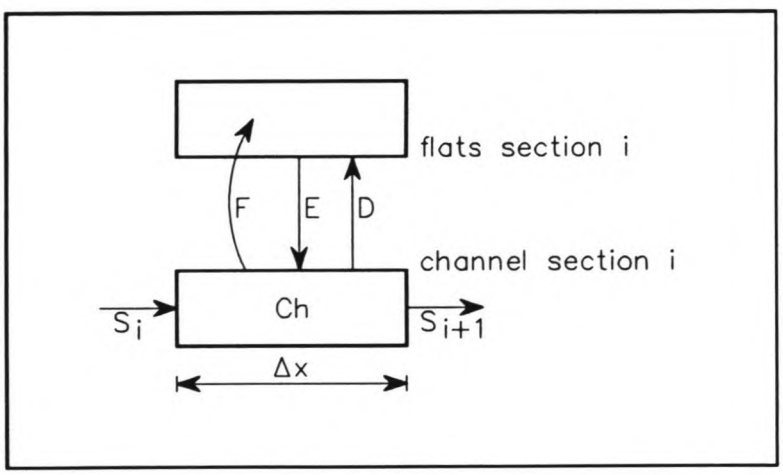

Fig. 4.4: Schematized sediment flow

The figure shows that sediment exchange occurs between two adjacent channel sections, denoted by S in the model. Sediment exchange between a channel section and a flats' section is more complicated. The model distinguishes between the sediment flow which changes the level of the flats, denoted F, and the flow that changes the horizontal area of the flats, denoted E for erosion and D for deposition. The inherent demand of the channel section itself is called Ch. These variables will be described in more detail below.

Ch is the inherent demand (sign is negative) or supply (+) to change the cross-section according to $\frac{\overline{A_c}-A_c}{\tau} \cdot \Delta x$ in one unit of time.
Ch is calculated with the above-mentioned equations. In the simulation, τ is set at 30 years, which is of the

same order as the inherent time-scale found in the Zoutkamperlaag by Biegel (1991b). Δx is taken as 1000 m in the simulation runs.

S_i inflow (+) or outflow (-) of sediment at the ocean side of the section i. In the most seaward section, S_o is calculated as

$$S_0 = \alpha \cdot (\overline{A_{fl}} - A_{fl}(t)) \qquad (4.4)$$

where S_o = exchange with the ebb tidal delta and/or the islands' headlands (m^3/year).

$\overline{A_{fl}}$ = total equilibrium flats' area, according to eq. (2.10) (m^2)

$A_{fl}(t)$ = total flats' area at time t (m^2).

Eq. (4.4) is based on chapter 3. Basins with less than the equilibrium flats' area will import sediment and basins with more than the relative area will export. Since this notion is only tentative, the equation has been formulated as a simple linear function.

F It is assumed that the flats will try to maintain a certain overdepth below HW. This can be understood in the following way: if the average depth over the flats increases, velocities decrease and (suspended) sediment will have the opportunity to settle. On the other hand, if the average depth decreases, the erosional capacity will increase. In the Oosterschelde basin, for instance, measurements indicate that erosion of flats is higher at neap tides when the average depth is smaller than during spring tides (Kohsiek et al, 1987). These two opposing mechanisms will cause the flats to "seek" an equilibrium overdepth. Because in the Zoutkamperlaag the tidal range is 2m. and the average flat level is around MSL, the overdepth in the model is taken as 1 m.
Consequently, in the case of a sea level rise or an increase in tidal range, the flats will demand sediment to raise their level. This demand can be calculated as follows

$$F = A_{fl,i} \cdot ((0.5 \cdot TR + MSL - flat\ level) - overdepth) \qquad (4.5)$$

where $A_{fl,i}$ = the section's flats' area
TR = tidal range

Sediment supplied from the channel and the flats' edges, eroded during storms, will determine whether or not this demand is met. In this regard the model differs from Peerbolte et al. (1991) who assumed that the demand will always be met at the cost of increased channel depth. In the model presented in this report it is possible that the flats' level lags behind the sea level rise. Especia-

lly when the relative area of the flats is large, drowning of the flats is a possibility.

E Erosion from the flats' edges (a decrease in the flats' area), on the other hand, takes place only during storms. Then, sediment is forced onto the flats (see F) or into the channels. In the model, the erosional capacity is expressed as

$$E = \mu \cdot A_{fl,i} \cdot height \qquad (4.6)$$

where $A_{fl,i}$ = the section's flats' area
height = the channel cross-sectional area divided by its width
μ = a dimensionless parameter

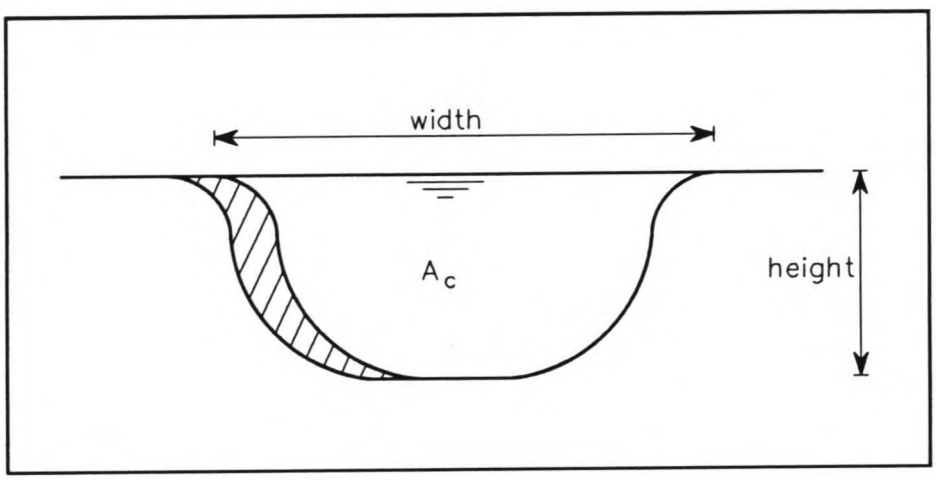

Fig. 4.5: Influence of bank height on erosion

The flats' area enters this equation because in nature a larger area of flats will be served by a greater number of individual channels. This will increase the length of the channel banks (and therefore the flats' edges) and consequently the total erosion in one section. The greater the difference in elevation between the channel bottom and the flats' level, in other words the higher the channel bank, the more of the flats' edge is exposed to erosion, see figure 4.5.
Since the erosion of the flats is storm-induced, E is autonomous and not dependent on a function of variables such as the channel cross-sectional area or the supply of sediment.

D is the increase of the flats' area. According to Kohsiek et al. (1987), sedimentation occurs during flood at the flats' edges and not on top of the flats themselves. This is due to effective wave breaking on the edge, consequent loss of wave energy and sediment transport capacity over the flats. Supply of sediment from the channel will therefore result in a growth of the flats' area before an increase of the level of the flats.

In the model, an increase in the flats' area is calculated as

$$D = \gamma \cdot (S_i + E - F + Ch) \qquad (4.7)$$

which states that a fraction of "superfluous" sediment will be deposited on the banks.
The higher the sum of the first three terms between parentheses, the higher the supply to the channel section. The larger the value of Ch, i.e. the smaller the cross-sectional area relative to its equilibrium, the higher the velocities will be. This results in a higher sediment transport capacity and a higher net sediment flow to the flats' edge. In the Oosterschelde basin, Kohsiek et al. (1987) noted a dependency of the accretion of the flats' edges on the sediment transport capacity in the channels.

4.3 Tidal basin simulation model

Based on the schematizations and equations in section 4.2, a simulation model was made in PASCAL.

Input parameters

The program asks for the following parameters:
- length of the tidal basin's main channel
- total basin area at $t = 0^-$ (before any changes)
- tidal range at $t = 0^-$
- relative equilibrium flats' area.
- duration of the simulation.

Input scenarios

The program gives a choice of the following scenarios which can be executed either singly or stacked.
- closure of part of the tidal basin
- sea level rise
- land subsidence (due to sand/gas mining)
- tidal range at $t = 0^+$
- varying tidal range due to the 18.6-year tidal periodicity

These scenarios will be discussed in more detail in section 4.4.

Simulation

The program follows the flow-chart of appendix 4A for every time-step and for every channel section. The flow chart works as follows:
First, it determines whether the channel section demands (Ch<0) or supplies (Ch>0) sediment. Following the right-hand branch (channel demand), it is determined whether sufficient sediment is supplied to fulfill its inherent demand. If so, the change in cross-section (dAc) will be equal to this demand. Superfluous sediment is passed on partly to the flats

(F and D) and partly to the next channel section. Growth of the area of flats is limited by a time-scale function similar to eq. (4.1):

$$\frac{\partial A_{fl}}{\partial t} = \frac{\overline{A_{fl}} - A_{fl}}{\tau_{fl}} \qquad (4.8)$$

where A_{fl} = area of flats in a section (10^6 m^2)
τ_{fl} = time-scale, which is an order larger than the channel time-scale. In the model it is set at 200 years.

If inherent demand is not met, all available sediment is used to adjust the channel, in which case the channel cross-sectional change dAc is smaller than the inherent demand Ch. This means that even if the flats demand sediment they will receive nothing.
Following the left-hand branch (Ch>0), it is first determined whether the flats' section and the neighboring channel sections demand more sediment than is produced in the channel section. In this case, the flow to the flats is limited.
If outside demand is smaller than production, all these demands are met. Here also the growth of the flats' area is bound by an inherent time-scale (eq. (4.8)).

The sediment flow to or from the channel section to the right of section i, S_{i+1}, follows from the conservation of mass. After all flow variables are known, the new channel cross-sectional area, the flats' area and the flats' level are calculated.

4.4 Scenarios

The model is run for different scenarios. The effects of these scenarios are shown for a "standard" basin with the following parameters:

Length	= 20000 m
Gross area	= $100 \cdot 10^6$ m^2
Tidal range	= 2 m
relative flat area	= $75 \cdot 10^6$ m^2 (equilibrium value)
duration	= 100 years
τ (channel)	= 30 years
τ (flats)	= 200 years
α (in eq. (4.4))	= 40000 (m/year)
γ (in eq. (4.7))	= 0.3 (-)
μ (in eq. (4.6))	= 0.0005 (-)

The scenarios will show the mechanisms that are invoked to attain equilibrium. The equilibrium situation will therefore be discussed last.

Partial closure

When part of a tidal basin is closed, the gross basin area is reduced. This means a reduction both in the tidal prism and, according to O'Brien's eq. (2.1), in the channel cross-sectional area. In the simulation, the basin with an original length of 20000 m is closed at 15000 m, leading to a sharp reduction in the tidal prism. According to eq. (2.10), the new, smaller basin will have a larger relative flat area as equilibrium. Since with the closure of the back part of the basin a relatively large area of tidal flats is cut off, the initial flat area immediately after closure will be smaller than this new equilibrium flat area, see Fig. 4.6.

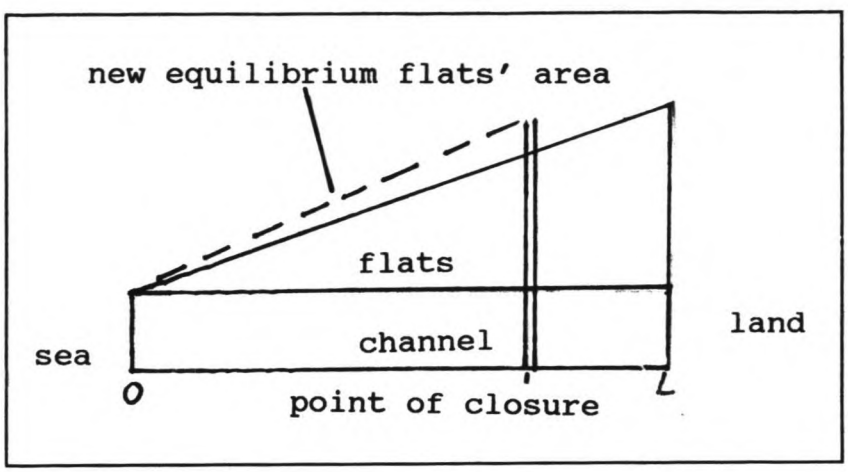

Fig. 4.6: Plan view of the situation before and after closure of the model basin (dimensions not to scale).

With eq. (4.4), this will lead to an import of sediment from the ocean. This imported sediment is used to adjust the most seaward channel cross-sections with their inherent time-scale according to eq. (4.1). This is shown in Fig. B-1 in appendix 4B for the first section at x=0. Because in this section the input exceeds the channel demand, some of the superfluous sediment is used to increase the section's flat area through 'D' in the model. The rate of this increase slowly declines in time. The rest of the sediment is passed on to the next section. Sediment continues being passed on as long as input in a receiving section exceeds demand.

Fig. B-2 shows that at x=8 km from the mouth, the sediment input from the sea does not reach this point until about 60 years from the start of the simulation. In the first 60 years, the only sediment input into the channel comes from the eroding channel banks (denoted by E in section 4.2). It is clear that in this simulation this lateral input is not enough to let the channel cross-sectional area adjust itself by its inherent time-scale. The erosion of the channel banks is visible as a decrease of flats' area in the figure.
At t = 60 years, sediment imported from the sea begins to

reach the section; more sediment is available to adjust the cross-sectional area. The change in the cross-sectional area becomes larger. From t = 60 to t = 64 years, the total input, both from the sea and from the banks is still smaller than the inherent demand, which results in the convex part of the graph. Only after t = 64 years does input exceed demand, just as it did at x=0. The channel adjusts according to the inherent time-scale (the concave part) and sediment is available to increase the flats' area.

Fig. B-3 shows that at x=14 km the sediment wave from the sea does not reach this section before the end of the simulation. The channel cross-sectional area is only decreased by lateral input from the channel banks. This input declines in time, since in eq. (4.6) both A_{fl} and the bank height (a function of the cross-sectional area) become smaller in time.
Lateral input from the banks into the channel has been measured in the Zoutkamperlaag and graphs show that this input is indeed declining in time (Oost, 1992 and Biegel, 1991b). A comparison to these graphs and data from the Zoutkamperlaag is included in section 4.5.

Sea level rise and land subsidence

Because of the much debated greenhouse effect, the earth's temperature might rise 4°C. The higher average temperature will melt the polar caps and expand the sea water volume. The predictions are that the sea level might rise 0.4 to 0.6 m in the next 100 years.

The effects of such a sea level rise are tested on the standard basin. The rate of sea level rise is set at 0.004 m/yr. Running the model in this way causes the rate of sea level rise to suddenly change from 0 to 0.004 at t=0, which is an unrealistic scenario in real life. However, it is expected that the greenhouse effect will cause a relatively large increase in the rate in a relatively short time span.

Fig. B-4 shows the section at x=0. Depicted are the channel cross-sectional area, the flats level relative to MSL at t=0 and the flats' surface area. The figure shows that because the sea level rises, the flats' level will try to follow the trend according to eq. (4.7). Sediment needed to raise the flats' level will come either from the ocean (external input), the channel cross-sections or the flats' edges.

Because at $t=0^-$, the system is in equilibrium, there will be no external input at first. Since the increase in sea level causes an initial increase in the tidal prism, the channel cross-section will begin to erode. Also, sediment is eroded from the channel banks, decreasing the flats' surface area. In the figure, it appears that this decrease is rather large but keeping in mind the (automatic) scale on the right side it is actually small. The eroded sediment from the banks and channels satisfies the demand of the flats in this section and their level will keep up with the sea level rise.

Because of the immediate erosion of the banks in all sections, the total surface area will become smaller than the equilibrium surface area and sediment will begin to be imported as from t=1 years. For section 0 this means that the availability of sediment more than satisfies the demand from the flats. The level of the flats linearly increases from 0 to 0.4 m at t=100 years, which means that the overdepth (MSL - flats' level) remains constant in time. The flats will even begin to grow in area again and sediment is being passed on again to the next section in a way similar to that described above.

Fig. B-5 shows the section at x=12 km. At first, there is no input from the seaward sections; the sediment wave has not reached this section yet. The flats will try to keep up with the sea level rise but they fail at that in the first 50 years for the following reasons. First, the area of flats in this section is much larger than the flats' area of section 0 because of the schematized triangular shape in Fig. 4.3. This larger area means a greater demand of sediment. Secondly, the supply by the channels ('Ch') is smaller than the supply in section 0 because of smaller absolute values of the cross-sectional area. Therefore, demand exceeds supply and the flats are unable to follow the sea level rise.

After 38 years, the external sediment wave will reach this section and more and more the (ever increasing) demand of the flats is met. After the 50nd year, supply exceeds demand and the flats in this section behave as the flats in section 0. As can be seen in the figure, the depth over the flats becomes larger in the first 40 years, then decreases from t=38 to t=50 years and remains constant from then on.

The time evolution for section 14 at x=18 km is shown in Fig. B-6. Here the flats' area is so large that demand is not met by supply from both the banks and the channel. Also, the sediment wave does not reach this section during the simulation. This means that the overdepth keeps increasing all the time in the most landward sections. This increased overdepth causes a larger prism and a larger cross-sectional area. The extra available sediment provided by the enlargement of the channel cross-section is still not enough to meet the demand.

The discretization of the flats allows an individual increase of each flats' section and because accretion of these flats is controlled by the supply from channels and banks, the most seaward sections, benefiting from the sediment wave first, raise their flats' level before the landward sections. This results in an uneven accretion of the flats and in fact a landward slope in the level. This is not likely to occur in a real tidal basin, since suspended sediment, which is not taken into account in this model, will spread more evenly through the basin. Here the model shows an important shortfall.

Land subsidence caused by gas or sand mining has the same effect as a rise in the sea level.

Increase in tidal range

After the closure of the Zuyder Zee in 1932, the tidal regime in the western Wadden Sea was changed. In one of the Wadden Sea's tidal basins, the Eyerlantse Gat, the tidal range increased from 1.4 to 1.7 m. Ribberink and De Vroeg (1991) noticed that after 1932 channels were scoured and that flats increased their level. With the model this can be explained as follows: the sudden increase in tidal range also increases the prism. Consequently, the cross-sectional area has to adapt to a new equilibrium. In the meantime, flats are demanding sediment to attain the critical overdepth below MHW again.

In Fig. B-7 this is shown for the standard basin which experiences an increase from 2 to 2.2 m. At x=0 km. the flats demand sediment to increase their level by 0.1 m. This sediment is delivered by the flats' edge (decreasing the flats' area) and by the scouring channel. The figure shows that the flats' demand in this section is almost instantly satisfied.

Figs. B-8 and B-9 show that this is not the case for x=12 and x=18 km. Just as in the sea level rise scenario, the flats' surface area and therefore demand is just too large to be met by the small supply. Because the surface area is eroded, the system starts to import sediment from the sea. This sediment wave propagates through the channel and when it reaches a section, the flats' demand is satisfied. This happens in Fig. B-8 at t= 12 years and in Fig. B-9 at t=30 years. At the same time, some of the superfluous sediment is used to restore the surface area to its original value at t=0.

After t=40 years, the channel cross-sectional area in all three figures begins to decrease again because the ongoing sedimentation on the flats heightens the flats' level and increases the tidal prism. When all the flats in the tidal basin have raised their level to the critical overdepth, the storage volume on the flats is back to its original value. The tidal storage in the channels (the tidal range · channel surface area) is larger than at $t=0^-$. The cross-sectional area will therefore continue to decline after t=100 years to a value slightly larger than the original value.

Both the sea level rise scenario and the tidal range increase scenario were simulated with a standard basin in equilibrium. This means that at t=0 there is no input of external sediment. This sediment wave is induced later when, because sediment is "borrowed" from the flats, the surface area falls below the equilibrium value. Simulating the scenarios in a basin under equilibrium at $t=0^-$ will help the elements reach equilibrium more quickly since external sediment is input from the start.

18.6-year periodicity

As explained in chapter 3, the vertical tide consists of numerous constituents. One of these has an extremely large period of 18.6 years. This is caused by the variation of the

angle between the plane of lunar motion and the earth's equatorial plane. For the Zoutkamperlaag, the variation in the tidal range has an amplitude of about 0.07 m. This slight variation may have a significant influence on morphology because the period has the same order of magnitude as the morphological time scale.

The effect of this periodicity is shown in Fig. B-10 for x=0. The simulation was run for an increase of the tidal range from 2 to 2.2+0.1*cos(2πt/T) where T is the periodicity of 18.6 years. The figure shows that as the equilibrium value which the cross-section wants to attain varies, the adaption of the cross-section also shows a variation, in fact a superposition of a negative exponential and a cosine. Fig. B-11 shows that the flats' top demands and supplies sediment during the cycle; the flats "breathe".

Equilibrium situation

In all of the above scenarios, the system variables are out of balance at $t=0^+$. The system tends to a new equilibrium by using the flats' surface area as a source of sediment to adjust the channel cross-sectional area and the flats' level to their new equilibrium values first. Also, by eroding the flats' surface area an external sediment wave is induced (according to eq. (4.4)) which helps to restore the system variables to their new equilibrium, starting in the most seaward sections. The result of these mechanisms is that the flats' surface area is adjusted to its equilibrium value last with its restoration also beginning in the most seaward sections.
As the channel cross-sections reach their equilibrium values, the gradient in the net transport capacity through all cross-sections becomes zero (analogous to chapter 3, page 25). Sediment transported through the channels will then only be used to build up the flats' surface area which has not reached its new equilibrium value yet. The increase in flats' area will, according to eq. (4.4), reduce the net sediment transport capacity. The most landward flats' section will be the last to reach its equilibrium value. When the flats attain their equilibrium value, the net sediment transport capacity will become zero and the system is in balance. Fig. B-12 shows the channel cross-sectional areas and the flats' areas in every cross-section in the case of equilibrium of the standard basin.

4.5 Hindcast of the Zoutkamperlaag

Schematization

The model is used to simulate the morphological behavior in the Zoutkamperlaag. This tidal basin has undergone great adjustments since the closure of the Lauwerszee in 1969, see Fig. 4.7.

As is shown in the figure, before 1969 the Zoutkamperlaag branched off into two main channels, the Oort channel and the

channel that is now called Lauwersmeer. In the model, the tidal basin is schematized as two separate systems, whose main channels are bundled together from the gorge at x=0 to x=9 km, done similar to Boon and Byrne (1981).

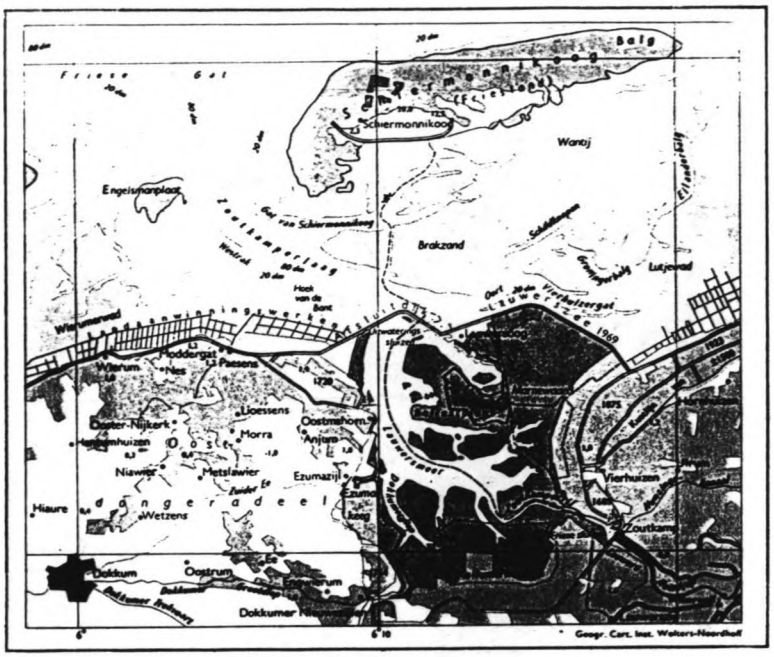

Fig. 4.7: Zoutkamperlaag after 1969

The schematization looks like this:

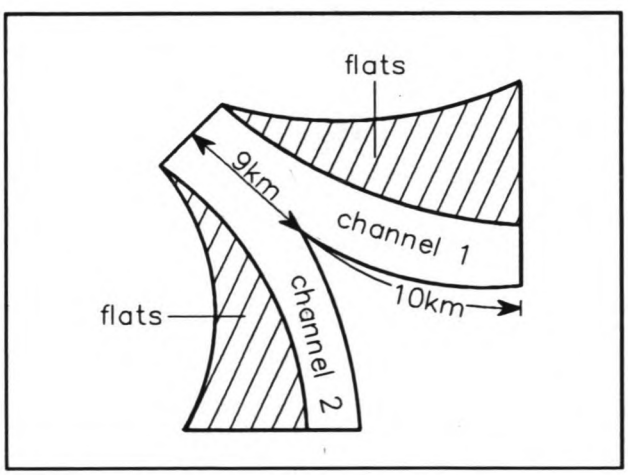

Fig. 4.8: Schematization of the Zoutkamperlaag before closure

The total basin area is 210 million m². The area that has been closed off, indicated by the dashes lines in Fig. 4.9, measures 90 million m², a reduction of 42% in basin area. With the new gross basin area of 120 mln m², the new equilibrium flats area measures 84.24 million m². The simulation was run with a sea level rise of 0.001 m, a new tidal range of 2.2 m due to a change in the tidal regime as described above, and a variation of the tidal range with an amplitude of 0.07 m and a

period of 18.6 years, a stack of all scenarios described in section 4.4.

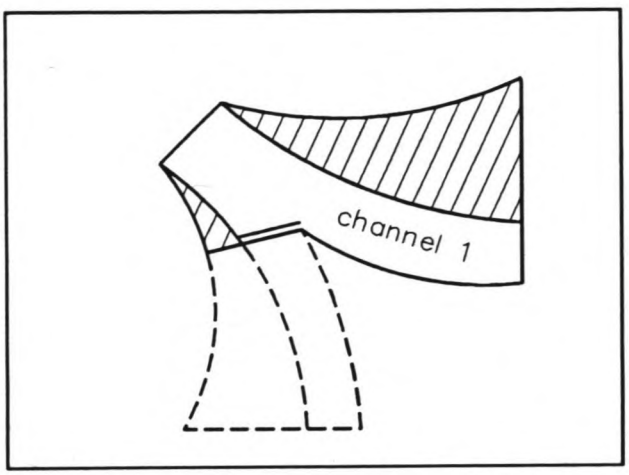

Fig. 4.9: Schematization of the Zoutkamperlaag after closure

Results

The results of the hindcast are compared to values calculated on the basis of measurements presented by Biegel (1991b), depicted in appendix 4C, Fig. C-1. These so-called "stamp graphs" show the change in cross-sectional area in 31 cross-sections, drawn in Fig. C-2. Unfortunately, these graphs are based on just 5 data points since measurements were only available for 1970, 1975, 1979, 1982 and 1987.

The first six cross-sections are situated in the ebb tidal delta and are not considered here. Cross-section 7 was used to tune the parameter τ_c. Cross-section 11 was used to tune both α and γ . μ was tuned in cross-section 22. O'Brien's constant c = $6.56 \cdot 10^{-5}$ was used.

τ_c = 15 (year)
α = 100000 (m/yr)
μ = 0.019 (-)
γ = 0.3 (-)

Fig. C-3 (Biegel's 7) shows the same features as Fig. B-1: the channel cross-sectional area decreases according to its inherent time-scale. Biegel's data points (the basis of the "stamp graphs" in fig. C-1) are marked 'X' in Figs. C-3 through C-11. Fig. C-4 will be discussed on the next page.

Figs. C-5 (Biegel's 11), C-6 (Biegel's 13) and C-7 (Biegel's 14) show the same behavior comparable to Fig. B-2. The cross-section is not able to decrease in area according to its inherent time-scale for about the first six years because of a lack of supplied sediment from the sea. These first years sediment is only provided by the channel banks. The decrease

of the rate of this supply, which has been noted by Oost and De Haan (1992) in the Zoutkamperlaag, is clearly visible and can be expected considering the gradual decrease of both the flats' surface area and the bank height in eq. (4.6). After the sixth year, the sediment wave from the gorge reaches these sections and the cross-sectional area decreases according to its own time-scale. Fig. C-8 (Biegel's 15) shows the same features, the sediment wave reaches this cross-section at t=9 years.

Figs. C-9 (Biegel's 18) and C-10 (Biegel's 22) show that the sediment wave does not reach this section in the simulation time. Only the channel banks provide sediment to decrease the channel's cross-sectional area.

Fig. C-11 (Biegel's 24) is exemplary of the behavior in the Oort channel, which was not closed. Here the prism increases because of the larger tidal range. This results in a growing cross-sectional area. The values are below those that have been measured by Biegel. This may be due to the crude schematization of the flats' area as a triangle. An important factor may be that the drainage divide south of Schiermonnikoog Island moved to the east after the closure. This would increase the prism and therefore the cross-sectional areas. The shift of the drainage divide has not been taken into account in the simulation model.

All graphs show that the closure of the Lauwerszee has the dominant effect upon behavior of the channel cross-sections. The increased tidal range only shows its effect in the Oort channel. Because of the short time-span, the sea level rise is almost immeasurable. The small amplitude of the 18.6-year periodicity has a negligible effect in this simulation.

The graphs produced with the simulation model show a strong resemblance with most of the "stamp graphs". This would indicate that this model, although based on rather crude assumptions, shows the essential features of the morphological process the Zoutkamperlaag is experiencing. Three types of adaption curves can be distinguished: an exponential adaption as in Fig. C-3, an adaption curve with a slowly declining rate as in Figs. C-9 and C-10 and a transitional 'S'-curve which shows both characteristics, see Figs. C-5 through C-8. It should be noted, however, that the low number of datapoints on which the "stamp graphs" are based limits the resolution of these graphs.

There are some "stamp graphs" that can not be reproduced by the model, for example Biegel's cross-sections 9, 12 and 21.
Fig. C-4 (Biegel's 9) shows that the model's values are lower than those calculated by Biegel. This is due to the fact that the cross-sectional area at t=0 in sections 7 to 10 is not decreasing down channel as would be expected according to O'Brien.
In cross-section 12 in Fig. C-1, there is a sharp decrease in area from the fifth to the ninth year. This cross-section is

situated just seawards of the Gat van Schiermonnikoog channel which is not included in the model as a separate branch. Sediment demand by this channel might have caused the large decrease in cross-sectional area.
At t=0, the area of cross-section 21 is much larger than the areas of surrounding cross-sections 20 and 22, see Fig. C-1. This large area could be due to the fact that the dividing line between channels and flats is sometimes hard to draw. Clearly this section does not fit the trend of decreasing cross-sectional areas down the channel.

4.6 Influence of changes in the tidal basin on other parts of the system

As explained in section 4.4, the tidal basin "demands" external sediment in the case of a closure, an increase in tidal range or a sea level rise. This sediment has to be provided by the other elements in Fig. 1.1, the ebb tidal delta and the barrier islands.

After a partial closure, the tidal prism is decreased considerably. According to Walton and Adams (1976), a smaller prism would require a smaller volume of the ebb tidal delta, see eq. (2.4). The excess sediment is then an obvious source of input for the tidal basin. This can be understood as follows: because the prism is decreased, flow velocities through the gorge are also decreased. Since the wave regime has remained the same, the balance of tidal and wave energy maintaining the ebb tidal delta is distorted. Sediment will be transported by the waves onto the shores and into the gorge.
Van Kleef (1991) notes that not all sediment in the ebb tidal delta is ready to be used as input because a large amount is stored below a depth where it can be moved by waves or currents. This part is inactive. De Vriend and Roelvink (1989) set the boundary between the active and the inactive part at -10 m MSL. Although the ebb tidal delta appears to be the logical source of sediment in this case, loss of sand at the barrier islands' beaches should not be ruled out.

After an increase of tidal range or in the case of a sea level rise, the flats may not keep up with the increase. This results in an increase in tidal prism and hence also an increase in the volume of the ebb tidal delta. As explained in section 4.4, the flats "borrow" sediment from the edges which would induce an influx of sediment into the basin to restore this. If this is true, both the basin and the ebb tidal delta demand sediment which could only be provided by the islands' beaches. The consequence of this is a high erosion of these beaches.
Another possibility would be that the ebb tidal delta acts as a buffer. In this case the delta would provide sediment to the basin even though it demands sediment itself. The restoration of the delta could then be accomplished by extracting sediment from the beaches on a larger time-scale.

Conclusions and recommendations

The aim of the research, of which this report is the product, is to simulate the morphological behavior in a tidal basin with a highly schematized model.

The underlying assumption is that the behavior of the basic elements, namely the channels and the flats, is controlled by certain variables which try to attain an equilibrium value. In this report three such variables have been acknowledged: the channel's cross-sectional area, the flats' surface area and the flats' critical overdepth.

The critical channel cross-sectional area is based on O'Brien's formula. The influence of the flats' surface area on the residual currents and therefore the morphological behavior of a tidal basin has been shown in chapter 3. The critical value has not been calculated. Instead, a formula based on data from existing basins has been used. The critical overdepth on the flats is assumed to be a constant value, independent of tidal range and mean sea level.

With the model based on these variables and on assumptions of the areal distribution of the flats in the basin, it is possible to predict the essential changes in the basin morphology. In the case of a partial closure, the model quite satisfactorily reproduces the process of cross-sectional change in the Zoutkamperlaag tidal basin. In the case of a sudden increase in tidal range, the model accurately predicts the trend in the morphological behavior in the case of the Eijerlantse Gat. The model shows its limitations in the event of a sea level rise. Because of the discretization of the flats into sections and the assumption that accretion of flats is ruled by supply and not by demand, the model shows a landward decline in flat level. The 18.6-year periodicity only shows a slight influence in the case of a partial closure.

In conclusion, this model, even though it is based on fairly simple equations and assumptions, seems to reproduce the trend of morphological changes in tidal basins.

On the basis of the results so far, I would like to make the following recommendations:

1) Results from this model, especially for the scenarios of sea level rise and an increase of tidal range, should be checked against data from actual tidal basins. In the case of a change in tidal range, data from the Eijerlantse Gat would be the most appropriate because it is small and data should be easily available. Data from various tidal basins should be used to verify or to negate the idea that in the case of a sea level rise the most seaward flats accrete sooner and faster than the more landward ones. In general, the model should be run with data from a tidal basin that is not as large and complex as the Zoutkamperlaag. One of the German Bight or American

east coast inlets could be used, preferably one that has undergone a partial closure or another large disturbance.

2) As this model shows the importance of the cricital stability parameters of the various controlling variables, more (fundamental) research is needed on this topic.
- The stability of the channel cross-section could possibly better be based on Bruun and Gerritsen's critical shear stress than on O'Brien's linear relationship between the cross-section and the prism. However, the shear stress and Q_{max} in eq. (2.3) will be harder to calculate than the tidal prism.
- The parametrization of the critical flats area warrants more attention. An empirical relationship of this critical ratio of flats area and gross basin area could be derived from data on a great number of flood-dominant and ebb-dominant tidal basins all over the world. Stevenson et al. (1988) made a start from a geological point of view. Also, an attempt could be made to derive the stability conditions from theoretical models in following Speer and Aubrey (1985).
- The notion of a critical depth on the flats should be verified theoretically or empirically. The balance of erosion and accretion on the flats will be a function of the wave-, wind- and current-induced sediment transport under various conditions (storms, spring tide, neap tide, etc.). The overdepth will also play a role in the ebb or flood-dominancy of the basin and should not be overlooked in determining the critical flats area.

3) Research has to be done on the parameters that influence the morphological time-scales of both channels and flats.

4) The sediment transfer mechanisms between channels and flats are insufficiently substantiated in this model. Through numerical modeling and/or in-situ measurements the underlying physical processes should be uncovered.

5) The model presented in this paper only deals with a part of the tidal inlet system as defined in fig. 1.1. The next element that should be investigated is the ebb tidal delta which probably plays a central role in the distribution of sediment. Sediment flow in and around the ebb tidal delta is controlled by both wave and tide-induced sediment transport which will surely complicate the schematization. One very crude first step is to schematize the ebb tidal delta as a semi-circle consisting of a central ebb channel, two shoal areas and two flood channels. Sediment flow will be around the terminal lobe of the delta, through the channels and over the shoals.

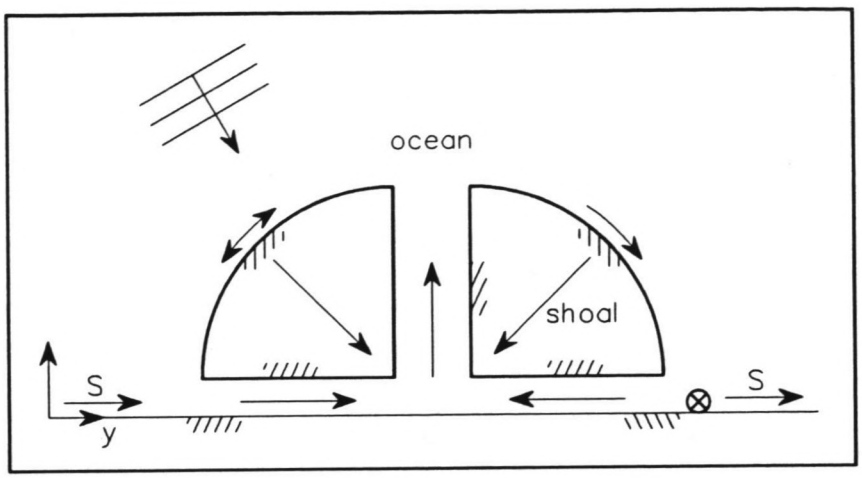

It might be possible to construct a model which, like the tidal basin model, tries to seek a certain equilibrium volume while exchanging sediment with the other two elements in the tidal inlet system.

REFERENCES

Allersma, E., 1988: 'Morphologisch onderzoek Noordelijk Deltabekken', DELFT HYDRAULICS, report Z71-03

Aubrey, D.G. and Speer, P.E., 1985: 'A study of non-linear tidal propagation in shallow inlet/estuarine systems. Part I: Observations', Est., Coastal and Shelf Science, vol. 21, p. 185 - 205

Aubrey, D.G. and Weishar, L. (eds.), 1988: 'Hydrodynamics and sediment dynamics of tidal inlets', Lecture notes on coastal and estuarine studies, vol. 29, Springer verlag, New York , 456 p.

Biegel, E.J., 1991a: 'De ontwikkelingen van de ebgetijde delta en het kombergingsgebied van het Friesche Zeegat in relatie tot de sluiting van de Lauwerszee (in Dutch)', State University Utrecht, Department of Physical Geography, Utrecht Report GEOPRO 1991.07

Biegel, E.J., 1991b: 'Equilibrium relationships in the ebb tidal delta, inlet and back barrier area of the Frisian inlet system', Rijkswaterstaat, Den Haag DWG GWAO-91.016

Boon, J.D. and Byrne, R.J., 1981: ' On basin hypsometry and the morphodynamic response of coastal inlet systems', Marine Geology, vol 40, p. 27-48

Bruun, P. and Gerritsen, F., 1959: 'Natural bypassing of sand at coastal inlets', ASCE, Journal of Waterways and Harbors Div, vol. 85: no WW4, p. 75 - 107

Bruun, P. and Gerritsen, F., 1960: 'Stability of coastal inlets', North Holland Publishing Co., Amsterdam 123 p.

Byrne, R.J. et al, 1974: 'Channel stability in tidal inlets. A case study', Proc. 14th Coastal Engineering Conf., ASCE, NY p. 1585 - 1604

Cronin, L.E. (ed.), 1975: 'Estuarine Research, vol II Geology and Engineering', Proc. 2nd Int. Estuarine Research Conference, Columbia, SC, Academic Press Inc., NY , 587 p.

Dean, R.G. and Walton, T.L., 1975: 'Sediment transport processes in the vicinity of inlets with special reference to sand trapping', in: Cronin, L.E., 1975, p. 129 - 150

Dean, R.G., 1988: 'Sediment interaction at modified coastal inlets: processes and policies', in: Aubrey and Weishar, 1988, p. 412 - 439

DELFT HYDRAULICS, 1991: 'WENDY one-dimensional mathematical modeling system, v. 3.00', Delft Hydraulics,

Di Silvio, G., 1989: 'Modelling the morphological evolution of tidal lagoons and their equilibrium configurations', Proc. XIII Congress of the IAHR, Ottawa, Canada , p. C169 - C175

Dronkers, J.J., 1964: 'Tidal computations in rivers and tidal waters', North Holland Publishing Co., Amsterdam , 516 p. (quoted in Speer and Aubrey, 1985)

Dronkers, J., 1986: 'Tidal asymmetry and estuarine morphology', Neth. J. of Sea Research, 20, p. 117 - 131

Escoffier, F.F., 1940: 'The stability of tidal inlets', Shore and Beach, vol. 8 no. 4, p. 114 - 115

Eysink, W.D., 1990: 'Morphologic response of tidal basins to changes', Proc. 22nd Coastal Engineering Conf., ASCE, New York, p. 1948 - 1961

Eysink, W.D., 1991: 'Simple morphological relationships for estuaries and tidal channels; handy tools for engineering', COPEDEC'91, Mombasa, Kenya , 11 p.

FitzGerald, D.M. and Nummedal, D., 1983: 'Response characteristics of an ebb-dominated tidal inlet channel', J. of Sed. Petrology vol 53 no 3, p. 833 - 845

FitzGerald, D.M., 1982: 'Sediment bypassing at mixed energy tidal inlets', Proc. 18th Coastal Eng. Conf., ASCE, New York p. 1094 - 1115

FitzGerald, D.M., 1988: 'Shoreline erosional-depositional processes associated with tidal inlets', in: Aubrey and Weishar, 1988, p. 186 - 225

Gerritsen, F. and De Jong, H., 1985: 'Stabiliteit van doorstromingsprofielen in het Waddengebied', Rijkswaterstaat Adviesdienst Vlissingen, nota WWKZ 84.V016, (quoted in Gerritsen, 1990)

Gerritsen, F., 1990: 'Morphological stability of inlets and channels of the western Waddensea', Rijkswaterstaat Tidal waters division, GWAO-90.019, 86 p.

Hageman, B.P., 1969: 'Development of the western part of the Netherlands during the Holocene', Geologie Mijnbouw, vol 48, p. 373 - 388 (quoted in Steijn, 1991)

Hayes, M.O., 1979: 'Barrier island morphology as a funcion of tidal and wave regime', in: Leatherman, S.P., 'Barrier islands from the Gulf of St. Lawrence to the Gulf of Mexico', Academic Press, New York , p. 1 -27

Hayes, M.O., 1991: 'Geomorphology and sedimentation patterns of tidal inlets: a review', Proc. Coastal Sediments Conf. , p. 1343 - 1355

Jarrett, J.T., 1976: 'Tidal prism area relationships', US Army Corps of Engineers, GITI report no. 3, 32 p.

Keulegan, G.H., 1951: 'Third progress report on tidal flow in entrances: water level fluctuations of basins in communication with seas', National Bureau of Standards Rep. no. 1146, Washington, DC 28 pp.

Kleef van, A.W., 1991: 'Empirical relationships for tidal inlets, basins and deltas', Institute of Geophysical Res., draft report, 51 p.

Kohsiek, L.H.M. et al., 1987: 'De Oosterschelde naar een nieuw onderwaterlandschap', Rijkswaterstaat DGW.AO 87.029, Den Haag 48 p. (in Dutch)

Kreiss, H., 1957: 'Some remarks about non-linear oscillations in tidal channels', Tellus, vol. 9, p. 53 - 68 (quoted in Speer and Aubrey, 1985)

Leatherman, S.P., 1982: 'Barrier island handbook', University of Maryland, College Park, MD, USA , 109 p.

Marino, J.N., 1986: 'Inlet ebb shoal volumes related to coastal physical parameters', Coastal and Oceanographic Eng. Dept., University of Florida, report UFL/COEL-86/017 (quoted in Marino and Mehta, 1987)

Marino, J.N. and Mehta, A.J., 1987: 'Inlet ebb shoals related to coastal parameters', Proc. Coastal Sediments Conf., p. 1608 -1623

Marino, J.N. and Mehta, A.J., 1988: 'Sediment trapping at Florida's east coast inlets', in: Aubrey and Weishar, 1988, p. 284 - 296

Massie, W.W. (ed.), 1986: 'Lecture notes f11: Coastal Engineering, vol 1: Introduction', T.U. Delft, Civil Engineering Dept., 212 p.

Moody, J.A., 1988: 'Small scale inlets as tidal filters', in: Aubrey and Weishar, 1988, p. 137 - 156

Mota Oliveira, I.B., 1970: 'Natural flushing ability in tidal inlets', Proc. 12th Coastal Eng. Conf. Ch III , p. 1827 - 1845

Niemeyer, H.D., 1986: 'Changing of wave climate due to breaking on a tidal inlet bar', Proc. 20th. Coastal Eng. Conf., ASCE p. 1427 - 1443

Niemeyer, H.D., 1990: 'Morphodynamics of tidal inlets', PATO - course coastal morphology TU Delft, Delft, the Netherlands , 41 p.

O'Brien, M.P., 1931: 'Estuary tidal prisms related to entrance areas', Civ. Eng., vol. 1 no. 8, p. 738 - 739

O'Brien, M.P., 1969: 'Equilibrium flow areas of inlets on sandy coasts', J. of the Waterways and Harbors Div., vol. 95, WWI, ASCE , p. 43 - 52

Oertel, G.F., 1975: 'Ebb-tidal deltas of Georgia estuaries', in: Cronin, L.E. (ed.), 1975, p. 267 - 276

Oertel, G.F., 1988: 'Processes of sediment exchange between tidal inlets, ebb deltas and barrier islands', in: Aubrey and Weishar, 1988, p. 297 - 318

Oost, A.P. and De Haan, H., 1992: 'Het Friesche Zeegat. Sedimentologische veranderingen 1970 - 1987', Instituut Aardwetenschappen, R.U. Utrecht

Peerbolte, E.B. et al, 1991: 'Morphological and ecological effects of sea level rise: an evaluation for the Western Wadden Sea', in: 'Ocean Margin Processes in Global Change', Mantoura, J.M. et al (eds.), p. 329 - 347

Pethick J.S., 1980: 'Velocity surges and asymmetry in tidal channels', Est. Coastal and Marine Sc. vol 11, p. 321 - 345

Pingree, R.D. and Griffiths, D.K., 1979: 'Sand transport paths around the British Isles resulting from M_2 and M_4 tidal interactions', J. of the Marine Biological Association of the U.K., vol. 59, p. 497 - 513

Renger, E. and Partenscky, H.W., 1974: 'Stability criteria for tidal basins', Proc. 14th Coastal Eng. Conf., ASCE, New York p. 1605 - 1618

Renger, E. and Partenscky, H.W., 1980: 'Sedimentation processes in tidal channels and tidal basins caused by artificial constructions', Proc. 17th Coastal Engineering Conf., ASCE, New York p. 2481 -2494

Ribberink, J.S. and De Vroeg, J.H., 1991: 'Kustverdediging Eierland (Texel)', DELFT HYDRAULICS, H 1241, 63 p.

Ritter, J.R., 1972: 'Sediment transport in a tidal inlet', Proc. 13th Coastal Engineering Conf., ASCE, New York p. 823 - 842

Seelig, W.N. and Sorensen, R.M., 1978: 'Numerical model investigation of selected tidal inlet-bay system characteristics', Proc. 16th Coastal Eng. Conference, ASCE, NY , p. 1302 - 1319

Sha, L.P., 1990: 'Sedimentological studies of the ebb-tidal deltas along the West Frisian islands, the Netherlands', Ph.D. thesis, publ. nr. 64, Geologica Ultraiectina, R.U. Utrecht

Smith, D., 1984: 'The hydrology and geomorphology of tidal basins', in: Huis in 't Veld, J.C. et al (eds), 'The closure of tidal basins', Delft University Press, the Netherlands Y5940

Speer, P.E. and Aubrey, D.G., 1985: 'A study of non-linear tidal propagation in shallow inlet/estuarine systems. Part II: Theory', Est., Coastal and Shelf Science, vol. 21, p. 207 - 224

Stauble, D.K. et al, 1988: 'Inlet flood tidal delta development through sediment transport processes', In: Aubrey and Weishar, 1988, p. 319 - 347

Steijn, R.C., 1991: 'Some considerations on tidal inlets (Literature survey)', Delft Hydraulics, H 840, 109 p.

Stevenson, J.C. et al., 1988: 'Sediment transport and trapping in marsh systems: implications of tidal flux studies', Mar. Geology, vol 80 p. 37 -59

Stive, M.J.F. and Eysink, W.D., 1989: 'Voorspelling ontwikkeling kustlijn 1990 - 2090, fase 3', Delft Hydraulics H 825 vol. 3.1, 66 p. (in Dutch)

U.S. CERC, 1984: 'Shore Protection Manual', U.S. Coastal Engineering Research Center, Vicksburg, Ms, U.S.A.

Velden van der, E.T.J.M., 1989: 'Lecture notes f7: Coastal Engineering', TU Delft, Civil Engineering Dept. 284 p.

Vriend de, H.J., 1987: 'Analysis of horizontally two-dimensional morphological evolutions in shallow water', J. of Geophysical Research, vol 92, No. C4, p. 3877 - 3893

Vriend de, H.J. and Roelvink, J.A., 1989: 'Innovatie van kustverdediging', Rijkswaterstaat nota Kustverdediging Technisch Rapport 19 / Delft Hydraulics H 825, 39 p. (in Dutch)

Walton, T.L. and Adams, W.D., 1976: 'Capacity of inlet outer bars to store sand', Proc. 15th Coastal Eng. Conf., ASCE, New York p. 1919 -1937

Wolff, W.J., 1986: 'De Waddenzee: eigenschappen van een dynamisch kustgedrag', Flevobericht nr. 252; RIJP, p. 11 -22 (in Dutch) (quoted in Steijn, 1991)

Zhu Weimin, 1991: 'Least-squares approximation program'

APPENDIX 3A

Set-up, amplitudes and phases of the least-squares approximation of the vertical tide in channels 1, 2 and 3.
Results are shown in figs. 3.12 and 3.13.
Set-up and amplitudes in meters, phases and lead in degrees.

channel	x(km)	η_o	M_2	M_4	θ_1	θ_2	ratio	lead
1	1	0.002	1.984	0.019	1.946	-70.648	0.009	74.54
	3	0.004	1.982	0.050	5.095	-67.081	0.025	77.27
	5	0.003	1.985	0.073	7.358	-65.191	0.037	79.91
	7	0.003	1.990	0.088	8.877	-64.126	0.044	81.87
	9	0.003	1.995	0.098	9.798	-63.597	0.049	83.19
	11	0.003	1.999	0.104	10.269	-63.610	0.052	84.48
	13	0.003	2.002	0.106	10.441	-63.757	0.053	84.64
	15	0.003	2.003	0.106	10.465	-63.892	0.053	84.82
2	7	0.003	1.986	0.085	8.804	-60.271	0.043	77.88
	9	0.002	1.991	0.102	10.193	-58.500	0.051	78.89
	11	0.001	1.995	0.128	11.805	-57.277	0.064	80.89
	13	0.001	1.998	0.134	12.209	-57.433	0.067	81.85
	15	0.001	1.999	0.135	12.243	-57.462	0.067	81.95
3	1	0.003	1.985	0.014	1.768	-76.285	0.007	79.82
	3	0.006	1.982	0.035	4.593	-73.610	0.018	82.80
	5	0.008	1.983	0.048	6.583	-71.145	0.024	84.31
	7	0.010	1.986	0.057	7.882	-69.025	0.029	84.79
	9	0.010	1.989	0.064	9.017	-66.626	0.032	84.66
	11	0.010	1.987	0.077	10.539	-63.552	0.039	84.63
	13	0.020	1.965	0.144	13.463	-52.576	0.073	79.50

APPENDIX 3B

Residual velocity fluxes over one tidal cycle (positive is inward) for channels 1, 2 and 3.
Results are shown in fig 3.14.

channel	x(km)	S_T (m^3/s^2)
1	6	74.007
	7	56.143
	8	39.919
	9	26.202
	10	15.531
	11	8.178
	12	3.494
	13	1.011
	14	0.131
	15	0
2	6	80.339
	7	61.205
	8	63.053
	9	65.641
	10	70.964
	11	29.270
	12	9.623
	13	2.159
	14	2.071
	15	0
3	6	31.325
	7	25.765
	8	24.659
	9	23.401
	10	21.492
	11	17.402
	12	10.216

APPENDIX 3C

Set-up, amplitudes and phases of the least-squares approximation of the vertical tide in channels 4, 5 and 6.
Results are shown in figs. 3.15 and 3.16.
Amplitudes in meters, phases and lead in degrees.

channel	x(km)	η_o	M_2	M_4	θ_1	θ_2	ratio	lead
4	5	0.008	1.986	0.040	6.246	-79.594	0.020	92.09
	6	0.009	1.988	0.048	6.918	-79.037	0.024	92.87
	7	0.010	1.990	0.050	7.444	-78.485	0.025	93.37
	8	0.010	1.991	0.053	7.926	-77.643	0.027	93.50
	9	0.010	1.993	0.055	8.452	-76.812	0.028	93.72
	10	0.010	1.994	0.059	9.040	-75.811	0.030	93.90
5	5	0.011	1.991	0.035	5.691	-84.918	0.018	96.30
	6	0.012	1.993	0.037	6.283	-84.449	0.019	97.02
	7	0.013	1.995	0.038	6.735	-84.353	0.019	97.82
	8	0.013	1.996	0.039	7.137	-84.062	0.020	98.34
	9	0.014	1.998	0.040	7.561	-83.570	0.020	98.69
	10	0.015	1.998	0.041	8.041	-83.222	0.021	99.30
6	5	0.012	1.986	0.025	5.265	-103.27	0.013	113.80
	6	0.013	1.987	0.025	5.800	-104.36	0.013	115.96
	7	0.014	1.988	0.025	6.206	-105.83	0.013	118.24
	8	0.014	1.988	0.025	6.562	-106.86	0.013	119.98
	9	0.015	1.988	0.024	6.988	-109.07	0.012	122.88
	10	0.017	1.995	0.023	7.639	-112.39	0.012	127.67

APPENDIX 3D

Residual velocity fluxes over one tidal cycle (positive is inward) for channels 4, 5 and 6.
Results are shown in fig. 3.17.

channel	x(km)	S_T (m^3/s^2)
4	6	12.957
	7	11.274
	8	10.209
	9	8.597
	10	6.480
	11	4.713
5	6	-6.046
	7	-2.373
	8	-2.780
	9	-3.150
	10	-2.118
	11	-7.733
6	6	-10.562
	7	-3.272
	8	-2.725
	9	-2.735
	10	-2.908
	11	-2.113
4a	6	3.122
	7	4.135
	8	3.079
	9	1.607
	10	0.397
	11	0.371
4b	6	-3.777
	7	-0.589
	8	-1.823
	9	-2.936
	10	-3.233
	11	-3.472

Appendix 4A

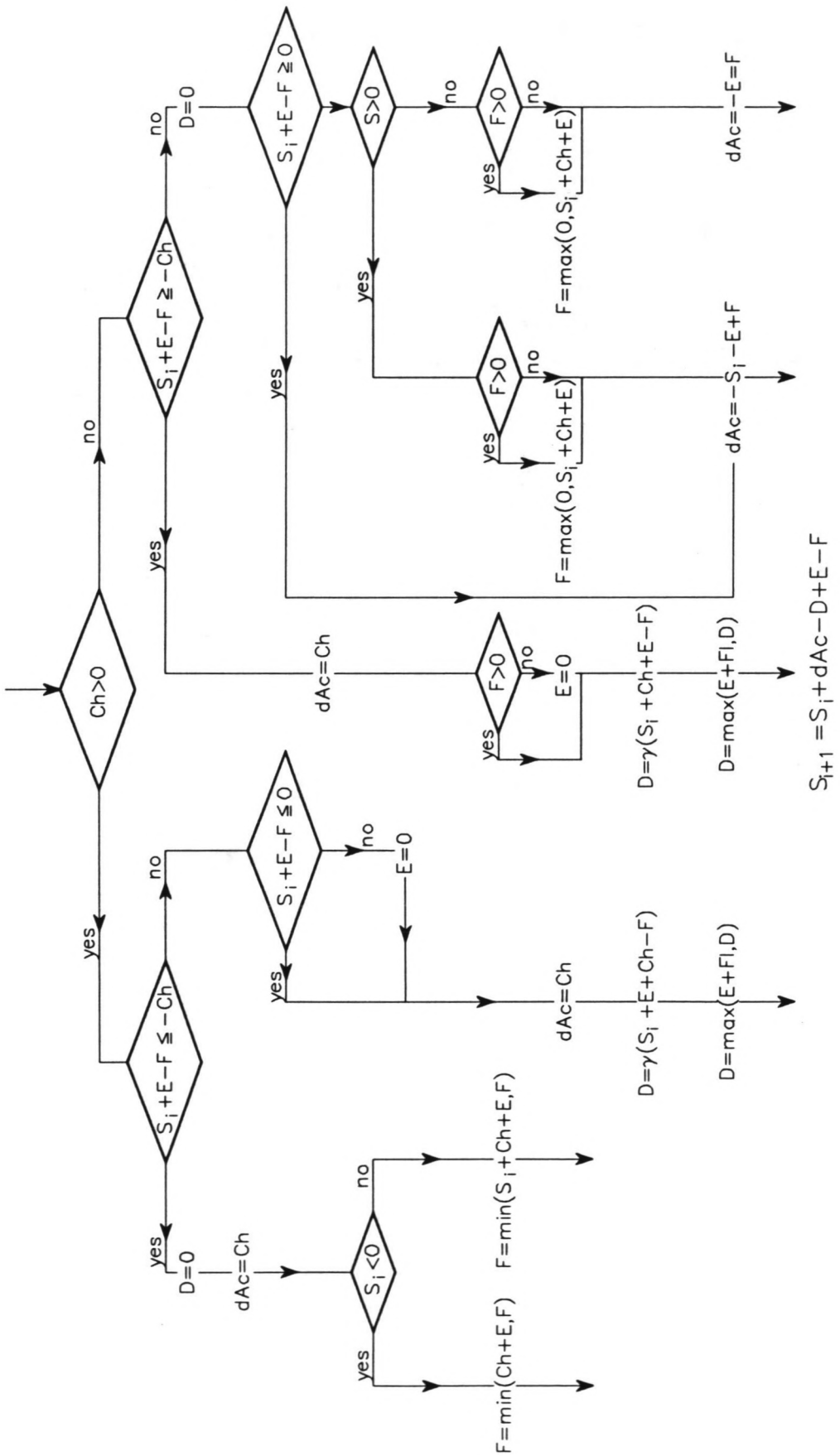
Ch>0
yes
no
Si+E−F ≦ −Ch
yes
D=0
dAc=Ch
Si<0
yes
F=min(Ch+E,F)
no
F=min(Si+Ch+E,F)
no
Si+E−F ≦ 0
yes
dAc=Ch
D=γ(Si +E+Ch−F)
D=max(E+Fl,D)
no
E=0
Si+E−F ≧ −Ch
yes
dAc=Ch
F>0
yes
E=0
D=γ(Si +Ch+E−F)
D=max(E+Fl,D)
no
D=0
Si+E−F ≧ 0
yes
S>0
yes
F>0
yes
F=max(0,Si +Ch+E)
dAc=−Si −E+F
no
F>0
yes
F=max(0,Si +Ch+E)
dAc=−E=F
no
Si+1 =Si+dAc−D+E−F

Appendix 4B

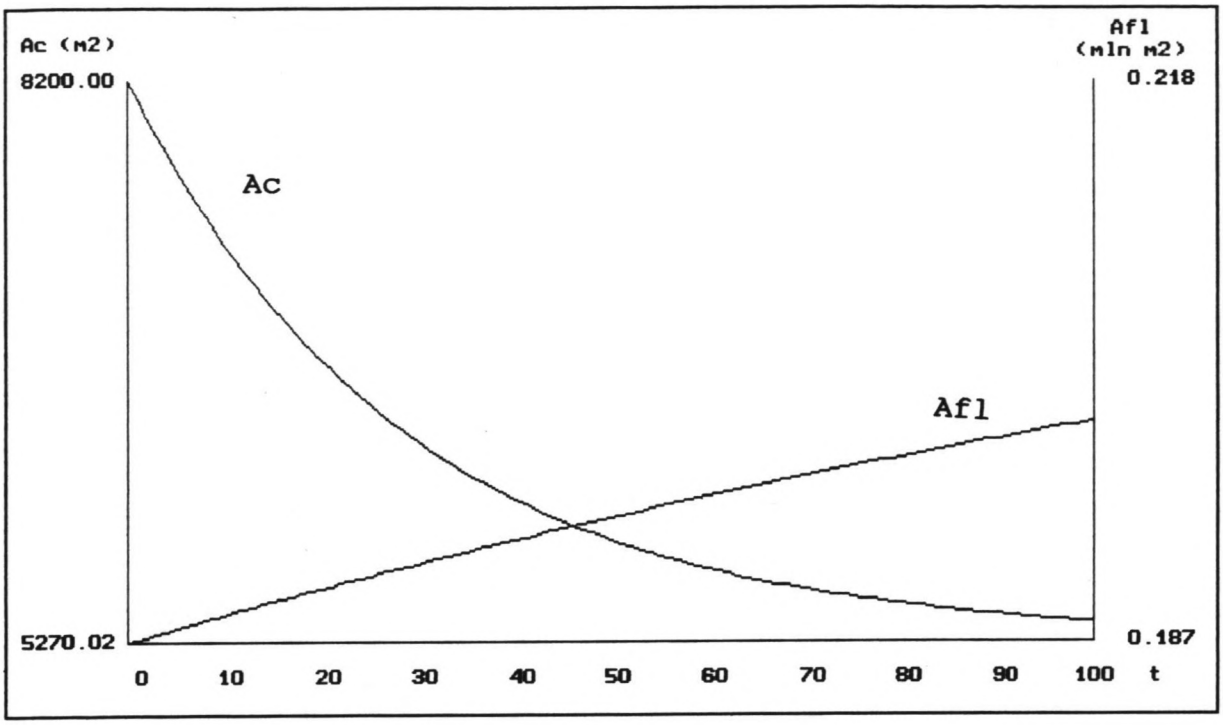

Fig. B-1: Partial closure scenario at x=0

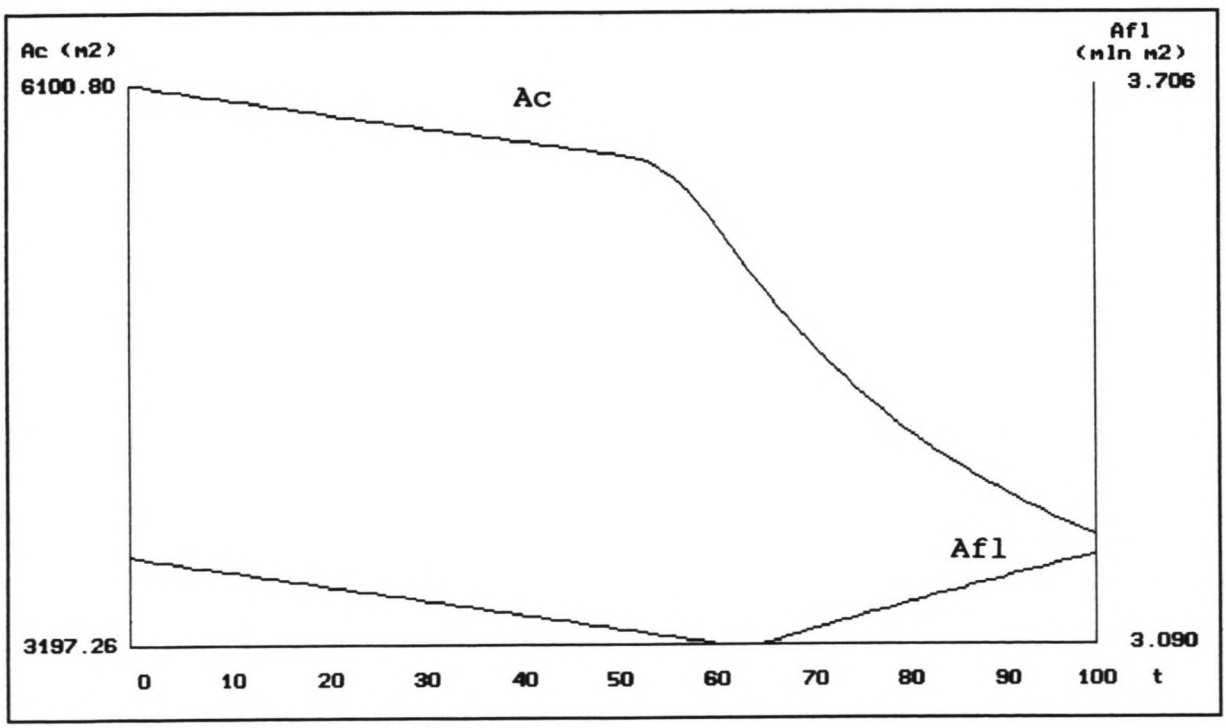

Fig. B-2: Partial closure scenario at x=8 km.

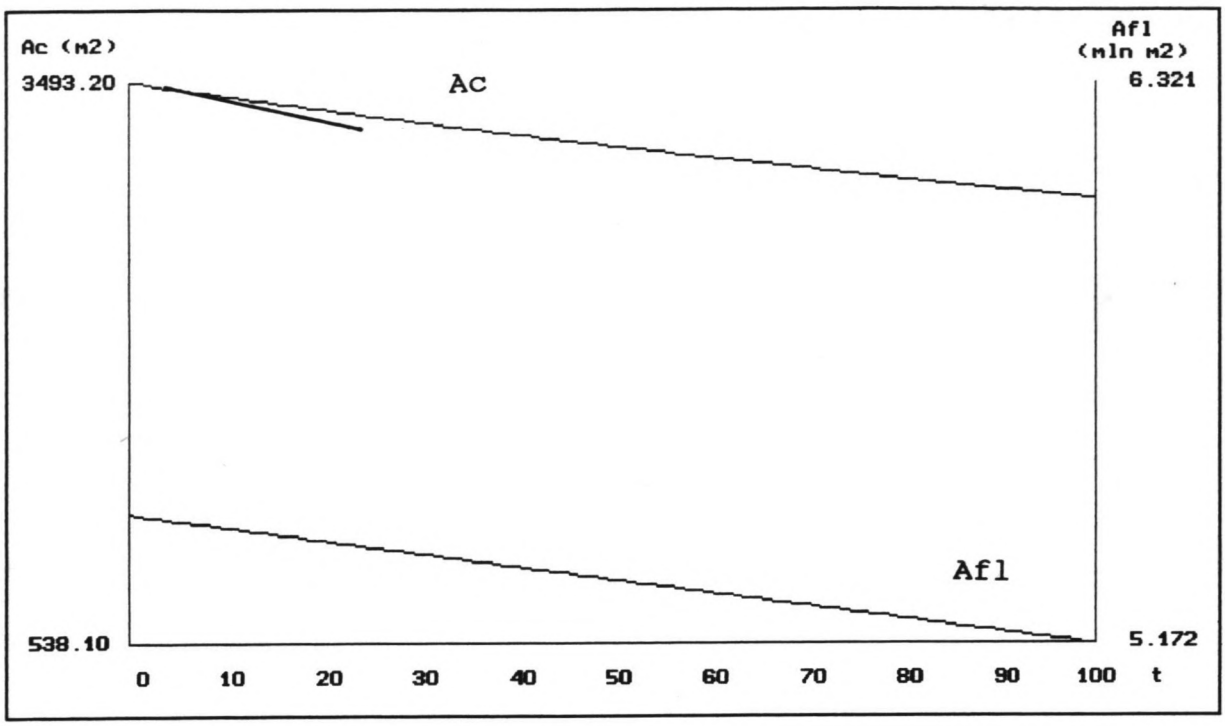

Fig. B-3: Partial closure scenario at x=14 km.

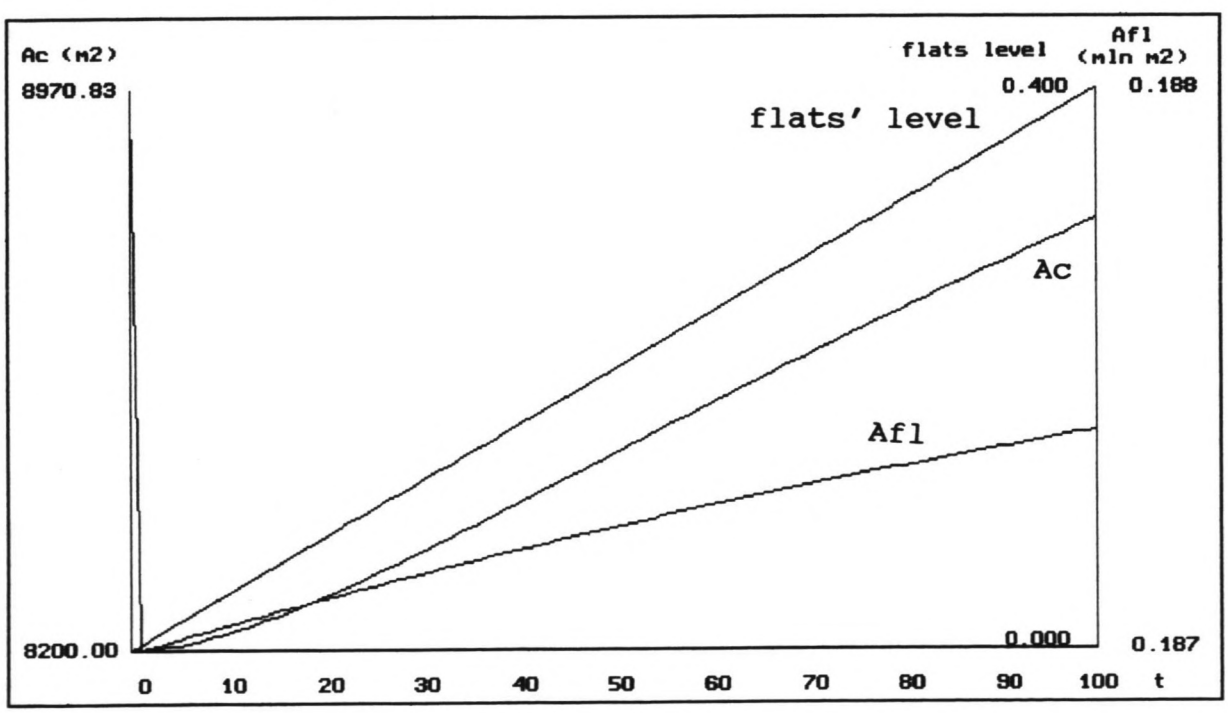

Fig. B-4: Sea level rise scenario at x=0

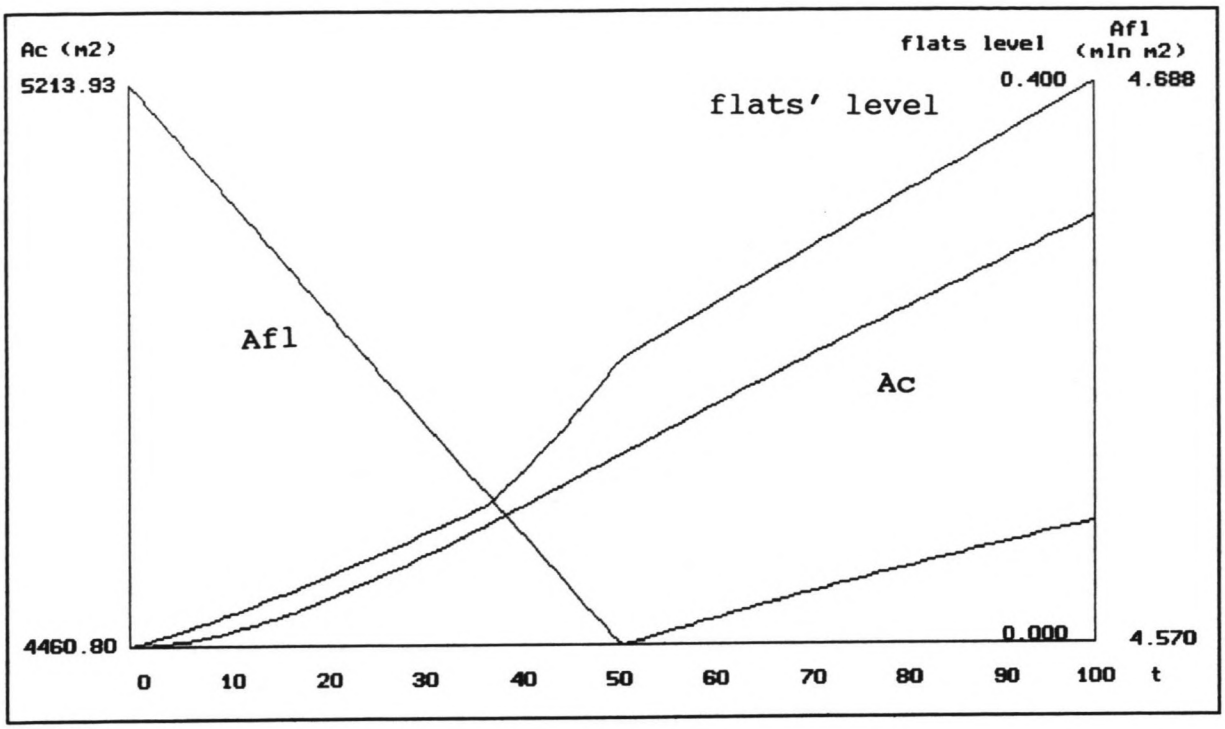

Fig. B-5: Sea level rise scenario at x=12 km.

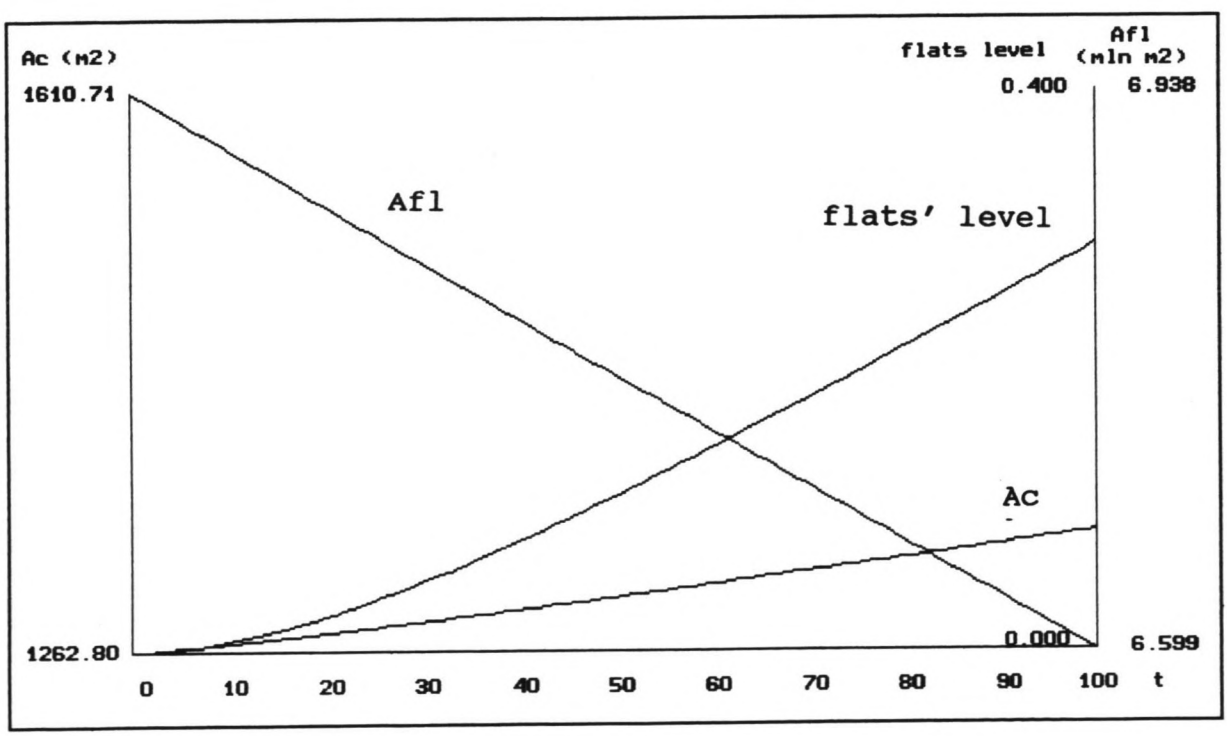

Fig. B-6: Sea level rise scenario at x=18 km.

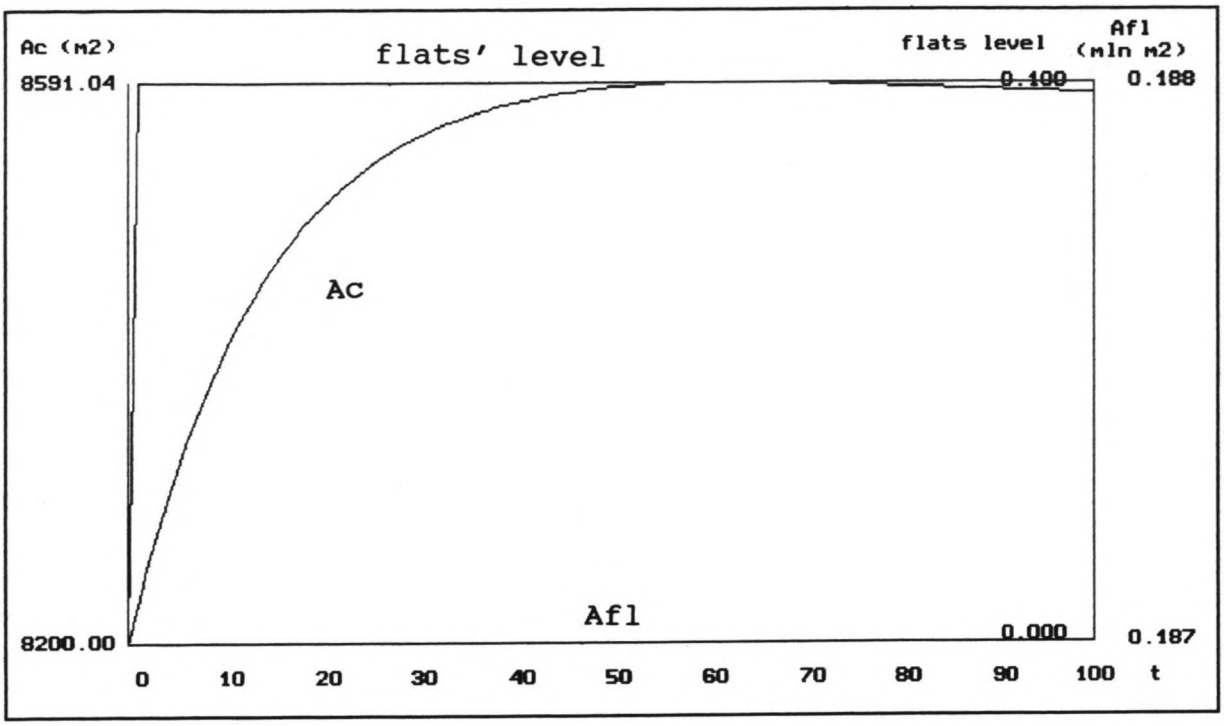

Fig. B-7: Increase of tidal range scenario at x=0

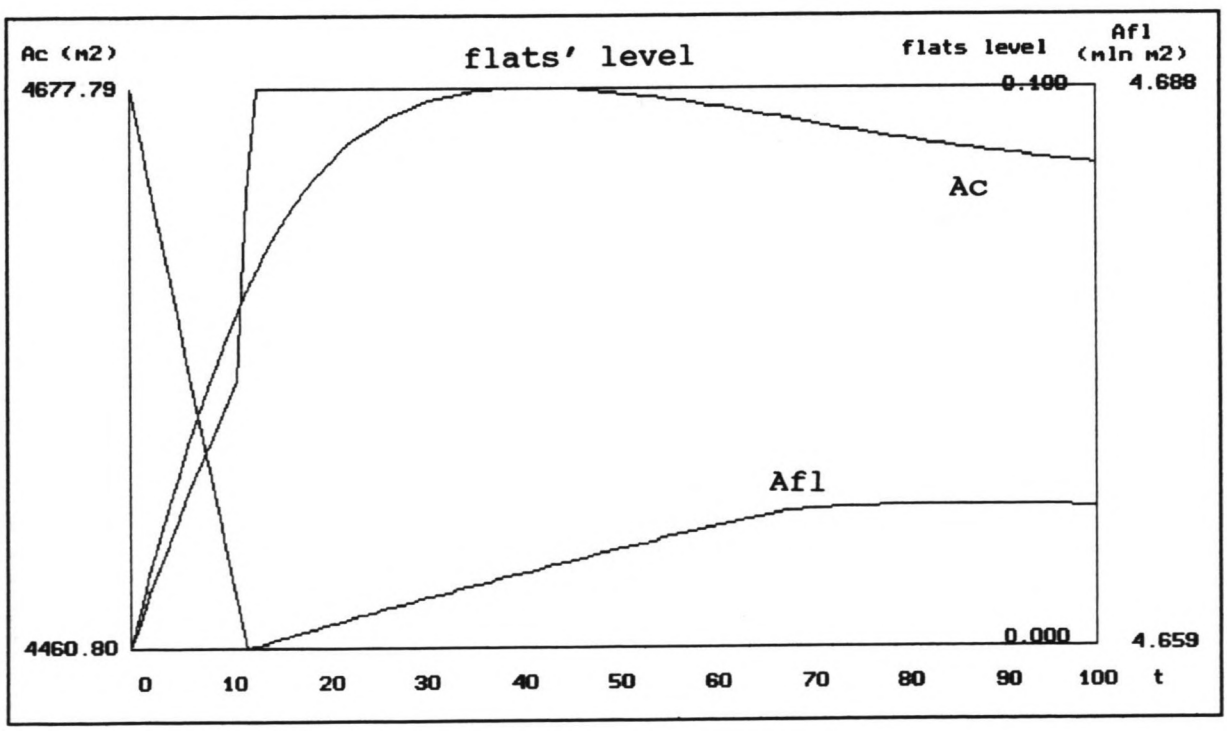

Fig. B-8: Increase of tidal range scenario at x=12 km.

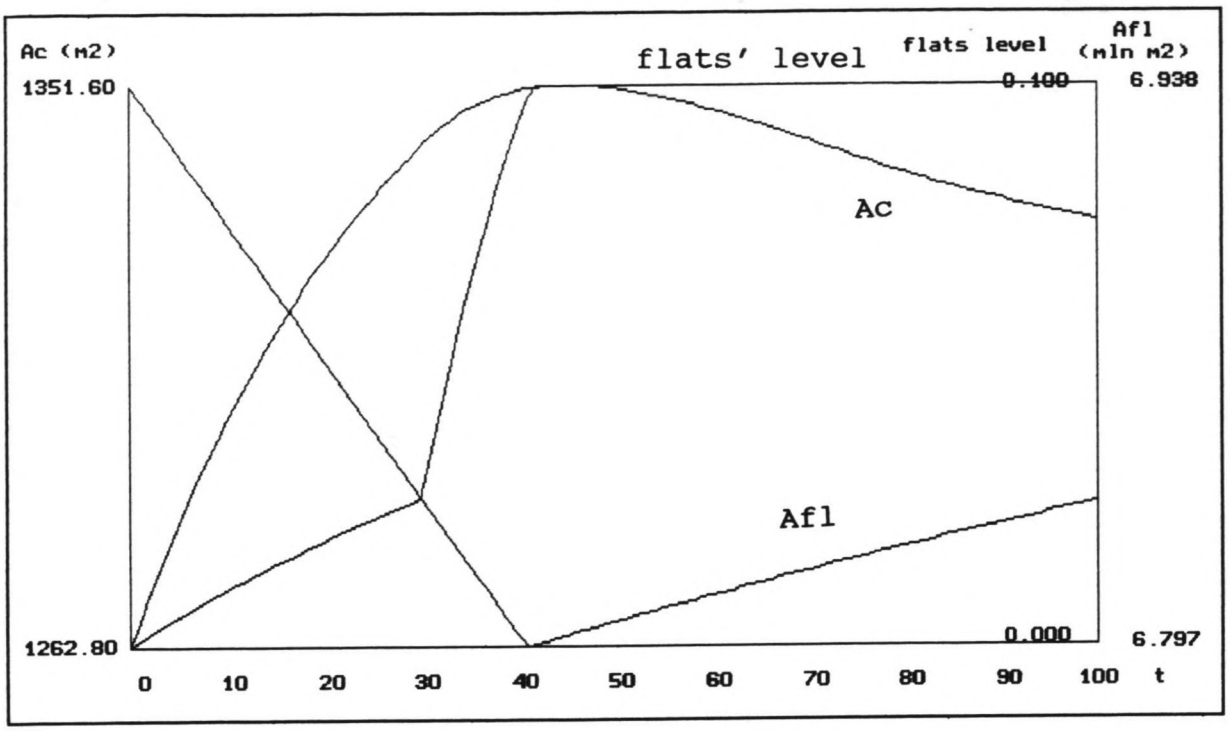

Fig. B-9: Increase of tidal range scenario at x=18 km.

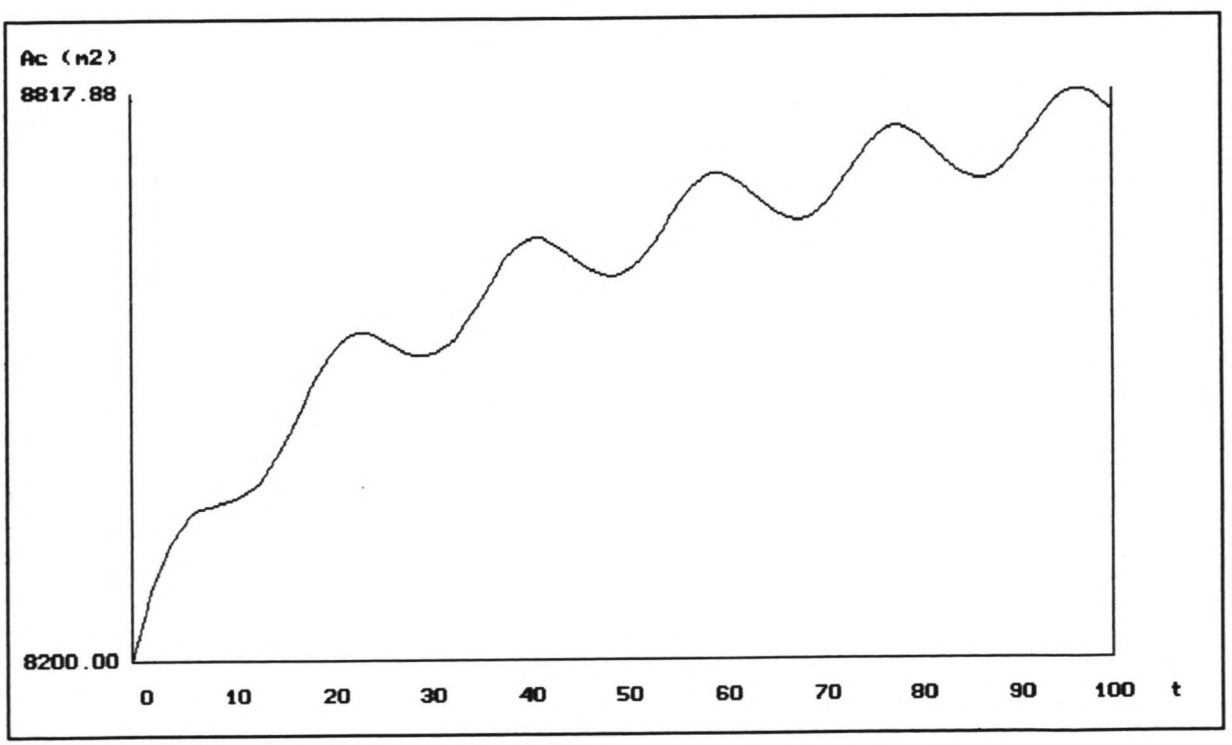

Fig. B-10: Tidal range periodicity scenario at x=0

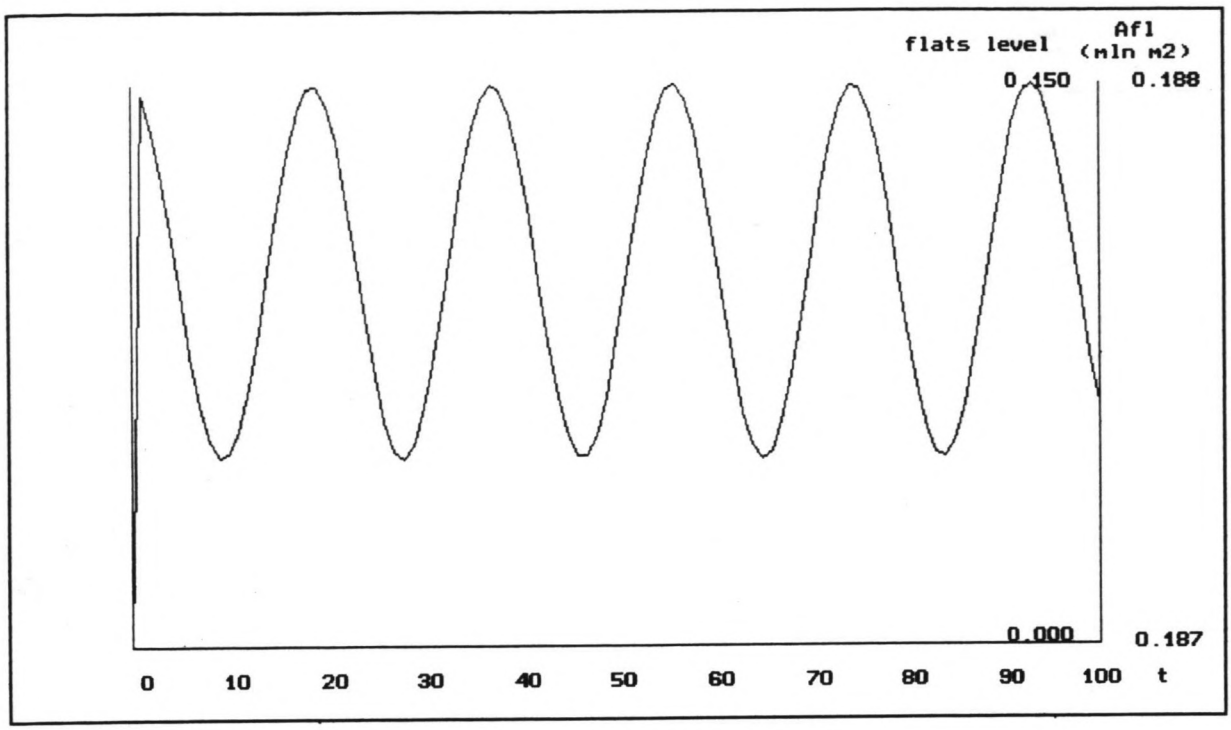

Fig. B-11: Tidal range periodicity scenario at x=0

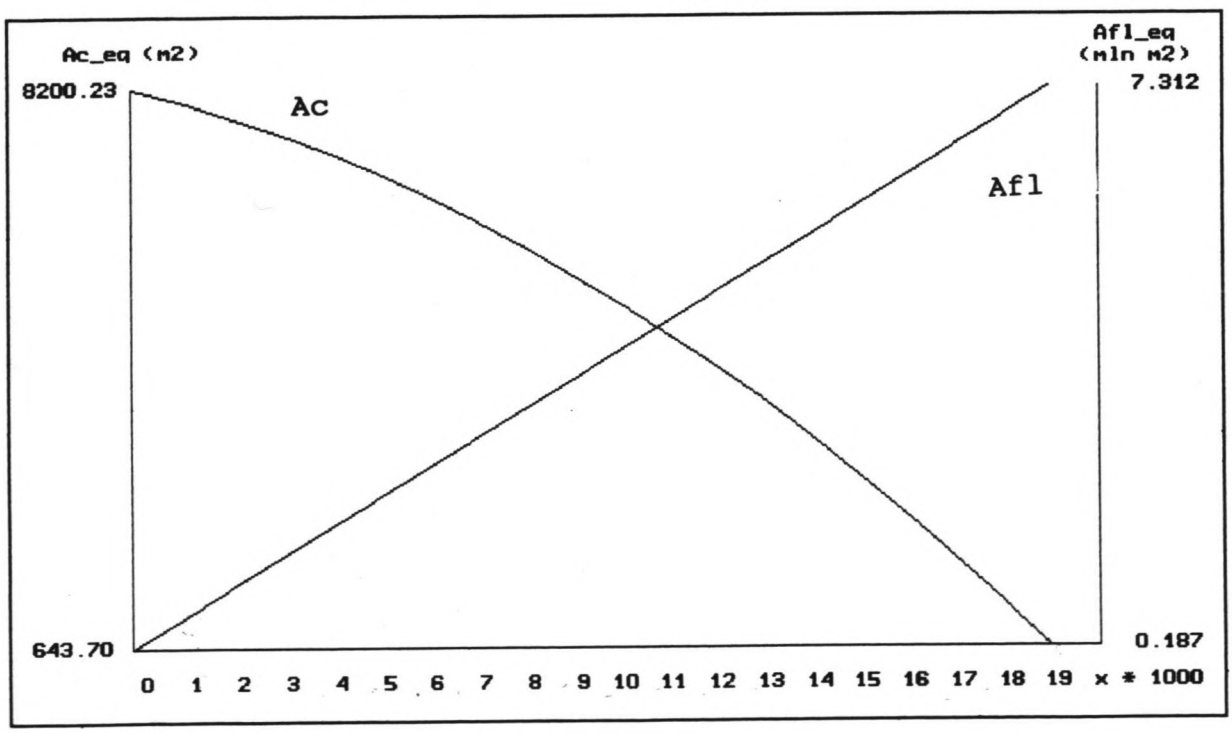

Fig. B-12: Distribution of equilibrium cross-sectional areas and flats' surface areas over the length of the basin

Appendix 4C

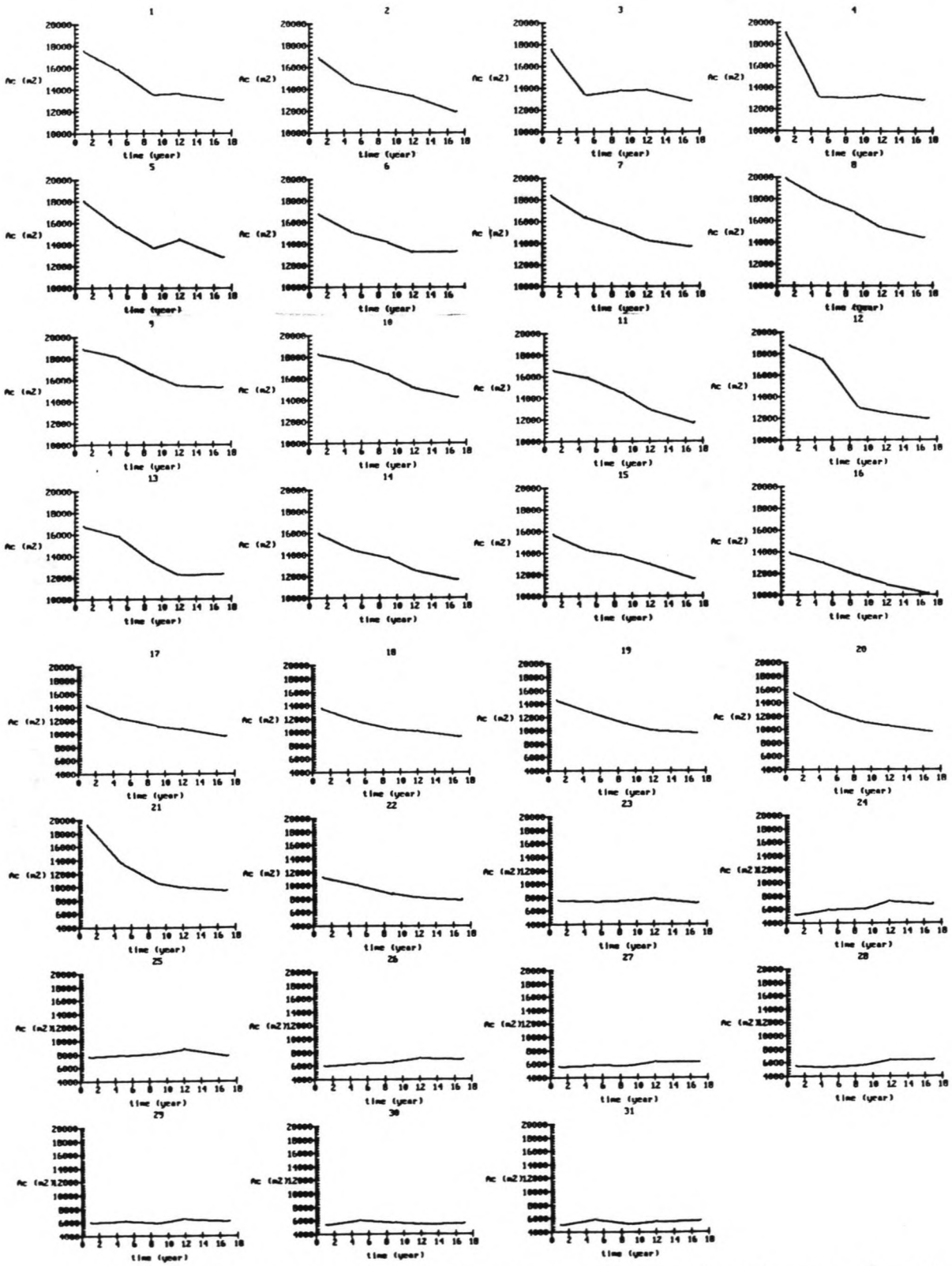

Fig. C-1: "Stamp graphs" of cross-sectional area in 31 cross-sections in the Zoutkamperlaag (from Biegel, 1991b)

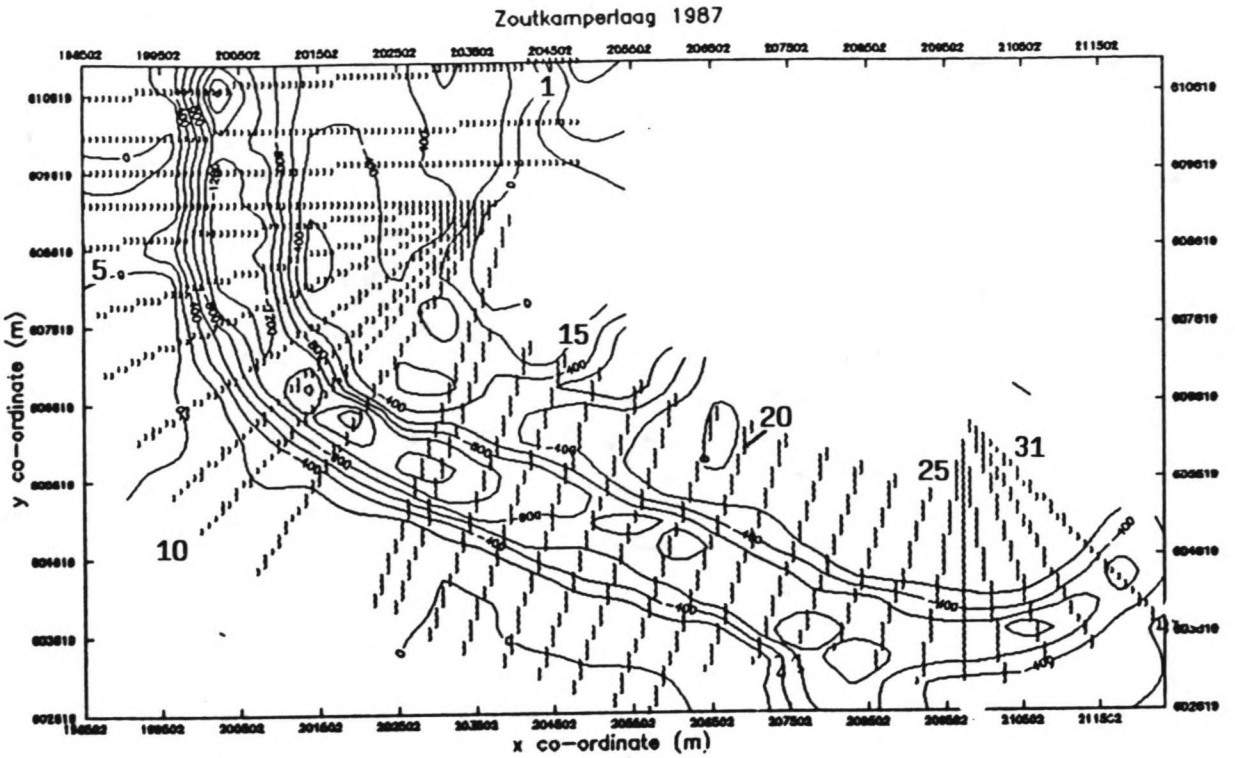

Fig. C-2: Location of cross-sections in the Zoutkamperlaag (from Biegel, 1991b)

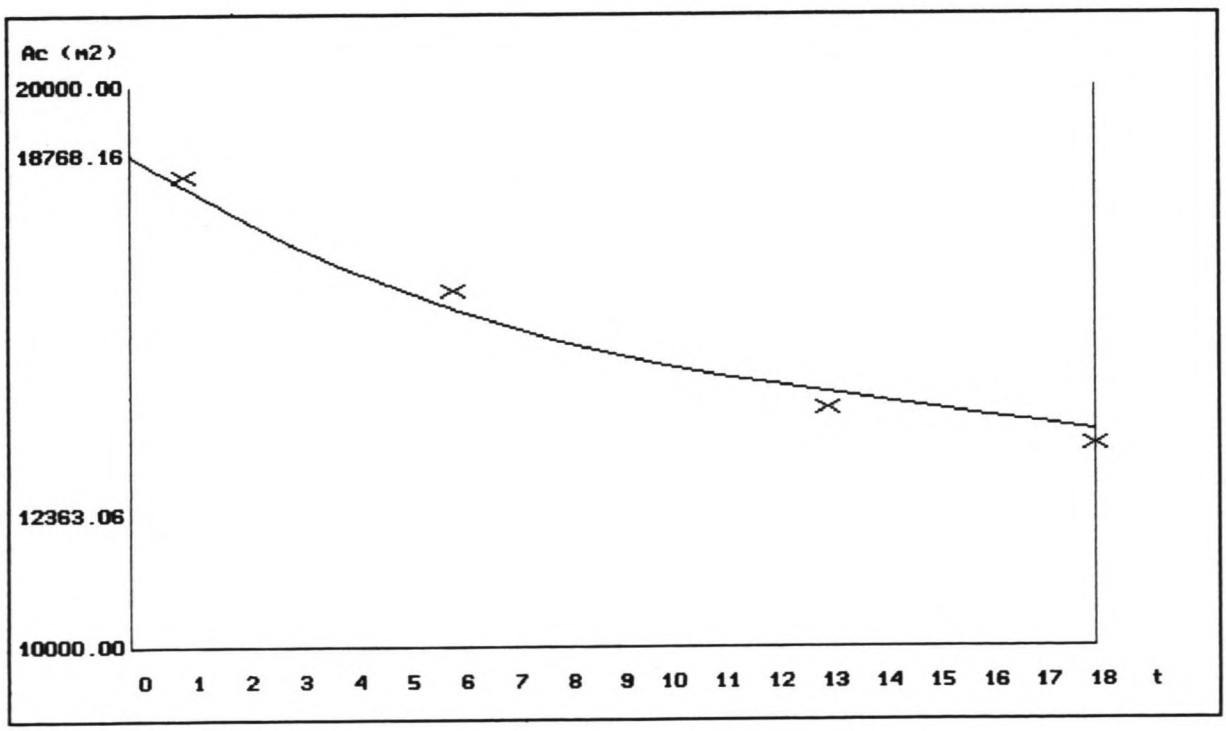

Fig. C-3: Time-evolution of the cross-sectional area at Biegel's cross-section 7

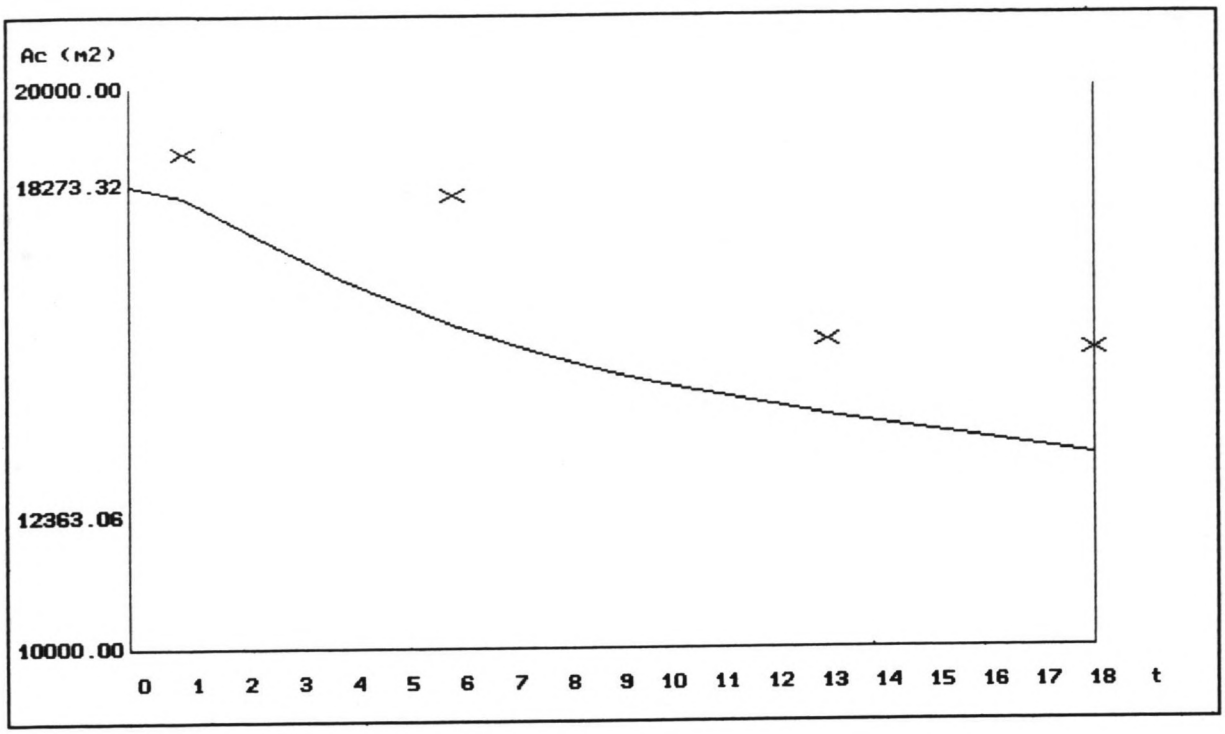

Fig. C-4: Time-evolution of the cross-sectional area at Biegel's cross-section 9

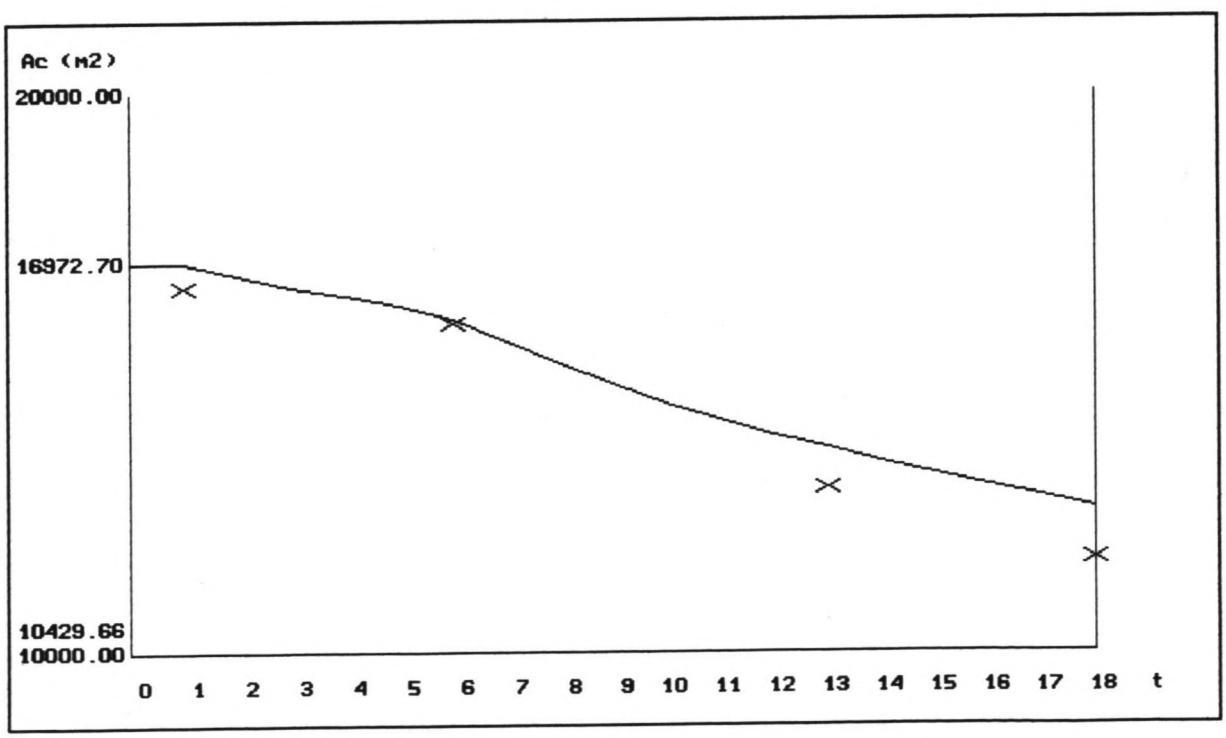

Fig. C-5: Time-evolution of the cross-sectional area at Biegel's cross-section 11

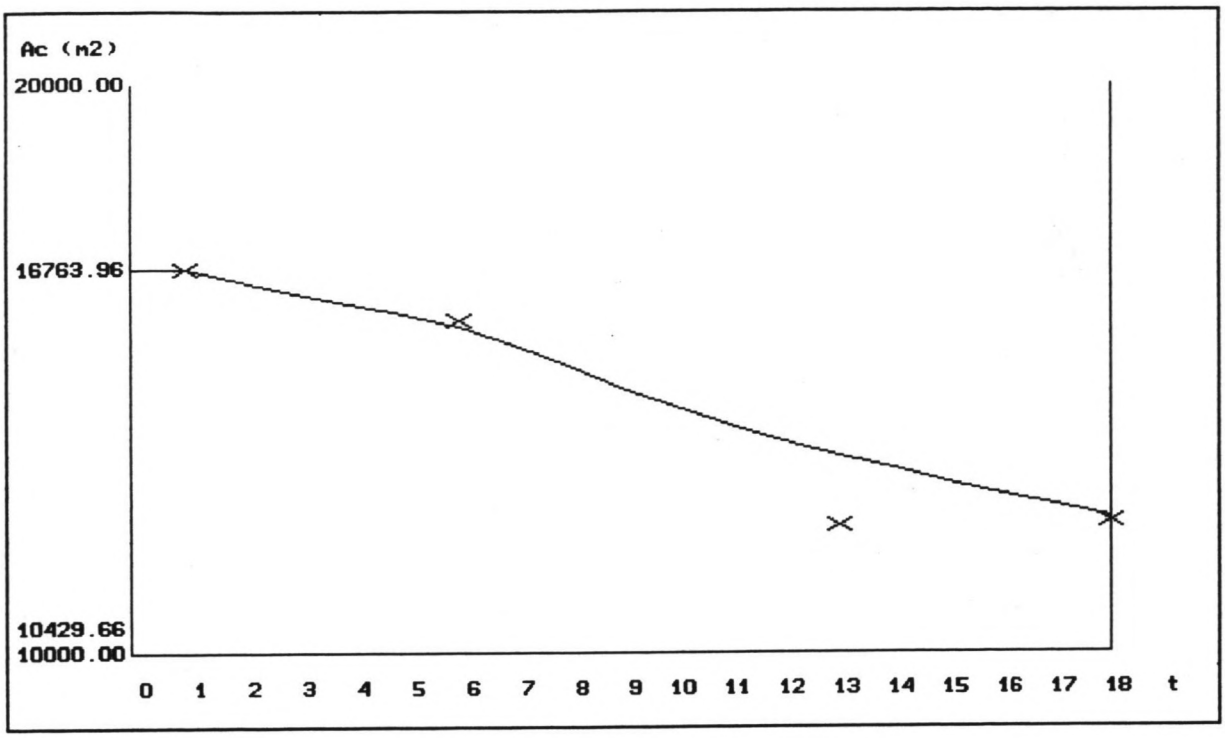

Fig. C-6: Time-evolution of the cross-sectional area at Biegel's cross-section 13

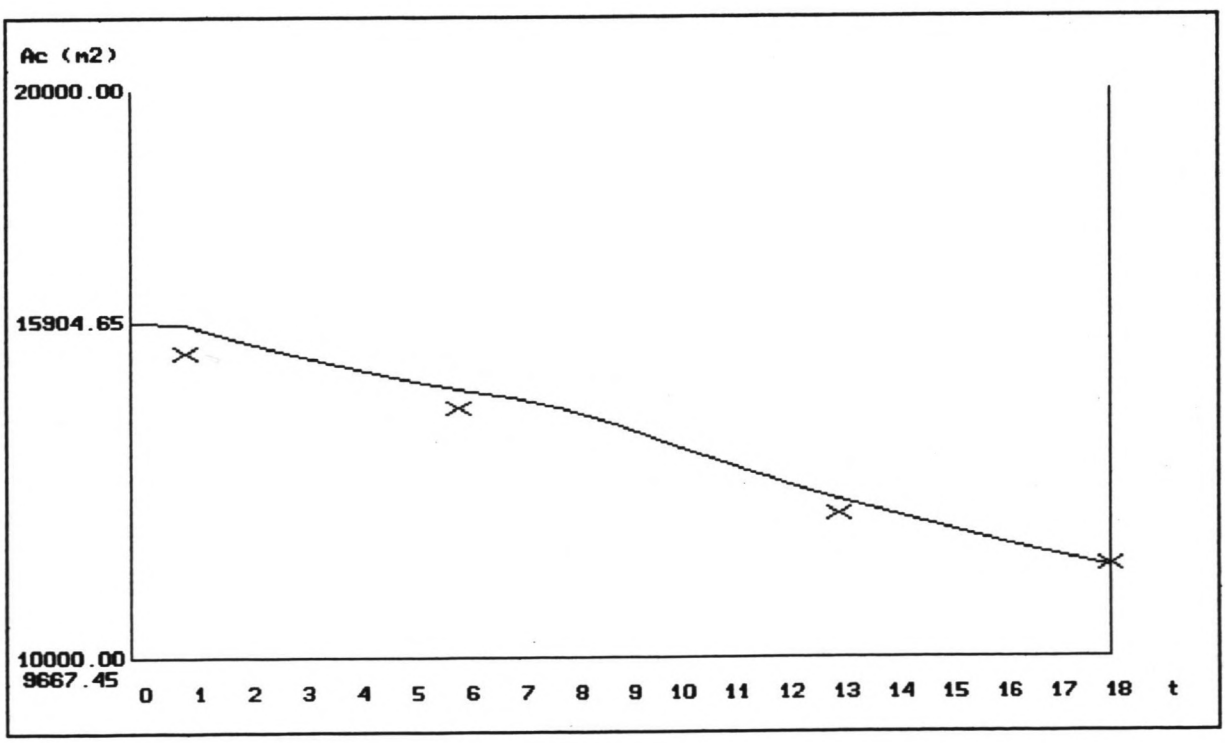

Fig. C-7: Time-evolution of the cross-sectional area at Biegel's cross-section 14

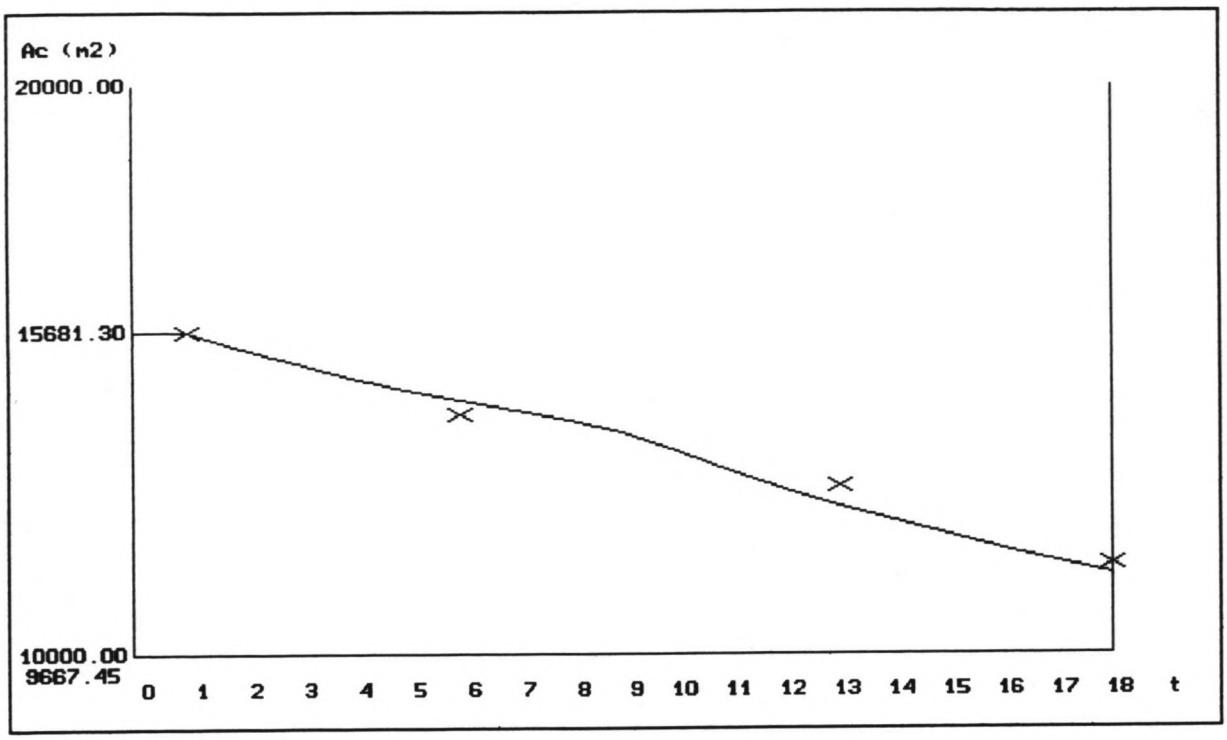

Fig. C-8: Time-evolution of the cross-sectional area at Biegel's cross-section 15

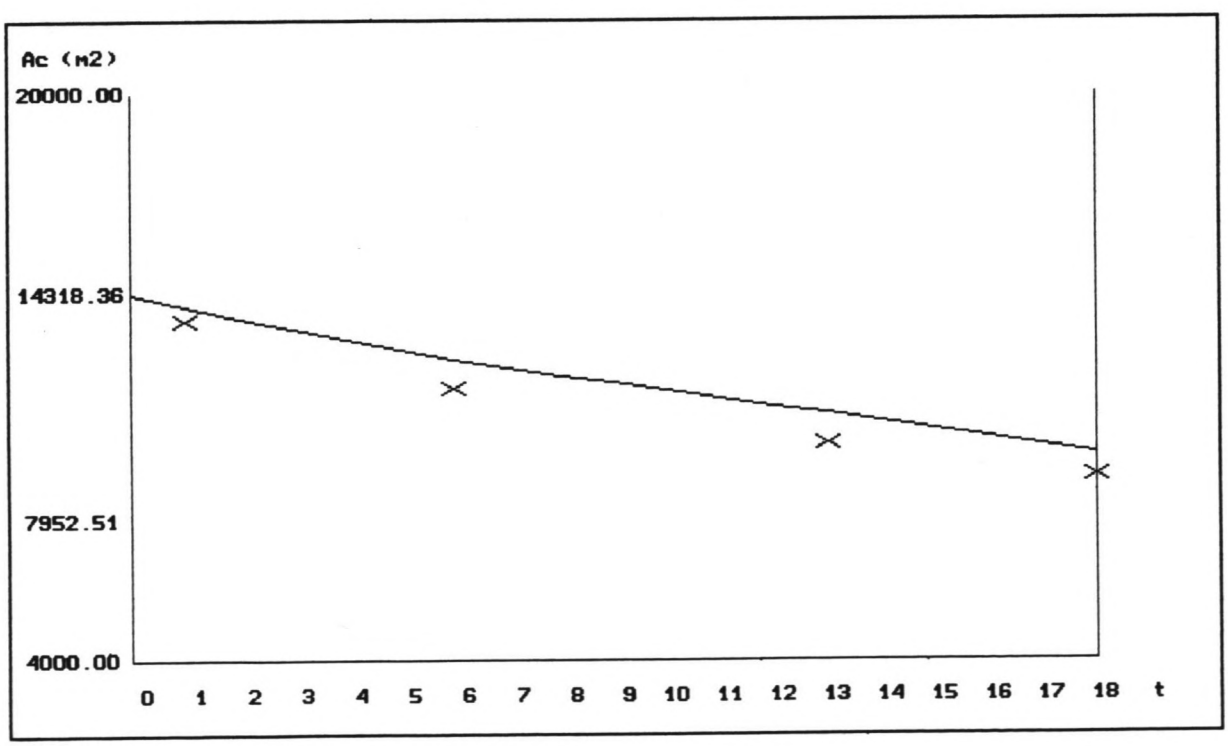

Fig. C-9: Time-evolution of the cross-sectional area at Biegel's cross-section 18

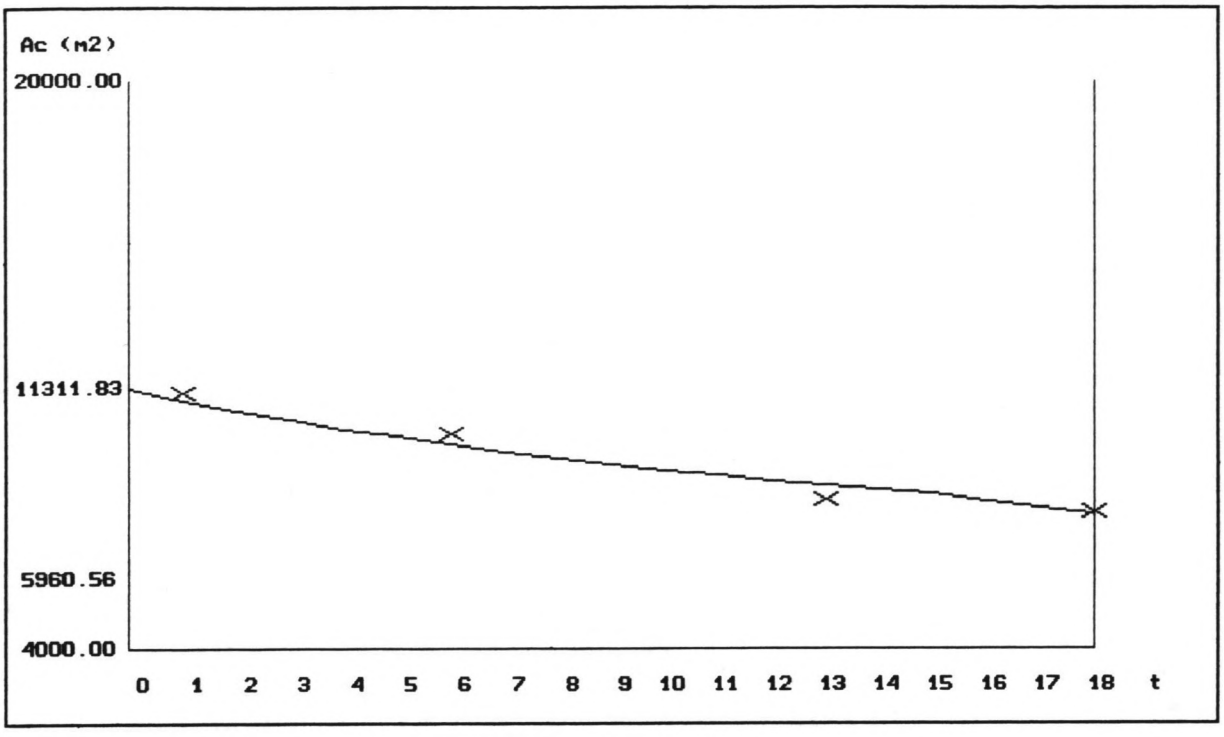

Fig. C-10: Time-evolution of the cross-sectional area at Biegel's cross-section 22

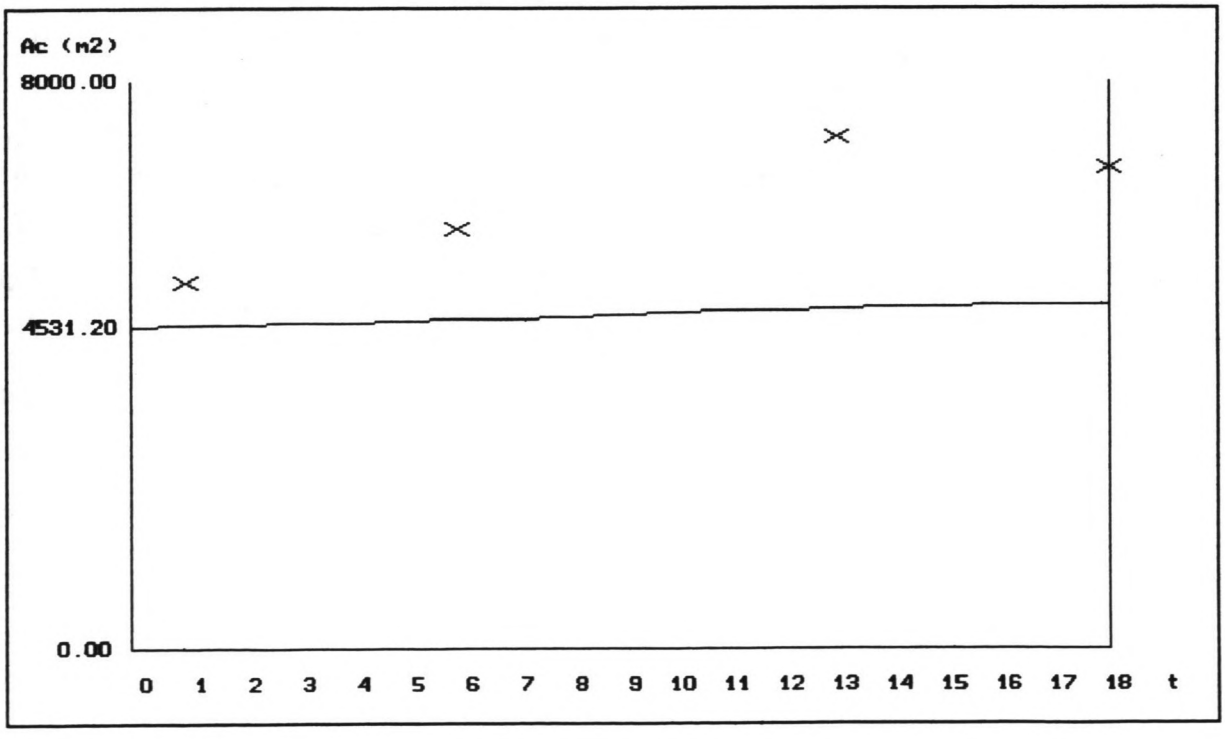

Fig. C-11: Time-evolution of the cross-sectional area at Biegel's cross-section 24

main office
Rotterdamseweg 185
p.o. box 177
2600 MH Delft
The Netherlands
telephone (31) 15 - 56 93 53
telefax (31) 15 - 61 96 74
telex 38176 hydel-nl

location 'De Voorst'
Voorsterweg 28, Marknesse
p.o. box 152
8300 AD Emmeloord
The Netherlands
telephone (31) 5274 - 29 22
telefax (31) 5274 - 35 73
telex 42290 hylvo-nl